Université catholique de Louvain
École polytechnique de Louvain (EPL)

Concentrated Solar Power: Plant Optimization for Energy Return on Investment and Deployment analysis for OECD Europe

A Dynamic Function for the EROI of CSP

Dissertation presented by
Julien Masson

for obtaining the Master's degree in
Mechanical Engineering - Energy

Supervisors
Hervé Jeanmart, co-supervisors: Elise Dupont, Gauthier Limpens

Readers
Gian-Marco Rignanese EPL, Camille Chardonnet Tractebel

Academic year 2016-2017

Abstract

A model of energy balance demonstrates that the solar technology owns the highest potential of evolution due to the future numerous installations and improvements of the technology. The Concentrated Solar Power (CSP) technology, producing electricity from direct irradiation, in the opposite of photovoltaic which produces power from diffuse light, is studied in details. The CSP perspectives in the future mix are analyzed. It appears that CSP towers, among the others CSP technologies, will have the lead of the future deployment.

A model computing the Energy Return on Investment (EROI = $\frac{\text{Energy}_{\text{delivered}}}{\text{Energy}_{\text{consumed}}}$) is used to evaluate the net energy return of the CSP technology. The EROI allows to assess the net potential that the technology is able to deliver to the society and enables the comparison of different energy sources. This dimensionless factor is used to analyze the integration of the CSP technology as an actor of the energy transition for OECD Europe.
The model, based on solar data from the NASA, simulates the hourly comportment of a CSP tower plant, during a year, for a given location. A study of life cycle assessments (LCA) allows to attribute energy cost to the defined plant, depending on its configuration. Then, the parameters impacts are analyzed. It appears that three main parameters, defining the plant configuration, critically impact the results given by the model. These parameters are: the capacity of the storage ratio, the power designed of the turbine and the size of the mirrors field.
From there, a static analysis of the EROI is performed and the optimal configuration in terms of EROI is computed. The optimal plant for Sevilla (Spain), one of the best region in Europe for CSP applications, has a 49 MW designed power, 20 hours of storage capacity at full load and a solar multiplicator of 2.84. The tests demonstrated that the optimal configuration depends on the location.
Afterwards, a dynamic analysis is performed. A program simulates the installation of these optimal plants in all OECD Europe. Sites are ranked by their level of direct irradiation. The availability, in terms of area, is defined for each site, and the program fills the sites with optimal CSP plants (with a configuration suited to the location, maximizing the EROI) until the site is full. Moreover, the evolution of technology is considered.

With an optimistic evolution of the technology, the study demonstrates a low net energy gain and question a sustainable deployment of CSP in OECD Europe. To complete the Advanced Energy Scenario of Greenpeace (430 TWh of electricity production in 2050), the model installed 80.5 GW, with 1807 plants, spread over Southern Europe. For this scenario, the mean fossil primary equivalent EROI decreases from 25 in 2015, to 15 in 2050. The electric equivalent EROI is constant at a value around 10. These results confirm the low net energy return of CSP technology for a deployment over OECD Europe, though the technological improvement was optimistic. Indeed, with a value found around 10 for the electric equivalent EROI, the energy sector scale would need to more that double, as the value of the current energy mix for the electric equivalent EROI is much higher than 10. Therefore, operating an energy transition in OECD Europe, with CSP technology as the main pillar, would change the way in which the energy is allocated in society, since the energy sector would need more energy to produce the same quantity than currently.
On the other hand, the results for North-Africa countries, due to the high lands availability, considering an optimistic evolution of the technology, show a rise of the electric equivalent EROI. Its value increases from 11 in 2015, to more than 15 in 2050, for a CSP installed capacity able to produce more than 2000 TWh per year in 2050. These results proved that a CSP delployment in North-Africa is interesting in terms of net energy gain.

Acknowledgements

I am grateful to my supervisor, Mr. H.Jeanmart, who gave me the opportunity to work on this subject. I appreciated the freedom I had to develop my own expertise on CSP technology, the support provided, and his reliance on my work. Moreover, I highly appreciated the possibility to link this subject to a global energy perspective.

I express my profound gratitude to my co-supervisors, E.Dupont and G.Limpens, for their continuous guidance and interest in my work. I really appreciated the interactions we had, sharing the improvements and results all along the study and challenging the concepts.

I also take the opportunity to thank the people I met at Tractebel during my internship and especially my supervisor, Ms. C.Chardonnet. This internship, constituating the majority of the first chapter of this thesis, gave me the opportunity to develop my energy perspective and vision as well as meeting people with interesting lines of thought about energy.

To conclude, I would like to thank my parents for their continuous support during my studies. As well, I thank my friends for the mutual encouragement we had, supporting each other for our respective Master Thesis.

Contents

Introduction **1**

1 CSP in the energy transition **3**
1.1 A model to represent a territory's energy balance 3
1.2 Perspective for the efficiency evolution & comparison with Greenpeace scenarios 10
1.3 The place of CSP in the energy transition 15

2 Focus on CSP technologies: synthesis of properties, performances and current researches **17**
2.1 Context, principle and historic overview 17
2.2 Review of the existing technologies 17
2.3 Subsystems and components 22
2.4 Perfomances 28
2.5 Summary and conclusion about CSP tower status 40

3 EROI and Life Cycle Assessment **41**
3.1 The EROI 41
3.2 Life Cycle Analysis 44
3.3 The EROI computation and the primary energy factor 46
3.4 Summary and conclusion about the EROI and LCA parts 50

4 Construction and validation of a model to evaluate the production of a CSP tower plant depending on its location **51**
4.1 The sun irradiations model 51
4.2 The plant model 55
4.3 Validation 61
4.4 Summary and conclusion about the plant model 63

5 EROI Static analysis: optimization of a plant depending on the location **64**
5.1 Analysing the results on a year 64
5.2 Configuration for a base load plant 66
5.3 Impacts of the different parameters 68
5.4 Finding the optimal plant 71
5.5 Impact of the location on the optimal plant configuration 73
5.6 Summary and conclusion for the static analysis 75

6 EROI Dynamic analysis: application of the model and optimization process to analyze a deployment of the CSP tower technology in OECD Europe from now to 2050 **76**
6.1 The land availabitlity 76
6.2 The technology evolution 80
6.3 CSP deployment for OECD Europe 83
6.4 Summary of the different assumptions and possible improvements 93
6.5 Conclusion about CSP deployment in OECD Europe 93

Conclusion **97**

Appendices **100**

A Definitions of the terms used for the balance energy model **100**
A.1 Resources 100
A.2 Technologies definition 101

B Defining the current and limiting values for each technologies **102**

C GP scenarios: representation of the evolution of the primary demand **116**

D Final values used in the energy balance model **117**

I Bibliography **120**

List of Figures

1.1 Global view of the bottom-up process. 3
1.2 Interface of the balance model. 4
1.3 General principle of the model. 5
1.4 Shape function of the efficiency evolution. 6
1.5 Summary of the hydrogen production. 7
1.6 Total Final Consumption from IEA data. 8
1.7 Total Primary Energy Supply from IEA data. 8
1.8 Mix used for OECD Europe region. 8
1.9 Results obtained with the IEA 2013 data. 9
1.10 Polynome approximating the production ratio evolution. 11

2.1 Representation of a parabolic trough collector. 18
2.2 Representation of a CSP tower plant. 18
2.3 Representation of a linear Fresnel reflector. 18
2.4 Representation of a parabolic dish system. 19
2.5 Principle of a CSP tower plant. 22
2.6 Simplified representation of power losses occurring in a SPT plant. 28
2.7 Optical losses occurring during the transmission. 29
2.8 Receiver's efficiency, details. 31
2.9 Plant efficiency from a basic model. 33
2.10 Distribution of the sun and receiver radiations. 34
2.11 Perfect selective absorber results. 34
2.12 Exergy analysis: parameters and scheme of the plant. 35
2.14 Exergy and energy efficiencies. 36
2.13 Map of the annual mean DNI on earth. 36
2.15 DNI influence on the exergy and energy efficiency. 37
2.16 Concentration ratio influence for the efficiency. 38
2.17 Results and comparison for the different plant configurations. 39
2.18 Exergy and energy, results and comparison for different DNI levels. 39

3.1 Static EROI analysis for a plant. 42
3.2 Dynamic EROI analysis method. 43
3.3 EROI: boundary of the model. 47
3.4 EROI: two methods of computation. 48

4.1 Beam radiations results for Tucson USA, on a year. 53
4.2 Beam radiations results for Tucson USA, on a month. 54
4.3 Beam radiations results for Tucson USA, in a day. 54
4.4 Efficiency for the zones of a heliostat field. 56
4.5 Representation of the main steps of the model. 59

5.1 Time operating at designed power per day on a year. 64
5.2 Comparison of energy produced, stored and received in a year. 65
5.3 Comparison of energy produced, stored and received in a month. 66
5.4 Comparison of energy produced, stored and received in a day. 66

5.5 Daily operating time compared with DNI levels. 67
5.6 Comparison of energy produced and received, for a base load plant. 68
5.7 EROI, production and operating time evolution according to the power designed. 70
5.8 EROI, LCA and production evolution according to the power designed. 71
5.9 EROI, LCA and production evolution with different storage capacities. 72

6.1 Types of area suited to CSP tower applications. 77
6.2 Process implemented to compute the CSP potential of a territory. 77
6.3 EROI evolution of Italy for a total filling of available lands with optimized plants. 79
6.4 EROI evolution for OECD Europe region. 80
6.5 Sunshot inniative (USA) goals for the CSP technology. 81
6.6 EROI evolution for OECD Europe, no land restriction and technology evolution. 82
6.7 Comparison of the impact on the EROI of technology components evolution. . . 82
6.8 Evolution of the primary energy demand. 83
6.9 Deployment in Europe. Test A: no evolution of the technology. 85
6.10 Deployment in Europe. Test B: moderate evolution of the technology. 86
6.11 Deployment in Europe. Test C: optimistic evolution of the technology. 87
6.12 The 119 sites of installations for the test C. 88
6.13 DNI levels, map of Europe. 88
6.14 Expected decrease of the PEF from a study. 89
6.15 PEF decreasing, deployment in Europe. 90
6.16 EROI without PEF, deployment in Europe. 92
6.17 EROI for wind turbines deployment. 93
6.18 EROIelec evolution for North-Afrcia. 95

C.1 OECD Europe, final energy demand, GP current sc. 116
C.2 OECD Europe, final energy demand, GP energy revolution sc. 116
C.3 OECD Europe, final energy demand, GP advanced energy revolution sc. 117

D.1 Efficiency values, energy balance model, part 1. 117
D.2 Efficiency values, energy balance model, part 2. 118
D.3 Efficiency values, energy balance model, part 3. 118
D.4 Efficiency values, energy balance model, part 4. 119

List of Tables

1.1 Use of final energy in refineries. 7
1.2 Values used for the efficiency of geothermal technologies. 13
1.3 Values used for the efficiency of biomass technologies. 13
1.4 Values used for the efficiency of geothermal technologies. 14
1.5 Differences from an accurate study about wind installation and use of mean factor. 15

2.1 Comparison of the four families composing the CSP technology panel. 21
2.2 Details of the optic efficiency. 29
2.3 Average efficiencies of the heliostat field. 30
2.4 Summary about receiver efficiency. 30
2.5 Types of power cycle configuration. 32

3.1 Examples of EROI studies for different technologies. 44
3.2 Cumulative energy demand for the different phases of a CSP tower plant. 45
3.3 Cumulative energy demand repartition for the E&M phases of a CSP tower plant. 46

4.1 The three types of power cycles used in the model. 57
4.2 The main parameters used to characterize the storage system in the code. 58
4.3 Summary of the formula used to compute the CED of a given plant. 60
4.4 The parameters of the model. 61
4.5 Validation: plants information. 62
4.6 Validation results. 62

5.1 The parameters used to configure the plant as a base load one. 67
5.2 The parameters describing the optimal plant in terms of EROI for Sevilla. 72
5.3 Optimization results for three locations. 73
5.4 Parameters influence on the optimization results. 74

6.1 Results for a total filling of available lands with an EROI optimization of plants. 78
6.2 Results for different types of plants, available areas entirely covered. 79
6.3 Parameters used for the different technology evolution scenarios. 84
6.4 Summary Results for OECD Europe Deployment 94

Introduction

The ongoing energy transition queries the current energy sources and launched the challenge of developing new renewable technologies. Solar technologies are an important source on which this transition relies. The integration of renewable technologies in the energy mix is slowed by the difficulties induced by the variation of the electricity production. Moreover, the renewable source quality, depending on the chosen site, is an important factor, directly impacting the production.

Concentrated Solar Power (CSP) plants, thanks to a thermal energy storage, has the possibility to tackle the variability of the energy provided by the sun. This quality has revived interests for the technology. Indeed, more and more projects arise and, CSP integration in scenarios implementing an energy transition is a reality. As a drawback, the sites quality is an important factor for the CSP efficiency. Moreover, the more the installed capacity, the less the quality of the remaining sites. On the other hand, the technology improvement could balance this trend.

The goal of this study is to set up a model to deeply analyze and characterize the deployment of CSP technology in OECD Europe. The relevance of a CSP deployment is not obvious. OECD Europe is not a highly sunny continent and the technology improvement should be analyzed carefully. This study does not give an opinion on CSP installation, it highlights the technological improvement conditions to achieve a sustainable deployment, given the land availability constraint.

In the first chapter, the construction of a model, to represent an energy balance, is proposed. The goal of this chapter is to analyze the different energy strategies for a renewable transition. From there, the current energy context and perspectives, as well as the place of CSP as an actor of these scenarios, are covered.
The second chapter sets up the required knowledge about CSP technology. The purpose of this chapter is to clarify the properties and main components of the CSP technologies. It also highlights the main possible innovations and analyses the performances and perspectives of improvement.
The third chapter introduces the Energy Return on Investment factor and describes its interest in the context of our study. As well, Life Cycle Assessments (LCA) are covered with a focus on the Cumulative Energy Demand (CED) for typical CSP plants.
The fourth chapter describes the methods used to implement a model able to compute the annual production of a plant for a given location. The model also computes the EROI of the plant, depending on its configuration.
Now that a model, able to compute the electricity production and EROI of a specific plant, is implemented, an optimization process is performed in the fifth chapter. The goal of this part is to optimize the EROI of the plant depending on its location. The importance of each parameter is studied and then an optimization process is performed.

In the end, the sixth chapter applicates the model to the deployment of the CSP technology, proposed by Greenpeace scenarios, over OECD Europe. First, the method to consider the land availability is explained. Then, the methodology to simulate the technology improvement is covered. Finally, the global process is applied for the OECD Europe region and the results are discussed. A special analysis is performed for the EROI factor, allowing to account for different energy points of view.

1 CSP in the energy transition

The goal of this chapter is to set up the current energy context and the different energy strategies for a renewable transition as well as the place of concentrated solar power plant, as an actor of these scenarios.

In the first section, the construction of a model to represent an energy balance at a territory scale is proposed. This model is then used, in section two, to analyze the relevance of transition strategy of the Greenpeace Scenarios.

1.1 A model to represent a territory's energy balance

This section describes the goal and the general principle and assumptions made to establish a balance energy model.

1.1.1 Objectives and perimeter

The objective of this section is to develop a full energy balance at a territory level, estimating the primary energy needs based on the final demand and the energy mix used. The model returns the annual primary energy supply, corresponding to each source, for the chosen year (see figure 1.1). There is no computation performed to estimate an optimal mix from a cost or environmental perspectives since the mix and the demand are considered as input. The model also returns the CO_2 annual production due to the energy production sector and proposes details about energy consumed for hydrogen production.

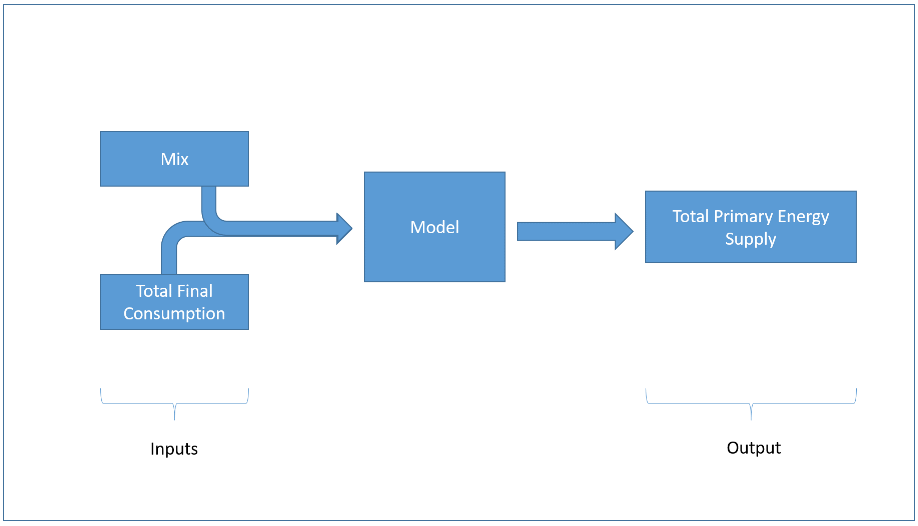

Figure 1.1: Global view of the bottom-up process used to find the Total Primary Energy supply (TFES) from the Total Final Consumption (TFC).

The model is restricted to the OECD Europe region. The main difference compared to the EU region is the addition of Turkey, Switzerland and Norway and exclusion of Romania and Bulgaria. This region comprises quite different shapes of demand and potential of renewable energy production. In the South (Italy, Spain, Turkey and Portugal), there is a high potential for solar energy production and a low heat demand for buildings. The North is more suitable for wind off-shore installations and, with the East part, has a good biomass potential.

1.1.2 Representation and general principle of the model

Representation of the annual energy supply and demand

A table was established to have a global view of an annual energy balance (see figure 1.2). The natural sources are classified in the first row of the table. All the final energy consumed is produced from these sources. The technologies are specified in the first column. This classification allows to assign a quantity of energy to each source, depending on the technology. A detailed explanation of each source and technology is proposed in the appendices (see points A.1 and A.2).

2050 Supply and consumption [MTOE]	coal	crude oil	Oil products	Natural gas	Uranium	Sun	Wind	Hydro	Geothermal	Biomass	Waste	Hydrogen	Electricity	Heat	Total
Production															
TPES	0,00	0,00		0,00	0,00	0,00	0,00	0,00	0,00	0,00	0,00				0,00
Electricity plants															
CHP plants															
Heat plants and direct heating															
Oill refineries															
Nuclear plants															
PV															
Solar thermal CSP															
Wind turbines off-shore															
Wind turbines on-shore															
Hydroeletric damps															
Tidal															
Hydrogen production															
Energy Industry own use															
Losses															
TFC	0		0	0						0	0	0			
Industry		/			/	/	/	/	/						
Transport		/			/	/	/	/	/						
Other		/			/	/	/	/	/						
Non enregy use		/			/	/	/	/	/						

Figure 1.2: The table, representing the demand and production depending on the sources and technologies for a specific year and scenario.

Heat and electricity are considered as energy vectors and then are represented in the two last columns on the right. The primary energy is transformed in energy vectors that will be used as another type of energy that doesn't exist in nature (as mechanical energy in an industry process). These energy vectors represent the most important part of the demand.
The demand is detailed in the bottom of the table (five last rows, see 1.2). The demand is categorized by sector and a cell represents a source. So, the demand could be of primary energy itself (coal, oil, etc.) or of energy vector as electricity or heat. As a simplification no demand for sun, wind, geothermal, hydraulic and uranium primary energy is considered.
Hydrogen is an energy vector too. No hydrogen suitable for human processes can be found in the nature. So, no primary value could be attributed for hydrogen and that's why the corresponding cell in the table (see figure 1.2, last column before electricity and heat) doesn't even display a zero, as for electricity and heat.

The general principle

From this classification of technologies and sources, the purpose is to find the primary energy consumption of each natural source knowing the final demand. From the data of the scenarios, we can deduce the distribution of the production (how much energy each technology should produce). So the repartition of the production is done for the ongoing year: a percentage of the total production is assigned to each technology according to a source (step [2] in figure 1.3). Knowing this mix and the total quantity to produce, only the step of conversion between the primary and final energy has to be performed. During this transformation, losses occur. The efficiency of the conversion gives the ratio between the production and the energy consumed; it contains the information of the losses that occurred. The evaluation of the efficiency for the conversion is done at the step [3] (in figure 1.3). From a bottom-up process, the primary energy supply is deduced for each source, (see point [4] in figure 1.3), and is written in the corresponding part of the table for each technology. The total of primary energy supply per source is then computed and displayed in the top of the table (see figure 1.2).

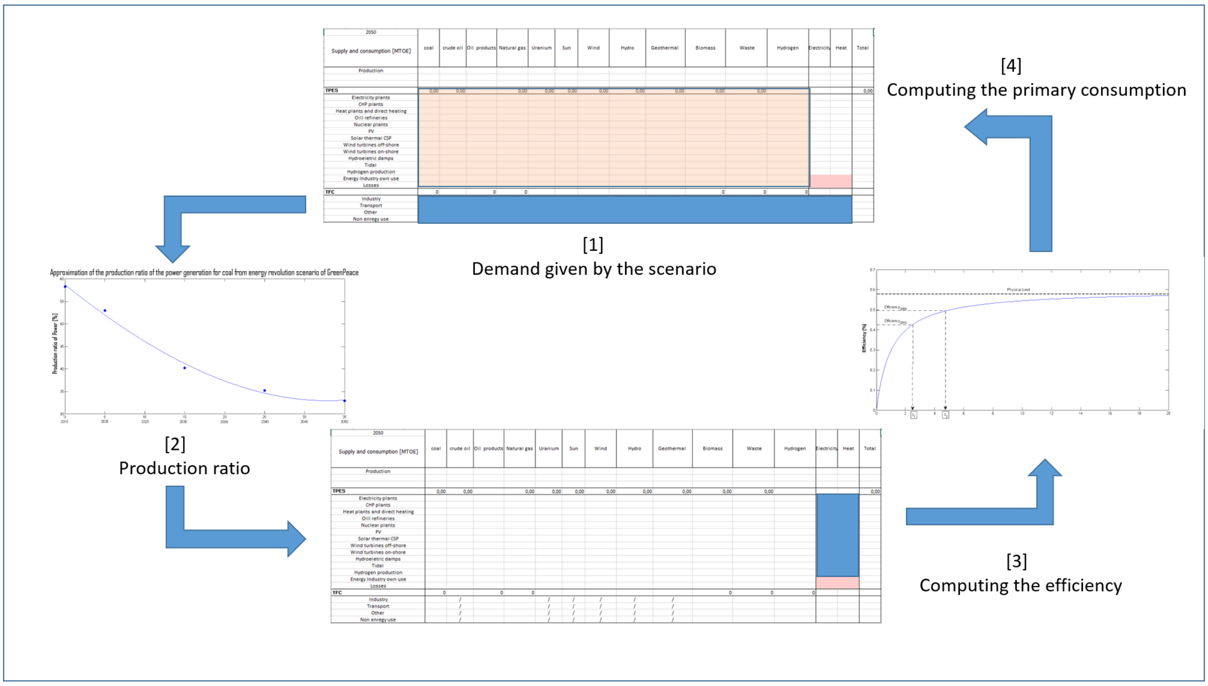

Figure 1.3: General principle of the model.

The efficiency of the conversion is different for each source and each technology. Moreover, it grows with time, as the technology is increasingly known and mastered and that the old production sites are replaced by new one. The question now is how to define a model of evolution for the efficiency.

1.1.3 The conversion: from final to primary energy

The efficiency of the conversion will determine the quantity of primary energy a technology consumed to create a certain amount of final energy. As explained in the previous point, the efficiency contains the information of the losses who occurred during the conversion. As the technology is more and more know and mastered the efficiency value for this technology increase and a better conversion is performed.

The model needs a value of the conversion efficiency, for each year, depending on the technology and source. As we want to be able to represent prospective scenarios, the evolution should be modeled. Then, a function will be developed to reproduced the improvement of the efficiency conversion, and such a function will be assigned to each technology depending on the source.

How to model the evolution of the conversion efficiency

The efficiency value increases with time. A global function can be attributed to each technology giving a physical limit as limited value of the function. The function used in the model is a negative exponential as presented in figure 1.4. The graph includes the representation of the physical value (divided by 100) as limit value in infinity. This kind of function allows to represent the fact that the more the technology grow the more it is difficult to improve it as the derivative is smaller and smaller. The function begins at zero (technology discovery or unused) to the physical limit (technology completely mastered). The equation is: $f(x) = -e^{(1+\frac{1}{ln(2)})} + 2$; an example is presented figure 1.4.

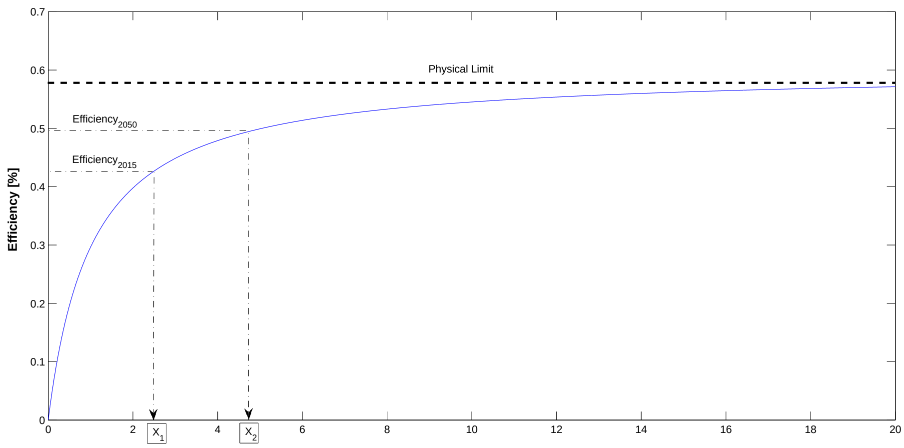

Figure 1.4: Shape function of the efficiency evolution for a certain technology and physical limit.

Three parameters are necessary to call the function to find the efficiency: the value of the current efficiency, the efficiency expected in 2050 and the physical limit. The function, knowing these efficiencies, can retrieve the x-value corresponding. For example, on the figure presented, x_1 corresponds to 2015 and x_2 to 2050. From there, dividing the interval by 35 we can attribute an efficiency to each year.

The goal now is to have a value of the current conversion efficiency for each technology and a forecast of the evolution, because we need to set a value for the efficiency in 2050. Moreover, the physical limit should be known to be able to shape the function. In the following paragraphs, a review of the current conversion efficiency for each technology is presented as well as perspectives of improvement. The first part is dedicated to all technologies and is followed by a paragraph dedicated to technologies consuming sun, ocean and wind sources. The reason of focusing such sources is because scenarios doesn't take into account the efficiencies of the conversion from these sources since these sources are almost infinite. The model here proposes to include or not the conversion factor for these sources. In the end, the third point covers different processes of hydrogen production. These data will serve to give the energy, from each source, necessary to achieve the hydrogen production included in the demand.

1.1.4 Assumptions and remarks about the model

Losses

The electricity losses in the transmission is estimated at 7% of total power generation. The heat losses during transmission is set to 15%. Both losses, then, do not depend on the scenario chosen.

Energy industry own use

The data found for EU indicated in 2014 a consumption of about 6.1% of the total final energy production (electricity and heat) for the energy sector. For the Europe of 18, the value is about 5.7%. In both case 80% of consumption is electricity and 20% heat. So, for the three scenarios, the consumption is set to 6% with same ratio between heat and electricity, independently of the scenario chosen.

Details about hydrogen production

The production of hydrogen, in the scenario rely on electrolysis process and the electricity needed is already included in the final demand; so, no need of specific efficiency calculation is needed. Different process could be achieved to produce hydrogen from green electricity as explained in the review above. Here the production ratio (mix) between the different processes could be changed and the energy needed per technology are showed in a table (see figure 1.5). These values do not impact the primary demand since the electricity needed was already taken into account in the scenario, but it permits to give an idea of how it is possible to produce hydrogen differently and at which energetic cost, depending on the evolution of the efficiency set. The detailed results are showed in a table, see figure 1.5. The computation for hydrogen production is separated from the main computation and can be launched independently. The result per source are written in the main table (see figure 1.2) at the row 22.

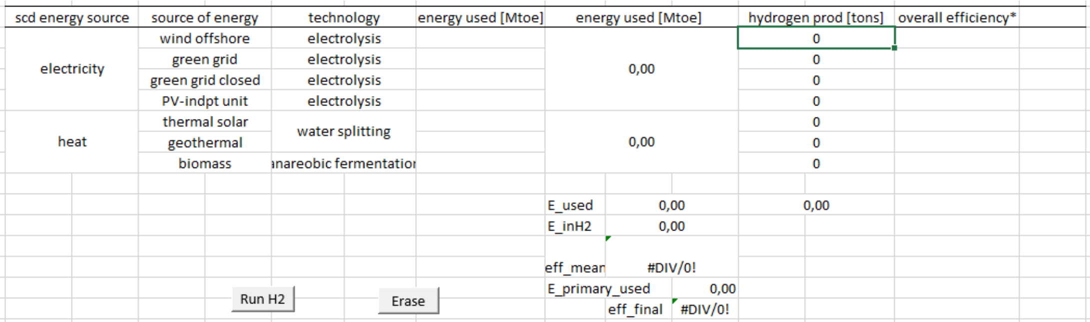

scd energy source	source of energy	technology	energy used [Mtoe]	energy used [Mtoe]	hydrogen prod [tons]	overall efficiency*
electricity	wind offshore	electrolysis		0,00	0	
	green grid	electrolysis			0	
	green grid closed	electrolysis			0	
	PV-indpt unit	electrolysis			0	
heat	thermal solar	water splitting		0,00	0	
	geothermal				0	
	biomass	anareobic fermentatio			0	

E_used 0,00 — 0,00
E_inH2 0,00
eff_mean #DIV/0!
E_primary_used 0,00
eff_final #DIV/0!
Run H2 — Erase

Figure 1.5: Summary of the hydrogen production. The mix is chosen by the user.

Refineries: from crude oil to oil products

This paragraph studies the energy consumption of the refineries sector. In overall, US refineries have an average efficiency of 87.8% and produce 46.7% of gasoline, 20% of diesel and 33.3% of other products [1]. Moreover, this article gives the energy used to produce each of these elements from 1kg of crude oil in these proportions (see table 1.1). From the bottom-up process

products energy use	electricity [kJ]	heat [kJ]
gasoline	53.9	183.3
diesel	9.3	39.4
others	38.8	426.5

Table 1.1: Use of final energy in refineries from 1 kg of crude oil (from [1]).

we have to find the quantity of crude oil (x in the following) and the energy consumed (y) for the oil products quantity (z). The transformation process leads to x equals z (more or less). From the table: $y = x * [\sum elec_{per-product} + \sum heat_{per-product}]$ so, we can find the energy consumed. The consumption in heat represents a big part of the heat consumed by the energy sector at the opposite of the electricity.

1.1.5 Application to IEA 2013 data

The purpose of this section is to validate the efficiencies attributed for the current values. The method consists in a comparison with the data of IEA 2013 for the OECD Europe region and the results of the model with the input 2013 demand from IEA for the same region. The TFC is clearly defined from the data of IEA (see figure 1.6) and is set as input (see the TFC part in figure 1.9). The repartition of the production per technology isn't well defined in the data and, so, the mix is inspired from Greenpeace data of 2012, which itself comes from IEA data, see figure 1.8. Now that both inputs are defined, the model can be launch and the results are show in the table, see figure 1.9.

	1990	2013	2020	2025	2030	2035	2040	2013
TFC	1 130	1 231	1 220	1 203	1 182	1 163	1 144	100
Coal	124	49	48	45	42	39	36	4
Oil	524	504	465	428	393	361	332	41
Gas	201	277	269	267	264	261	254	22
Electricity	193	266	277	286	293	300	306	22
Heat	40	47	49	51	52	53	55	4
Bioenergy	46	82	101	111	120	128	136	7
Other renewables	1	6	10	14	17	21	25	0

Figure 1.6: Total Final Consumption from IEA data.

	1990	2013	2020	2025	2030	2035	2040	2013
TPED	1 631	1 760	1 711	1 658	1 620	1 586	1 554	100
Coal	452	314	278	236	192	156	134	18
Oil	616	559	508	463	422	385	354	32
Gas	260	421	408	430	432	436	434	24
Nuclear	205	229	224	198	205	208	202	13
Hydro	38	50	52	54	56	57	58	3
Bioenergy	54	141	166	182	196	208	219	8
Other renewables	6	46	74	95	117	136	154	3

Figure 1.7: Total Primary Energy Supply from IEA data.

OECD EUROPE 2015	coal	oil	oil prdt	gas	uranium	Sun	wind	hydro	geotherm	biomass	waste	hydrogen	Electricity	Heat	
Electricity plants	57,08		4,00	33,81					0,82	4,29	0		37,34		100%
CHP plants	34,78		4,90	43,88					0,44	15,20	0,80	0,00	19,00	8,25	100%
Heat plants and direct heating	38,86		27,51	21,60					0,04	12,00	0			91,25	100%
Oill refineries															
Nuclear plants					100								24,00		100%
PV						100							1,90		100%
Solar thermal						100							0,00	0,50	100%
Wind turbines off-shore							100						1,92		100%
Wind turbines on-shore							100						3,84		100%
Hydroeletric damps								100					12,00		100%
Tidal								100					0,00		100%
Hydrogen															
Energy Industry own use													4,8	1,2	
Losses													7	15	
												TFC+losses:	100%	100%	
	15% heat perdu en transmission				7-15% elec supply losses										

Figure 1.8: Mix used to define the energy repartition per technology in 2013 for OECD Europe region.

The figure 1.7, looking at the data for 2013, allows to compare the TPES from IEA data and the one of the model (see figure 1.9). The first thing to compare is the global TPES. The one from IEA is 1760 Mtoe and the one from the model is about 1753. These values are close, which demonstrates that the mix and the efficiencies defined are similar from the reality, since the data used here come from real value and not from a prospective scenario.

The primary energy supply for hydro is at 47 Mtoe for the model and 50 Mtoe for IEA. This result suggests a lower efficiency than the one defined before. In final, the efficiency doesn't play an important role on such small values and the difference should come from the mix definition.

The RES information given in IEA data are the sum of all RES sources which is 46 Mtoe. By definiton of our model, the RES primary demand is set to zero, and 6 in the IEA data. If we add

Supply and consumption [MTOE]	coal	crude oil	Oil product	Natural gas	Uranium	Sun	Wind	Hydro	Geothermal	Biomass	Waste	Hydrogen	Electricity	Heat	Total
TPES	336,04	542,45		410,20	246,78	7,00	20,39	46,95	13,14	130,08	0,79				1753,82
Electricity plants	207,78		14,29	81,07					10,12	13,82	0		135,75		
CHP plants	60,44		4,85	42,69					2,98	16,47	0,79	0,00	67,27	4,51	
Heat plants and direct heating	18,82		13,89	9,45					0,04	13,29	0		-6,37725	49,84	
Oill refineries		542,45											-1,32	-8,41	
Nuclear plants					246,78								81,44		
PV						6,73							6,73		
Solar thermal CSP						0,273161							0,00	0,27	
Wind turbines off-shore							6,80						6,80		
Wind turbines on-shore							13,60						13,60		
Hydroeletric damps								46,95					42,49		
Tidal								0,00					0,00		
Hydrogen production				0,00		0,00	0,00	0,00	0,00	0,00	0,00				
Energy Industry own use		9,74											-14,93	-0,56	
Losses													-21,77	-7,05	
	49	0	504	277						80	0	0	311	47	
Industry	30		28	91						22		0,00	98	15	
Transport	0		303	0						13		0,00	6	0	
Other	16		123	170						45		0,00	207	32	
Non enregy use	3		50	16											

Figure 1.9: Results obtained for the IEA 2013 demand and the mix defined in the previous figure.

this value to the ones of Sun, Wind and Geothermal we obtain 46.53 Mtoe, which is really near the IEA value of 46. For the Sun and Wind source it allows to justify the accuracy of the mix since the efficiency is 100% for these sources. For the geothermal values, it permits to justify the accuracy of the efficiencies chosen.

For the nuclear source (uranium), the result of the model is higher than the one of IEA (247 vs 229, Mtoe), sugaring to raise the efficiency which was set to 34%. After different input, the value of 36% was defined to match the IEA value.

For the natural gas source, the small gap, in percentage, between both TPES couldn't be filled with efficiencies variation: the electricity plants at 56% is a quite sure value, the heat plant has a to small utilization to impact the value by changing the efficiency and the CHP was changed but does not impact a lot (-2% gave +2Mtoe). So, the efficiency will stay as before since only a change in the mix could fill the gap. This difference is also true for the coal: a change in the efficiency couldn't fill the gap. The difference in the mix seems to be shared between coal, gas and crude oil which doesn't permit to draw conclusion about efficiencies. A more precise data set, with the production per technology type and not only the source, would have allow us to go further.

1.2 Perspective for the efficiency evolution & comparison with Greenpeace scenarios

1.2.1 Details about the scenarios and data utilization

In this second part, the model is used with scenarios of Greenpeace. The goal is to evaluate the efficiencies applied in these scenarios and discuss the differences from the ones set in the model. First, the particularities of a scenario are covered and then the three scenarios are described. In the following, the way of extracting the information given by the scenarios, and use them to build a continuous demand curve, is explained. Now that the inputs definition is done, the program is launched and for each scenarios, we discussed the difference with the efficiencies. In the end, the program is used with the three scenarios and a difference is done for a compilation with a non-improvement (flat curve) and a full improvement (physical limit reached in 2050) for all technologies. The interest to achieve high efficiency for a certain technology is then discussed, depending on the scenarios.

Discussion about the scenarios

According to a study from the International Journal of Green Energy, analyzing a holistic method to design an optimized energy scenario [2], it exists three types of scenarios: the extrapolation of the past, the normative scenario and the exploratory scenario. The normative scenario is based "on a set of features that the world should possess"[2]. The exploratory one, has the goal of giving perspectives and explore a future possible configuration for the region studied. According to the authors, most of the sustainable scenarios are based on exploratory scenarios. From an abstraction process, they described six main features that a sustainable energy scenario should own: consideration of environmental impact, utilization of renewable energy sources, minimization and optimization of energy conversion, utilization of the optimal energy source for each application, choice of power plant types according to locally available energy sources and planning planning of integral energy systems. From there to design the system constituting the scenario, the authors focus on two main points: choosing future energy sources and future conversion technologies in accordance with the six key features presented. In the application here described, three scenarios of Greenpeace for OECD Europe region were implemented. They are summarized here below with the critera described before (see [3] for more details about the scenarios).

For these three scenarios, the population development is based on the United Nations Development Program (UNDP), which is the basis of IEA studies too, and is expected to reach 604 million of people in OECD Europe region from 2050. The GDP mean growth used in this region from 2015 to 2050 is +1.5%.

GP:current policies

This scenario is completely based on the IEA WEO 2014 scenario until 2040 and then extrapolate to 2050. As an extrapolation of the past, it assumes that no new policies will be apply except in electricity and gas market where reforms would progress. Policies to combat carbon emissions up to 2014 are taken into account as well as policies about the liberalization of energy trades through borders.

The demand of both electricity and heat is increasing as no strong policies are applied. The future energy sources are based on the current ones and a continuing slow increase of the renewable sources. The future conversion technologies are still based on fossil sources and complemented by some renewable technologies.

GP:Energy [R]evolution

The goal of this scenario is to propose a path to reach an annual emission of Co_2 below 4 Gt per year accounting for 2050 and, so, to achieve staying below a global warming of 2°C while phasing out of the nuclear production.

The global demand is decreasing, due to new policies for the transport, industry and private sector. The future energy sources are the current ones with a global confidence in renewables ones, helped by a decreasing cost of investment. There is also the apparition of the hydrogen as energy vector. The future conversion technologies pillars are the PV and CSP technologies.

The fluctuation is managed to maintain a secure capacity. A quite strong improvement of efficiency in RES as well as a large deployment is taken into account. No biomass trades (importation - exportation) are taken into account and an evolution of the grid is assumed. The electricity demand increase due to the heat generation by heat pumps and electrification of the transportation sector. In this latter sector, a change in mobility pattern is assumed as well as anti-fossil policies.

GP:Advanced Energy [R]evolution

The goal of this scenario is to propose a path to reach a 100% renewable energy supply continuing reforming the electricity and gas market. The way to achieve this goal is the same as in the previous scenario except that the massive use of new technologies and especially in the transport sector, leads to a total decarbonization of the power, heat and transportation sector. Electricity play a major role in all sector (heating, transportation, hydrogen production) and, assuming only produced by renewable sources, become the main energy vector.

Use of the data to recover the annual production

From the baseline of the scenario (e.g. leaving nuclear in 2030) and these data at some years, it is possible to fit functions to estimate the repartition of the production between all technologies. The model uses polynomes to approximate the evolution of the repartition, as it can be seen on figure 1.10.

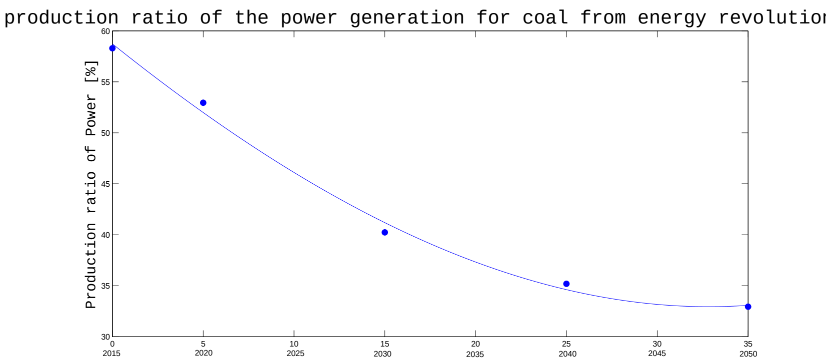

Figure 1.10: Evolution of the share of the power production by coal for the energy revolution scenario of Greenpeace. The dots are the real data given by the scenario, the curve is the polynome approximating the production ratio evolution.

In the electricity category, the focus is done on renewable energy, in a sense that the ratio of electricity plants production (mainly fossil in 2015) is the rest of the total production minus all other productions (mainly green). So that the ratio of the production in green is well established and the electricity plants production is there to complete the gap between the demand and production of the renewable.

In the CHP, electricity plants and heat plants categories, the repartition between the sources used has always one source which is used to fill up the gap between the demand and the production. For example, for scenarios achieving an energetic transition, the natural gas is used as a buffer, adapter, to fulfill the demand, given the production of the other sources. It can easily be seen in the trends of such scenarios (example of Greenpeace energy revolution detailed further; see Appendices figure C.2) that the gas is used to allow a transition from fossil to renewable while always matching the production and demand.

1.2.2 Methodology to assess the efficiency evolution considered in the GP scenarios

The idea is to have an approximation of the efficiency used to build the scenario of GP. In the data of the scenarios, the final primary energy demand is given by source and not by technology. But, by changing the efficiency of the technologies used, running the program, it is possible to find more or less a value to approximate the efficiency used in the scenario. It is important to notice that for ocean, sun and wind energy an efficiency of 100% is used by convention.
In summary, the three-step process is followed:

- Compute the primary energy per technology
- Add primary energy used to achieve a total for each source
- Comparison to the total primary energy demand by source from Greenpeace scenarios

A plot of the evolution of the primary energy demand was done (see Appendices C.1, C.2, C.3) for each scenario with the value of efficiencies found here below. The results for the three scenarios are explained in the following. All values defined as efficiency for the different technologies and depending on the scenarios are fully showed in the Appendices (see D.1,D.2, D.3 and D.4).

Results for the current policies

It is quite difficult to found the efficiencies used to build this scenario. The difference occurring by changing the values of the efficiencies for the source like sun CSP, hydro, biomass and geothermal is not really visible since these sources are no enough used. In the opposite, the coal, oil and gas are highly used but the efficiency doesn't seem to evolve. It is quite difficult to pretend something sure since the final energy demand by industries, transport and others sectors is really high for these sources, meaning no conversion efficiency studied here is used to transform these quantities. See the plot of the evolution of the primary energy supply in the appendices, figure C.1.

Results for the energy revolution

The wind suited well (logical since the efficiency is always 100%) , hydraulic and uranium (38 to 39% improvement) too and crude oil [1] also. But the demand for "Sun" is only really well fitted when the efficiency of CSP technology in 2050 is estimated really closed to the Carnot physical limit but with high temperature (900°C), meaning that new materials for turbines would be used to resist to the high working temperature. CSP is used as a pillar for the scenario, meaning that a good improvement is plausible since the economic attractivity of the technology; but the real improvement would be more in the light-energy absorption part than in the thermal. The

[1] with oil products equals 99% in mass of crude oil at the end of the transformation process

assumption made here seems too inappropriate. See the plot of the evolution of the primary energy supply in the appendices, figure C.2.

Geothermal

Geothermal	Electricity plants	CHP heat	CHP elec	Direct heating plants
η_{2015} [%]	12	50	6	45
η_{2050} [%]	16	53	**11**	51

Table 1.2: Values used for the efficiency of geothermal technologies, energy revolution scenario.

The first value for the CHP_{elec} efficiency was first assigned to 9%. It seems that a more optimistic value is ecessarily to achieve to a closer geothermal primary consumption. It could be due to the fact that the discussion higher for geothermal is more centered on EU but the Turkey, here in the scenario, has a great potential and could up the average, since the site itself (not only the technology advancement) has a capital impact on the geothermal efficiency. The CHP efficiency was chosen to receive the impact since it is the main contributor for the conversion of geothermal sources in the scenario.

Biomass

It is more challenging to find a good approximation of the efficiency used since the part of waste, which has a much lower efficiency conversion, is not mentioned in the data. To achieved a primary energy demand similar to the ones in the scenario, the portion of waste in total biomass grew from 5% in 2015 to 30% and then falling to 20 in 2050 and these values of efficiency where used:

Biomass	Electricity plants	CHP heat	CHP elec	Direct heating	CHP heat wastes	CHP elec wastes
η_{2015} [%]	42	36	34	40	30	22
η_{2050} [%]	45	45	45	**57**	40	28

Table 1.3: Values used for the efficiency of biomass technologies, energy revolution scenario.

The no increase of electrcity plants efficiency is due to the fact that coal is phasing out the scenario (no co-firing possible) but the others technologies efficiency grow as discussed before. The most challenging point is the improvement of direct heating, which will cover the direct housing heat demand that heat pump and district heating are not covering.

Natural Gas

The results fitted quite well but since are a bit too low and then too high, if amelioration is made the lower part will be lower and compensate the gain at the end. It means that the current efficiencies of the technologies used should be lower and the final one higher. The efficiency of electricity plants is near the Carnot efficiency (56 to 59%). So, we cannot really play on this parameter, the direct heating efficiency is equivalent to boilers one which is already quite high (92%) and will not improve a lot, means than we have to lower the current efficiencies of CHP plants but it doesn't seem clever since the value are realistic. Then we can impute the approximation to the lack of data.

Results for the advanced energy [r]evolution

Firstly, the scenario was launched with the same efficiency values for each technology than for the energy revolution one. The results showed a perfect match with the coal, oil and natural gas sources. The efficiency for the technology using these sources is set to (almost) not evolve due the abandonment of these technologies. It is quite great that the value of the efficiency of the technologies using natural gas permits to fits the curve, it showed that the values used in the previous scenario that could not be verified were pertinent. The other efficiencies are exactly the same also (the same big improvement for the CSP, nuclear and hydro constant), only the geothermal (see table 1.4) values need to be adapted. See the plot of the evolution of the primary energy supply in the appendices, figure C.3.

Geothermal	Electricity plants	CHP heat	CHP elec	Direct heating plants
η_{2015} [%]	12	50	6	45
η_{2050} [%]	17	53	13	51

Table 1.4: Values used for the efficiency of geothermal technologies, advanced energy revolution scenario.

In conclusion, all these scenarios considered an improvement of the technologies, meaning a better efficiency of conversion from primary to final energy. The one accorded to CSP technologies seemed a bit optimistic, from a thermal point of view. In the following, we will highlight these possible improvements in a way to characterized the possibility of CSP as a pillar of the energy transition.

1.2.3 The interest of achieving a high conversion efficiency

The idea is to find the differences of primary energy used between a first computation with no evolution in the efficiency and a second one where all technologies reach their physical limit. Now, real efficiencies for renewable sources are introduced. It means that the current efficiency and the physical limit, for example, for PV, take into account the fact that all energy in the light captured is not converted in electricity. For the PV, the efficiency used is 15% with a physical limit up to 50% (for a global light, three layers, see section 3.2.2.2). The wind power is limited by the Letz limit, and the current efficiency is about 38%.

For the current scenario, in terms of cumulative primary energy saving, the technologies using oil products source has the more potential of saving. In this scenario CHP technologies are not so well developed and, so, the gain (about 5000 Mtoe each) is made with electricity plants and direct heating using both oil products. To reach it, the main parameters are that the electricity plants using coal reach Carnot efficiency and that boiler reach a 100% efficiency. The big gain in primary energy saving due to electricity plants is due to the high difference between the current efficiency and physical limit; the big gain about direct heating using oil products is not due to this difference but his high utilization. The total CO_2 emission (by technologies using oil products) saving is about 36000 Mt, the triple than the one due to improvement in coal and ten times the one for natural gas. In second amount of primary energy saving the biomass is before coal (4400 > 3330 Mtoe) and the Sun technologies are following, despite their pore use, before the nuclear.

For the energy revolution scenario, in terms of cumulative primary energy saving, the technologies using sun source has the more potential of saving. The PV accounting for 6400

Mtoe and the CSP for 2300 Mtoe. Biomass is following with almost 4000 Mtoe of savings with geothermal and oil products following. For the advanced energy revolution scenario, in terms of cumulative primary energy saving, the technologies using sun source has again the more potential of saving, far away of any others source. The solar has a high potential rate of improvement, and could be install more and more, making it an interesting source to invest in, to impact the primary energy demand.

The improvement in hydro technologies does not impact the primary demand for any scenario (about 155 Mtoe for each) because of utilization small and constant and improvement stuck. It is the same for the tidal efficiency because the utilization is small. In fact, improvement in efficiency for technologies using biomass impact all scenarios. Biomass seems a great source of improvement, it doesn't depends too much about the localization, in the contrary of solar and wind technologies and offers a quite good potential of improvement.
In conclusion, for an energy transition scenario, the potential gain of primary energy by a great evolution of the CSP and PV is high.

1.3 The place of CSP in the energy transition

Solar technology seems to be the most promissing technology as the perspective improvement combined with a large utilization in the future energy mix seems to lead, as seen before, to a large primary energy saving.

CSP technology has a good place as a serious candidate to supply renewable electricity in the future energy mix, according to energy transition scenarios of Greenpeace. Indeed, its potential of improvement seems interesting, even if the technology evolution seems a bit high in the advanced energy revolution scenario. A deeper analysis of its real potential will be performed through this work.

Greenpeace Scenarios:	Current	Energy revolution	Advanced energy revolution
Production needed [TWh]	828	1592	2351
From GP			
Installation [GW]	310	570	831
From Dupont et al. [4] :			
Mean capacity factor*efficiency land [%]	24	19.3	17.7
Installation [GW]	350	764	1228

Table 1.5: Table showing differences from an accurate study about wind installation (Dupont et al. [4]) and a mean factor for the OECD Europe region, from Greenpeace [3].

To rely on a technology, we should also take care to the land availability and the evolution of the quality of the renewable source on these lands. Indeed, for example, the study for wind turbines from Dupont et al. [4], shows a high difference for OECD Europe installation between previous scenarios covered and their detailed study, see table 1.5.
Moreover, the technological improvement should be also considered. Indeed, the possible grow in conversion effeciency should be analyzed and described precisely to be able to set up perspectives.

In the following chapter, a detailed review of the technology is proposed. This chapter sets up the necessary knowledge to pursue an analysis of the CSP technology. Then, thanks to these informations, we will be able to establish a model, taking into account the land quality and development of the technology.

2 Focus on CSP technologies: synthesis of properties, performances and current researches

The aim of this chapter is to clarify the properties and main components of the CSP technologies in the purpose of achieving a global comprehension of these technologies. It also clarifies the main innovations possible and analyses the performance and perspective of improvement. This chapter is necessary to set up the basis to be able to perform a life cycle assessment (see 3.2) and to implement a model of production.

2.1 Context, principle and historic overview

CSP is the only technology, with PV, to convert the energy contained in sun rays into electricity. A CSP plant is based on the same principle that all power plants: heat a fluid and transform the equilibrium difference with the ambiance into mechanical energy and then electricity. Instead of burning a fuel to heat a fluid, solar radiations are concentrated to act as the primary energy. The direct solar radiations are concentrated on a small area, called receiver, thanks to mirrors. The receiver converts the solar irradiation into heat which is transferred to a primary heat transfer fluid (HTF). From there the HTF flows directly through a turbine or a secondary power cycle. On his way, the HTF can also store heat or be heated by a thermal energy system.

In 2016, 90% of installed capacity were located in Spain (around 50 commercial plants, 2300 MWe in 2015) and USA (1600 MWe in 2014) [5]. The future of CSP seems bright as the thermal storage principle is a great benefit on the other renewable technology and the number of possible sites is high. Many other countries are implementing projects or already constructing new plants. The website of the National Renewable Energy Laboratory [6] reported 22 projects under construction and 22 others under development. The countries are varied as for example two solar power tower projects under construction in Chile (total of 370 MWe), a soon terminated solar power tower plant of 121 MWe in Israel, another power tower, also soon operational, of 200 MWe in China, a parabolic trough concentrator plant of 200 MWe in Morocco as well as a tower power of 150 MWe, another parabolic plant of 100 MWe in South Africa, a tower plant (finished recently) supplying heat, electricity and fresh water in Australia, etc. Beginning with the two pioneer countries, all the five continents are now rising the number of CSP plants.
Different technologies inside of the CSP family exist and are presented below.

2.2 Review of the existing technologies

It exists fourth types of CSP technologies. The most mature design is known as parabolic trough collectors family. The most growing installation rate and "second most mature" [7] is the solar power tower system. The cheapest design is known as the linear Fresnel reflector plants and it exists a modular system knew as parabolic dish system.
The principle of each of these technologies is covered in the following paragraphs. A specific table summarizes more detailed characteristics about these technologies and allows to discuss and compare them in the last paragraph.

2.2.1 Parabolic Trough Collector (PTC)

A Parabolic Trough Collector (PTC) system, is composed of curved mirrors linked to a tubular receiver. The sunrays are concentrated on the receiver located at the focal line of the parabolic mirrors. A thermal fluid, flowing into the tube and extracting the heat of the receiver (composing the circumference of the tube), is used as primary fluid or will directly expends in a turbine as working fluid. This technology is widely installed and accounts for several projects of large scale (for example the 250 MW Genesis Solar Project in California [8], operating since 2014).

Figure 2.1: Representation of a parabolic trough collector, from http://www.seia.org/policy/solar-technology/concentrating-solar-power.

2.2.2 Solar Power Tower (SPT)

In a Solar Power Tower (SPT), there is only one receiver point for all mirrors. The mirrors are slightly curved and track the sun. An entire field is covered of these heliostat collectors, reflecting the sunrays on the single receiver, located on the top of the central tower. The receiver converts the rays in heat and a heat transfer fluid (HTF) is used to transfer the heat to the secondary power cycle unless direct generation occurs. Since all mirrors concentrate sun radiations at the same point, the working temperature is high and allows to reach high level of efficiency value in the thermal cycle. A lot of technical concepts are possible (several towers for one generation block, secondary cycle or not, different kind of heat thermal storages, different heliostat field configurations, etc.) which makes this technology quite flexible. The world biggest installation is located in California, a three towers-power generation systems, which has, since 2014, an installed, net turbine capacity of 377 MW [9].

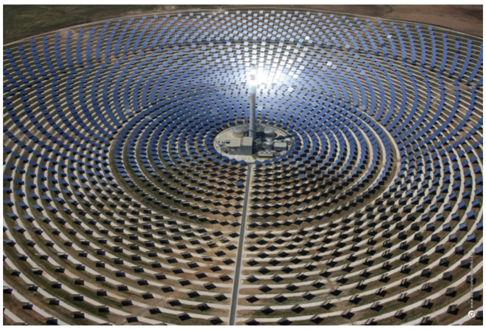

Figure 2.2: Gemasolar CSP tower plant in Sevilla Spain, from http://www.torresolenergy.com/TORRESOL/gemasolar-plant/en.

2.2.3 Linear Fresnel Reflector (LFR)

Linear Frenel Reflectors (LFR) are constituted of a linear fixed receiver. The mirrors, reflecting the sun rays, are flat and arranged in long rows. The design is simple as well as the direct steam generation process. The steam flowing in the receiver is directly sent to the turbine. Sometimes the steam is directly used in industrial applications. The first Fresnel plant was installed in 2009 in Germany (1.4 MW) followed later by another one in Spain (30 MW) [7].

Figure 2.3: Typical linear Fresnel reflector installation, from http://www.areva.com/EN/solar-220/areva-solar.html.

2.2.4 Parabolic Dish Systems (PDS)

For the Parabolic Dish Systems (PDS), the sunrays are concentrated on a central point above the dish, containing the receiver and the engine. Both are moving in tandem, as the system tracks the sun during the day. The sunrays are directly converted into electricity in the engine after passing through the receiver and being converted into heat. The system does not need cooling water and neither a heat transfer fluid. This leads to the highest sun-to-electricity efficiency but also the highest cost and smallest production capacity. The modules are independent and produce about 10 kWh or less. The first installation was performed in Arizona in 2010 with an installed capacity of 1.5 MW [7].

Figure 2.4: A parabolic dish system installation, from http://www.areva.com/EN/solar-220/areva-solar.html.

2.2.5 Comparison of the CSP Technologies

The table 2.1, presents detailed characteristics from different sources and allows to compare the different technologies presented. In the following paragraphs, other facts presented allow to have, in addition to the table 2.1, an idea of the more advantageous one.

The advantage of the PTC is its long term proven reliability [10]. The main advantage of the SPT is the high efficiency achieved and the promising evolution in perspective (see table 2.1). The LFR main advantages are its simple configuration and low cost. For the PDS, the main advantage is the modular units composing it, which allow to change the configuration and even move the plant. To produce big amount of energy the PTC and SPT design distinguish themselves from the two others. The LFR has a too low operational temperature and so its efficiency and the PDS does not allow thermal storage (which is the greatest advantage of CSP on PV, even with the highest current efficiency of the CSP technologies) and is particularly expensive. We could also have mentioned the existence of a fifth technology, the concentrated solar thermo-electric, which is composed of thermal collectors and thermoelectric generators. A thermal resistance creates a temperature gradient (depending on the heat flux) between the fluid and the absorber plate. This technology is stuck because of the high price of the thermoelectric material [7].

The PTC is ranked number one in the CSP installed capacity but the SPT technology, always second, is rising. In 2011, 96% of all installed capacity was PTC technology [7] and 3% SPT. In 2016, the PTC declined to 82% and the SPT was raised to 13% [10] and for the projects in development, SPT technology has reached 71.43% and PTC only 28.57% [11]. The improvement perspective of the PTC technology is weak in comparison with the SPT (see table 2.1). Moreover, the SPT technology is quite flexible in its configuration and the limited working temperature of the PTC technology encourages companies to install and invest in SPT projects, which has a greater potential of cost reduction [12]. The complex design of SPT and the scale-up difficulties have led to a delay in comparison with PTC systems [13]. Moreover, most of CSP plants are located in arid or desert place since the direct radiation level need to be great. Supplying water has a real economic and environmental cost and the SPT high working temperature allow to use dry cooling without impacting seriously the efficiency of the thermal cycle. Thanks to a central receiver, the quantity of heat transfer fluid (HTF) is reduced in comparison with PTC, which needs the fluid to flow in all the field [5]. These HTF are constituted of molten salt in most of the case, for heat thermal storage reasons, and their economic and environmental impact are important. Reduce the quantity of HTF is then essential, and overall in a large scale deployment of CSP technology. The SPT technology allows more energy to be stored per mass of HTF (molten salts) since the temperature range at the thermal energy storage (TES) system is higher [14]. SPT plant, with a TES of 15 hours is already technically feasible and some plants work as baseload electricity power source[1]. The levelized cost of electricity (LCOE) has fallen of 42% between a PTC plant, with any thermal storage capacity, to a current-generation power tower, with 10 hours of storage capacity, in USA [14].

Nowadays, the number of SPT plants and researches is rising and a shift between these both technologies (PTC to SPT) applications is occurring. Since this article is turned towards the future potential of CSP, the focus will be done on the most promising technology, which is considered as the SPT one.

[1] But with a gas turbine back-up system.

	PTC	**SPT**	**LFR**	**PDS**
Solar collector [12]	line focus	point focus	line focus	point focus
Solar receiver [12]	mobile	fixed	fixed	mobile
Power conversion cycle [10] [12]	steam or organic Rankine, CC	Steam Rankine, gas Brayton, CC	steam or organic Rankine	Stirling engine, Steam Rankine, gas Brayton, CC
Operating receiver temperature range [$°C$] [10] [7]	150-400	300-1500	150-400	300-1500
Relative cost [7] [10]	low	high	**very low**	very high
Relative land occupancy [7]	large	medium	medium	small
Cooling water [L/MWh] [12] [7]	3000 or dry	1500 or dry	3000 or dry	none
State of the art annual $\eta_{\text{sun-to-elec}}$ [15] [10]	15-16	16-17	8-12	20-25
Concentration ratio [7] [12] [10]	50-90	600-1500	35-175	1000-3000
Typical capacity [MW] [12]	10-300	10-300	10-200	**0.01-0.025**
Typical capacity factor without storage and back-up[%] [7] [12]	25-28	24	22-24	25-28
Typical capacity factor with storage and back-up[%] [7] [12]	29-43 (with 7h storage)	up to 75	/	/
Development status [12] [10]	**commercial proven**	commercial	pilot project	demonstration stage
Improvements [7] [12]	limited	**very significant**	significant	if mass production
Relative rise of efficiency after improvement [%] [15]	20	**40-65**	25	25

Table 2.1: Comparison of the four families composing the CSP technology panel. For each CSP technology, the main characteristic which distinguishes it the most from the others is written in bold text.

2.3 Subsystems and components

In this section, the focus is done on the central tower receiver technology. Each part composing the process is covered as well as the future possible improvements.

First the mirror field layout, tracking the sun (heliostat field, see figure 2.5), is covered. Then the different systems use to receipt the concentrated rays, the receiver types, located in the central tower, are described. From there, the fluid heated in the receiver, the heat transfer fluid and its characteristics are explained, as well as different types of thermal storage systems. In the end, some possible configurations for the power generation system are covered.

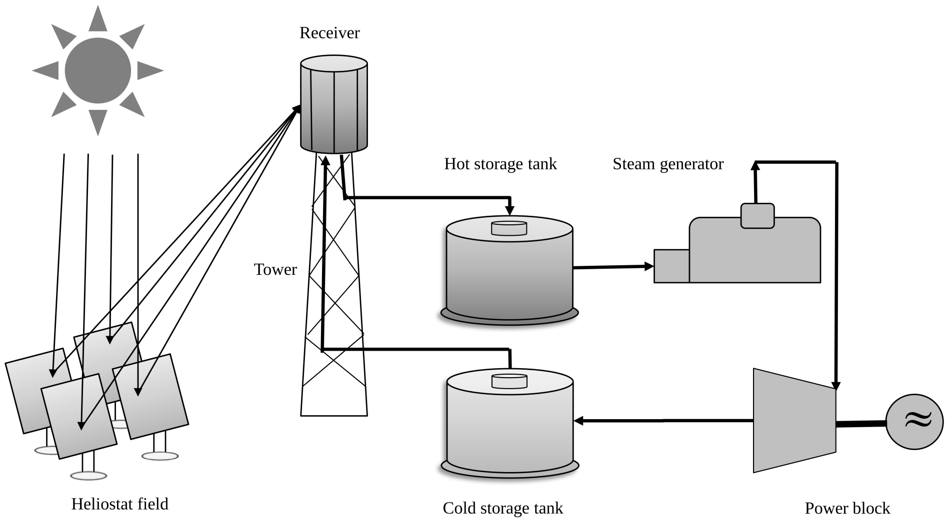

Figure 2.5: General scheme representing the principle of a CSP tower plant, from li et al. [16].

2.3.1 Heliostat field

The moving mirrors are called heliostats since they are tracking the sun. Each heliostat is composed of mirrors linked to a frame. They are moving thanks to a control system, which is guided by a tracking system and the all thing is fixed by a structure foundation. The purpose of this heliostat field is to reflect the direct irradiations from sun to the central receiver tower. The critical parameters are the heliostats disposition and the tracking and control system. The heliostat system has a real importance since half of the investment is granted to it [12] and account of about 47% of annual energy losses [17].
A summary of currents uses and researches about layout and tracking system is proposed below.

Layout

The optical efficiency is constrained by the cosine effect, the shadowing effect, the receiver spillage and the blocking effect [12]. As well the atmospheric attenuation and the mirror reflectivity should be considered [17]. Since the mirrors reflect the sunrays on the receiver, the normal of the mirror surface exactly forms the bisector of the angle between the sun and the tower. Then, the mirrors surface is not normal to the sunrays and the solar irradiance falling on it is not maximum. The solar irradiance would be reduced by the cosine of the angle between the surface normal and a central ray of the sun, which constitutes the losses by cosine effect [18]. Spillage losses is due to the portion of reflected radiation which could not reach the receiver because of the tracking accuracy or the quality of the mirror itself [17]. We can imagine than the more the mirror is far from the receiver, the more its quality should be controlled and that it is better to place the mirrors near the tower. The blocking effect means that the radiation reflected by the heliostat are stuck by the back side of a neighbor heliostat. The shading effect is due to the unused part of the surface which could not be hit by the sunrays since a neighbor heliostat is shading it. Depending on the visibility and the distance to the receiver, the reflected irradiations are affected by the atmospheric attenuation [17].

Depending on the configuration of the heliostat field, each of these losses takes important role or not and the purpose is to find the optimal layout of heliostat field leading to the optimal optical efficiency. A lot of field designs are possible as the cell wise procedure, the radial cornfield or staggered arrangement, the North-South cornfield or staggered arrangement and the idea of spiral arrangement which could reduce the land area and increase the optical efficiency [12]. The optimal design could also vary according to the location, from example depending on the sunshine duration. A lot of studies are still researching an optimal algorithm to configured a heliostat field. Eddhibi et al. [17] proposed a new mathematical model to optimize the optical efficiency and showed that the development of the new method, defining new referential to compute the blocking and shadowing losses, can improve the current ones. Collado et al. [13] proposed a new code to allow accurate and fast computation of shadowing and blocking effect for each heliostat constituting a field composed of thousand of them. The code can perform an optimization task, processing while the layout is changing. They linked the tower height to the field efficiency but remind that the geometry of the receiver itself is an important parameter that should considered. The authors complained about the lack of accurate data to be able to establish procedures to link the annual energy required with the number of heliostats, height tower and receiver dimensions, in order to optimize the layout. We should also mention the design of the mirror itself which could be squared or circular. The shape of the heliostat play an important role in the shading and blocking effect. Leonardi et al. [19] proposed a code allowing to compute the optical efficiency with squared and circular shapes of the mirrors, and, in a way to optimize the efficiency, proposed to mix both.

Tracking the sun

The right positioning of the heliostat, which means that the normal to its surface is the bisector of the angle between the sun and receiver (minimizing the cosine effect), is assured by a tracking and control system. As explained in the review about central receiver of Behar et al. [12], it exists two ways to track the sun: the open and closed loop system. The open loop system consists of a general computer control system based on astronomic formulae. According to this article, the cost is low. The sun position is computed by a geometrical system. The open loop one is a direct method: the sun is spotted thanks to sensors. This method is more accurate that open loop, except if the weather is cloudy, and is more applied to small field [12]. The control process could be achieved by two ways: using a rotation around the spinning axis or an elevation one [2]. The spinning axis allows to rotate the mirrors around an axis passing through the center of the mirrors surface and perpendicular to it (but then, this method does not have any sense for a circular shape of the mirror). The elevation rotation is turning around an axis passing through the center of the lateral edges of the mirrors surface. Chen et al [20], by a comparison between circular heliostats with elevation control and rectangular ones with spinning control achieved to a reducing spillage losses of about 10 to 30%. From this study, the spinning system provide better uniform rays on the receiver and the variation during the day would be reduced in comparison with the elevation system. Moreover, according to Chong and Tan [21] the energy consumption on the total year for a spinning system is lower than for an elevation one.

As we saw before, the study of Leonardi et al. [19], proposed a mix of both shape and so, the rectangular heliostats should be control by a spinning system and the circular ones by

[2] ...in addition to a rotation around the azimuthal one.

the elevation method. This example show the complexity of designing a heliostat field. The common point about the design of a heliostat field is that the closer of the tower the greater the density and the smaller the dimensions of the heliostats. But the number, the shape and the dimensions of the heliostats as well as the high of the tower, the layout (circle, spiral,...), the type of control and tracking systems is currently discussed and a lot of studies are on their way to optimize the optical efficiency.

2.3.2 Receiver

The receiver is the most critical component of the SPT plants. All the concentrated, per thousand of mirrors, sun radiations are concentrated on the receiver which converts them into heat. The review about central receivers CSP plants [12] computed that, on the 274 articles reviewed, 45% of the articles covered the receiver subject, only 16% the heliostats layout and 9% about tracking and control, explained in the previous subsection. It exists currently three families of receiver for SPT plants: volumetric receiver, cavity receiver and particles receiver. The review about central receivers [12] computed that, on the 274 articles reviewed, 26% covered the cavity receiver type, 14% the volumetric receiver family and 5% the particles receiver systems. A brief review of these families and about absorber materials is proposed below.

Volumetric receiver

The volumetric receiver is composed of a porous structure which absorbs the concentrated rays. The porous surface allows to increase the heat transfer surface area and the gas theoretically reach the temperature of the material. By acting as a convective heat exchanger with a gas passing through it, it converts the radiations in heat [10]. Then the hot gas is directly used in a gas turbine or will heat another fluid from the secondary circuit. In general, the gas is air and the porous material is made of ceramic [12], to resist to high temperature among others. The drawbacks are the non-uniform heating which leads to local failure in the receiver material due to high local pick of temperature [10]. According to this article of Xu et al., some researches try to design more suitable cavities for the porosity to enhance the uniformization. The cavity family could be divided in four sub groups depending on the air pressure and the material used (metal or ceramic) [22]. In this review about volumetric receivers of Avila-Marin of 2011, the characteristics of more than twenty different technologies of each families are described. The final gas temperature varies from 563 to 1200°C and have an overage about 750°C if the production is larger (real tests out of laboratory). The efficiency varies from 50 to 80% and the average is about 70%. In general, the more the output temperature of the gas, the more the emissivity losses and the lower the efficiency. Currently the air receivers have an open configuration, absorbing the air at an ambient pressure, for example the Jülich power plant, which returns the air at a temperature of 680°C [23]. According to this same source of Hoffschmidt, closed volumetric receivers are in pilot-phase. In a close volumetric receiver, the inlet air is pumped to the top of the tower, flows near a receiver window (which closed the receiver), through the porous material and leaves the receiver. The receiver is composed of a secondary concentrator, with a nozzle form which concentrate the rays on the receiver window. According to Hoffschmidt, the low thermal reradiating, the low pressure drop and the high possible outlet temperature (more than 1000°C) at an efficiency greater than 80% is achievable. Metallic tube receivers are also studied in a pilot project (Abengola Solar NT) to heat pressurized air up to 800°C with high efficiency and achieving higher outlet temperature in a already planned future project [23].

Cavity-external receiver

The cavity receiver collects the radiations in a box-like structure. The face in front of the heliostat is open and the radiations are reflected on a wall and then undergo a heat exchange on

a specific surface. It is opposed to an external receiver.
The heat receiver could be a gas or a liquid contained in pipes. In general, the efficiency is higher for liquid than gas since the heat transfer coefficient and the thermal conductivity of the liquid is higher than the one of the gas. The problem due to liquids is the corrosion, leakage and the cyclic fatigue effect due to the thermal stress [10]. As explained, a theoretical efficiency of about 90% could be achievable but the working temperature is more limited than for a gas, at about 650/700 °C. A thin film fluid, flowing on the absorber, could also be used to capture the heat from the absorber and theoretical efficiency of about 90% could be reached [10]. As well, external receivers using pipes exist and are widely used. They also reach an efficiency near 90%.

Particles absorber/receiver

Used in a cavity receiver, particles, acting as absorbers is one particular subject of research for the development of new receivers technology. A continual flow of tiny falling particles is used, in the receiver chamber (cavity receiver), to capture the heat and transfer it to the air surrounding them. The risk of damages due to high temperature is low, the solar absorption is high, and the efficiency could reach 90% percent for a 700°C output air temperature [10]. This technology is less known and only 5% of the paper reviewed by [12] are dedicated to this subject. The temperature reached could be really high (>1000°C) since the damage risk due to local pick of temperature is low [7].

Absorbers

The absorber is a part of the receiver system. He has the critical role to absorb the radiations, re-emits as less as possible of them, and convert them into heat. The heat is then transferred to a fluid or gas. The absorber type depends on the receiver design chosen. The absorber materials could be metals for temperature between 800 and 1000°C and ceramics to achieve temperature up to 1500°C [22]. The radiation losses increase dramatically with the temperature since the emissivity is proportional to the temperature exposed to four (Stefan-Boltzmann law), and so, low emittance material are necessary to reach high peak of temperature, allowing a better thermal-electric yield. From the article of XU et al. previously cited [10], selective materials could reach high temperature with an high efficiency (>90%). But such material should also be low cost and have a long-life cycle. A study of Burlafinger et al. [24] analyzed the possible gain by using absorbers with selective absorption properties with an optimal working temperature. By using a nonrealistic material with a perfect cut-off property (0 or 1 in absorption), meaning zero width transition, and a high absorption value, they show a possible overall efficiency of 73% for the all plant at a concentration ratio of 2000 and 65% for a more realistic absorber. As explained before, the authors remind that this material should also be reliable and owns good thermal stability for its all life and so the research has still a lot of work before achieving such a material.

XU et al. previously cited [10] proposed a summary of the different materials used to achieve low emittances but high absorption.
Intrinsic selective materials as transition metal and semiconductors has an optic absorption dependent on the wavelength and so could be used as cut-off materials. The wavelength range is dependent on the plasmon frequency for the transition metal and dependent on the bandgap for the semiconductors.
Semiconductor-metal tandem could be used as a photothermal wavelength selective material too. The selection of photons according to the wavelength is done by the semiconductor (Si, germanium or lead sulfide) depending on its bandgap and reflected by the metal if the photon has a too low energy and is not absorbed by the semiconductor. The emittance factor is low (0.016 at 400k and 0.073 at 1000K) and the absorptance value is high, between 0.79 and 0.89.

Multi-layer absorbers consist of metal dielectric thin layers. The constitution and dimension of the layers allow to define the range of wavelength absorbed. The materials used are tungsten, titanium and aluminum. A theoretical value of 0.97, for the absorptance, and an emittance value of 0.06, at 450K, could be achieved.
Metal dielectric composites consist of metal particle dispersed in dielectric phases. The metal chosen has a high melting temperature but silica or alumina could be used too. With tungsten and silica combination, emittance value of 0.042 and absorption value of 0.979 was achieved at 400K.
Photonic crystals, a periodic arrangement of two materials with different dielectric constants could be used to achieve an ideal (theoretically) solar selective absorber. Nanowires silicone coupled to a silicon surface form a thin transition width, which is near a perfect cut-off wavelength. Development has still a lot to explore since 2D and 3D photonic crystals are not strongly studied for the moment.

As showed in this section the design of the receiver is still evolving a lot as well as the absorber material. A lot of possibilities and improvement are available.

2.3.3 Heat transfer fluid

The heat transfer fluid (HTF) is passing through the receiver to collect the heat. Then, it will undergo a direct expansion in a turbine, be stored or provide heat to a secondary fluid. In the case of storage use, it should be possible to store directly the HTF, to skip another heat exchange. The HTF could be a gas or a liquid. The HTF needs to own a low melting point temperature to avoid freezing risk, high thermal stability (up to 700°C) and should be cheap [10]. This perfect fluid does not exist yet and different ones are used as: air, steam, thermal oils and organic molten salt. A brief review of each of them is proposed below.

Air

The main advantage of air as a HTF is its free cost. The drawbacks are the low thermal conductivity and viscosity [10]. If a secondary circuit is implanted, air is rarely used. If air is heated by the receiver, it will directly be used into the combustion chamber of a gas turbine.

Water/Steam

Water/steam is used in several plants. This liquid owns a low viscosity at high temperature. The main drawback is the scarcity of water in desert region and the storage properties [10].

Thermal oils

Thermal oils include mineral, silicone and synthetic oils [10]. The thermal properties are better, in general, than the ones of air and water but the limiting stability temperature and the price is an important drawback.

Organic molten salt

Organic molten salt seems to be the most important contender for HTF because of its good thermal stability and properties at high temperature [10]. According to this article, the commercialized ones are the alkani nitrate and nitrite (as the Solar Salt, Hitec and HitecXL). Carbonate salt are analyzed also to provide cheaper HTF which could not depend on rare materials [25], this study from Wu et al. reported good results and research is ongoing.

2.3.4 Thermal energy storage

The storage ability of the CSP technology is the main advantage it owns on the other renewable technologies. The thermal storage system has a higher potential than the mechanical and chemical ones in terms of capital cost and operating yield [10]. According to this article, three parts are defining the TES system: the thermal storage medium, the HTF and the containment system. It should be noted that the storage is required for no more than one day since the plant produce heat each days.
The medium stores the heat in a sensible, latent or a combination of both modes. The sensible system consists of raising the temperature of a sensible heat material as rocks or concrete. The latent one is an isothermal process which has a larger capacity storage than the sensible one. Moreover the temperature difference, since it is isothermal, is quite low which is recommended for the thermal cycle and the other components of the plant. The hybrid system uses a latent mode for the vaporization of the fluid and the sensible mode for the preheating and the superheating. The HTF is used to transfer the heat to the storage medium but also collect it and was already covered in the previous section. The containment system holds the medium, and could be composed of one or two tanks.
According to Xu et al [10] three generations exist for thermal storage system. The first is a direct storage system with tanks. One tank is used for the hot fluid and the other for the hot one. The medium of the storage is the HTF itself. According to this article it is the most commercialized and mature storage system. The second generation is composed of only one tank. The principle is based on the stratification between the top (hot) and bottom of the tank (cold). The gradient of temperature is maintained by the buoyancy effect. An isolation is planned to impede mixing. The third generation is the upgraded second one, the tank is now filled with packed solid material and the heat is store in the material as well as the HTF contained in the tank. This system combined sensible and latent heat storage and so reduce the temperature difference between the HTF and the storage medium [10].

2.3.5 Power conversion cycle

All the achievement described had only one goal: use the sun to heat high quantity of fluid. Now, the heat (energy) will be converted into mechanical one (by the turbine) and then electrical one (by the alternator). To achieve it, well known cycles could be implemented, as the Rankine, Brayton, combined cycles or a gas turbine. Choosing the power cycle often requires to know almost all the configuration of the plant, so this subsection presents some different CSP tower configurations. It should also be mentioned that some of the currently operating CSP plants own a back-up generation system (gas or oil) which, with the TES, regulate the output power to a constant value and sometimes allow to use CSP plants as a baseload power source [7]. The challenge of CSP is the location, most of the time in desert region, which lead to water scarcity. So, the cold source of the cycle could not be water in most of the cases and dry cooling need to be considered. The dry cooling could be direct or indirect. It could save up to 90% of water consumption [10]. From this article, dry-wet cooling would be promising. This system is alternating between both systems, depending on the air temperature and could save up to 80% of water.

Brayton

The classic configuration of such concept in a CSP plant consists of a heliostat field - volumetric air receiver - gas turbine (converted). The air is compressed in the compressor of the gas turbine, then heated in the receiver of the tower and finally flows into the combustion chamber of the gas turbine. An alternative to this hybridization could be a supercritical CO_2 cycle. The CO_2 acting as the HTF does not limit the working temperature. The study from Turchi et al. [26]

analyzed different transformations of a simple supercritical CO_2 Brayton cycles according to CSP condition (e.g. dry cooling). They found that by utilizing compressor intercooling, splitting the turbine, incorporating fluid reheating and optimizing the rotation speed of each turbine and compressor by a dual shaft, the efficiency of such cycle could reach 50%. A study from Chacartegui et al. [27] demonstrated that add an ORC cycle to the supercritical dioxide one does not worth it since the losses in the HRSG was too high.

Rankine

The Rankine cycle is the most classical cycle used in CSP applications. The steam is heated by a HTF. Then, the steam is used to expand in a turbine, be condensed, compressed and undergo the cycle again. According to a study of Zoschak et al. [28], the best way of using the solar heat in a Rankine cycle is to use it for the vaporizing and superheating phase and not in feed-water heaters. Commonly subcritical Rankine cycle use in CSP plants have an annual efficiency about 35 to 45% [26].

Combined Cycle

The Brayton-Rankine combined cycle consists of air that is compressed and sent to the tower, then goes to the combustion chamber and flow through the gas turbine. Then a heat recuperating system allow to heat, with the exhaust gas, the steam of a Rankine cycle. This kind of cycle was never tested for CSP applications [12]. Also, some configurations use a gas turbine to directly heat the HTF when needed. This method is used as back-up system and allows to control the temperature of the HTF. As well some people imagine the use of organic Rankine cycle, using this cycle as the cold source of a Rankine one.

2.4 Perfomances

An efficiency study of a SPT plant could be divided in three blocks as the ones showed in figure 2.6. The first losses occur during the transmission of the sun power, by the heliostat field, to the tower. Then losses occur during the conversion of the radiations power in internal energy (heat) by the receiver and by the convection effect between the air and the receiver. Then, irreversibilities occur within the power cycle (and in the thermal storage system) and the output is the electricity on the grid.

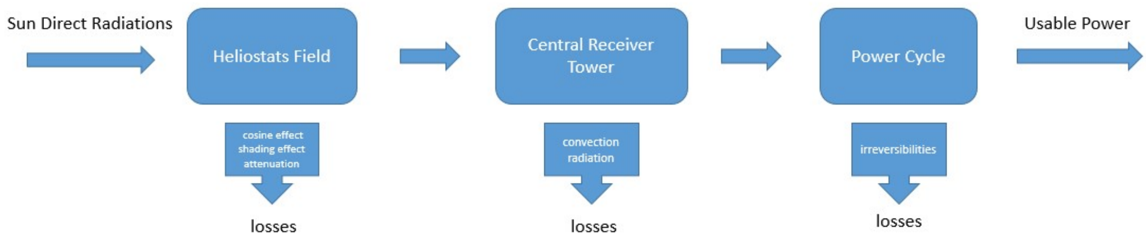

Figure 2.6: Simplified representation of power losses occurring in a SPT plant.

In the following subsection, a detailed summary of the efficiency is proposed for each step of the process. First, the efficiency of a heliostat field is analyzed. Then, the losses occurring in the receiver are described and the efficiency of different power cycle configuration are analyzed. In the end, the limit of the efficiency for an overall STP plant is computed from different ways.

2.4.1 Heliostat field efficiency

The heliostat efficiency or optical efficiency, is defined by the quantity of radiations reaching the absorber divided by the whole quantity of the energy captured which means the total direct radiation captured by the mirrors surface. Optical losses occur due to the mirrors positioning, quality, and physical phenomena (as attenuation or cosine effect). The figure 2.7, represents the different effects to consider. Each of them will be briefly described but were already introduced in the previous paragraph about heliostats. The table 2.2 describes the time and field layout dependence of each of them.

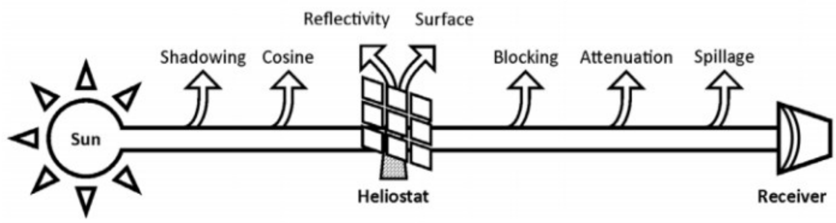

Figure 2.7: Optical losses occurring during the transmission, by the heliostat field, of the sun radiations to the tower (from [29]).

dependence:			time	field layout
heliostat field efficiency	$\eta_{\text{optic}} = \eta_{\text{cos}}\, \eta_{\text{atm}}\, \eta_{\text{refl}}\, \eta_{\text{sh-bl}}\, \eta_{\text{sp}}$	η_{cos}	yes	yes
		η_{atm}	no	yes
		η_{refl}	no	no
		$\eta_{\text{sh-bl}}$	yes	yes
		η_{sp}	no	no

Table 2.2: Summary of the efficiencies and their influencing parameters on the optic efficiency of the heliostat field.

The cosine efficiency (η_{cos}) is defined hourly for a heliostat field. The losses occur since the mirrors are not normal to the direct radiations since they have to reflect them on the tower. The efficiency is equal to the cosine of the angle between the heliostat and the tower. The angle depends on the placement of the heliostat and the sun position and varies hourly. The layout of the heliostat is studied to reduce this loss on the year. The atmospheric efficiency, losses occurring from the attenuation during the path of the rays to the tower, of one heliostat (η_{atm}) is not time dependent but depends on the distance heliostat-tower. The global (average) atmospheric efficiency of a heliostat field then depends on its layout. As well as the atmospheric efficiency, the reflectivity efficiency (η_{refl}) is not time dependent. It is a constant value that depends on the degradation and cleanness of the mirrors. An average value for the all field is then similar to a value of any heliostat. The shadowing-blocking efficiency (η_{sh-bl}), due to the shadows generated between the heliostats themselves, depends on time since the sun position is critical to compute it. It is defined hourly, depending on the season (date), for the all field. It is of course dependent of the layout of the heliostat field and the dimensions of the heliostat. The spillage efficiency (η_{sp}) depends on the tracking accuracy and mirror quality. It is defined as the relative quantity of reflected rays who do reach the receiver.

To study the efficiency of a hypothetical plant, the atmospheric attenuation and mirror reflectivity can be set as constant. Indeed, some values from existing plants could be reuse as the mirror and ordinary defaults are not expected to change. Then, for the cosine, atmospheric and blocking-shading efficiencies it exists three options: decide of a layout and compute the efficiency at the plant position, take real efficiencies values of a real layout from an existing plant (but the location is not the same and so it is not so accurate) or design a code to find the optimum layout depending on the position of the plant and then compute the efficiencies.

As explained in this section, some efficiencies change during the day, due to the sun position. The most accurate way of defining the average annual efficiency of a heliostat field of a SPT plant, located at a given position, is to compute and multiply the hourly efficiency of each parts, for all operating hours and divide it by the total operating hours on the year. As an example, the study presented by Eddhibi et al. [17] computed the efficiency of the PS10 CSP tower in Sevilla (first purely commercial CSP tower of 2007 [3]), implementing their own code. Their results are presented in the table 2.3 and give an idea of typical values. Their results were compared to other studies values and are similar. They compared the results with other studies and found similar values. The global field efficiency, from these values, is 0.636. This result confirms the citation from the heliostat paragraph arguing that 40% of the losses come from the reflecting part.

η_{cos}	0.8283
η_{atm}	0.9498
η_{refl}	0.88 (arbitrary)
$\eta_{\text{sh-bl}}$	0.9255
η_{sp}	0.9926

Table 2.3: Results from a study of Eddhibi et al. [17] about the average efficiencies of the heliostat field of the PS10 plant in Sevilla.

2.4.2 Receiver efficiency

The efficiency of the receiver is characterised by three losses: the convection between the surrounding air and the receiver, the radiations reemit by the receiver and the part of the radiations reflected by the receiver. A simple way of computing the efficiency is proposed by Xu et al. [10]. The losses by reflections are taken into account by the capacity of absorbance of the receiver. The Stefan-Boltzmann law of radiations is used to compute the losses by radiations and the losses by convection are determined setting a value for the coefficient of convection (see table 2.4).

Receiver efficiency	$\eta_{\text{re}} = \frac{\alpha Q_{in} - Q_{loss}}{Q_{in}}$	$Q_{in} = \eta_{\text{optic}} E_{DNI} C$ $Q_{loss} = \epsilon \sigma T_r^4 + h(T_r - T_{amb})$	

Table 2.4: Summary about receiver efficiency, as proposed by Xu et al. [10].

The efficiency is then the effective heat captured by the receiver (corresponding to αQ_{in}, so without the reflected radiations) from the whole concentrated radiations minus the losses due to convection and re-radiations (Q_{loss}) divided by the whole energy from the heliostat

[3] see NREL web site for more technical information `https://www.nrel.gov/csp/solarpaces/project_detail.cfm/projectID=38`.

field and reaching the absorber (Q_{in}). The absorbance factor (α) could be seen as the efficiency of the material composing the absorber to convert photon's energy, from the radiations, in internal (thermal) one. The value of this factor depends of the wavelength of the radiations beams and the temperature of the absorber (internal energy); some values were presented before in the receiver section. The whole energy from the heliostat field, reaching the absorber, is defined as the multiplication of the optical efficiency of the field (η_{optic}), multiplied by the concentration coefficient and the direct normal irradiation (E_{DNI}). The convection losses are computed multiplying the convection factor (h) by the temperature difference between the absorber and the ambient one (T_{amb}). The radiation losses depend on the emittance factor ($\epsilon = \epsilon(\lambda)$), the Stefan–Boltzmann constant (σ) and the temperature of the absorber (T_r). In the equations, the concentration ratio (C) is the result of the division of each members by the receiver surface, defining it as:

$$C = \frac{\text{mirrors total area}}{\text{receiver area}}$$

.

A study of Clifford et al. [30] examined central receivers. In fact, from this study, the simplified losses equation above should take into account a radiative view factor from the receiver area to the environments (from 0 to 1) and a convective heat losses multiplier (0 and greater than 1). Indeed, the author remind that for a cavity receiver, this convective factor could be up to two times greater than the one of an external receiver since the surface of the internal one is larger. The figures 2.8 allow to see the influence of these factor on the efficiency. The DNI level is set to 1800 kWh/m^2, the absorbance and emittance of the absorber are respectively 0.95 and 0.85. The concentration factor is defined as 900, the field efficiency 0.6 (common value and near the approximation from previous paragraph), the ambient temperature 20°C and the coefficient of convection 10 W/m^2K. We can observe that a quite big difference is due to the irradiance factor and that this difference is more and more critical the greater the temperature. The losses due to the convection factor are already present at low temperature but does not become so important at high temperature. It shows the importance of the design of the receiver on the receiver efficiency, which is not only impact by the thermal properties of the absorber material. It should be noticed that the equations here are not accurate since the emittance and absorbance are taken as constant but, in fact, should vary depending on the temperature of the absorber and the wave length of the sun radiations. Moreover, the convection should be computed separating the forced and natural parts [29]. These details are more required to design the receiver than having an idea of its efficiency.

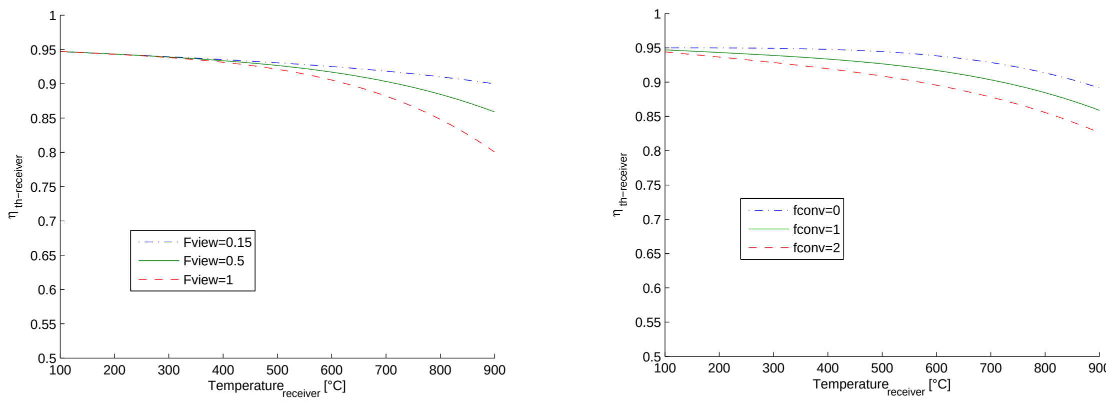

convective factor equals to 1.

Radiative view factor equals to 0.5.

Figure 2.8: Receiver's efficiency depending on its temperature for different values of the convective and the radiative view factor.

2.4.3 Thermal cycle efficiency

The thermal efficiency depends on the design of the plant (outlet and inlet receiver temperature chosen), the use of the plant as base-load plant or not, the presence of a storage system and the presence of a secondary fluid which means the need of a new heat exchanger and so supplementary losses. In the table 2.5, three types of CSP configuration with different power cycles are presented. A focus is done on these configurations since no gas turbine are necessary (in the contrary of other Brayton cycles and combined cycles). As a reminder, solid particle receivers are not operational yet and the value for the SC Rankine and Brayton with supercritical gas are then theoretical.

	Sub-C Rankine	SC Rankine	Brayton ($s-CO_2$)
Configuration:	$Steam\ Turbine$	$Steam\ Turbine$	CO_2
	Molten Salt	Solid Particle Receiver	Solid Particle Receiver
High T [°C] [31]	540	580	700
Pressure [MPa] [31]	13	24	25.0
Yield Power Cycle [31] [26] [14] [27]	35-45	40-50	45-55

Table 2.5: Three types of CSP configuration with different power cycles, adapted from Sakadjian et al. [31], Turchi et al [26], Charcartegui et al. [27] and the Sunshot initiave resume [14].

2.4.4 The limit of the global efficiency

Firstly, the goal is to define the highest possible limit ever achievable. The efficiency of the heliostat field is then set to one, as well as for the receiver and storage system. The efficiency of the power cycle is limited by the Carnot efficiency. Concretely, for the heliostat field, it means that the angle between the sun and the tower at each heliostat is infinitely small, that all heliostats are closed to the tower and that the mirrors reflect perfectly the sun radiations, also, that any shadows occurred during the all sun path during any days on the year between the heliostats. This is unachievable for sure but allow to construct a real maximum. The receiver efficiency set at one would mean that a perfect absorber material would absorb all radiations ($\alpha = 1$) and emits any thermal ones (= 0). Moreover, the design of the receiver would be perfect as no convection occurs. The temperature achieved by the receiver would be the one of the HTF and the thermal energy storage (if there is one) would store thermal energy with a perfect insulation. The power cycle would be a Carnot machine, with a lower temperature equals to the ambient one and a higher temperature equals to the one of receiver. In the end, the efficiency achieved would depend on the concentration factor setting the receiver temperature and so cycle temperature. The more the temperature of the receiver, the more the Carnot machine's efficiency. So, the result would be, for a given mass flow of HTC, to achieve the most high value of C which means more surface of mirrors and so a smaller field efficiency which contradict the hypothesis of a perfect heliostat field and demonstrates that the hypothesis is too strong.
In conclusion, to compute the physical limit for the efficiency of a CSP plant, the maximum reachable temperature bearable for a cycle should be put as the high temperature of the Carnot equation. For example, setting a temperature of 2000K, the maximum efficiency, with an ambient temperature of 300K would be 0.85. This value, as explained before, is not achievable but set a maximum.

A second approach more realistic would be to set the value of the concentration ratio and use a black body model for the receiver. This model considers the losses due to the radiation emission by a black body (then emittance, ϵ, equals the absorbance factor, α, equals one). Using the formula of Stefan-Boltzmann saw previously, keeping the field and storage system efficiency to one and the ambient temperature to 300K, the global efficiency would be computed as:

$$\eta = \eta_{receiver} * \eta_{Carnot-cycle} = (1 - \frac{\sigma T^4}{DNI * C}) * (1 - \frac{T_{receiver}}{300})$$

The terms $\frac{\sigma}{DNI}$ could be replace by a constant.

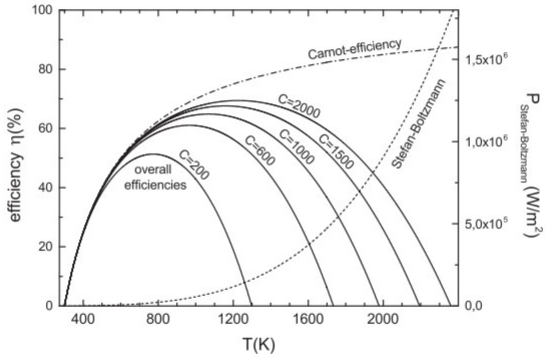

Figure 2.9: Plant efficiency from a basic model of a black body receiver and a Carnot machine, depending on the receiver temperature. The heliostat field efficiency is set to one. In other words, only the radiative lost emitted by a black body receiver are taken into account and the trends are represented by the dashed line. [24]

Burlafinger et al. [24] proposed a comprehensive plot of this curve, setting in relation the radiative losses and the Carnot efficiency, see figure 2.9. This model allows to conclude that the more the concentration ratio, the more the global efficiency. It also gives a comprehensive limitation for the receiver temperature which appears to be about 1350K. The increase of the concentration ratio generates high efficiency difference for values between 0 and 600 and then the rate of increase is smaller and smaller to finish as insignificant.

Another model, is here proposed to consider the selective properties of future absorbers. As presented before, in the receiver subsection, black body absorbers, with selective properties, could absorb the radiations only for a certain range of wavelengths. It would mean that the temperature achievable could be higher than for a black body, since the radiations emittance would be really low, and that the Carnot machine efficiency would be higher. Burlafinger et al. previously cited proposed an analyze of such a model. The fact is that the sun radiations lies at wavelengths smaller than the one emitted by a black body for classical temperature of a receiver. As explained in the article, the long-distance sun-earth and the atmospheric attenuation decrease the sun light wavelength's range. At the earth crust level, the magnitudes of these radiations are comparable to the one of a black body and intersect at a point characterized by a wavelength, which is called the cut-off wavelength. The idea is then to create a material (see section about receiver and crystal receiver) which has a high absorbance value below the cut-off wavelength and an almost zero value for the one higher, since the total energy between the emissions by the black body and the absorption would be negative, see figure 2.10. On the figure inserted, the absorbance characteristic of the absorber could be seen, as equals to one below the cut-off wavelength and zero for higher ones. The emittance value is set to one, always.

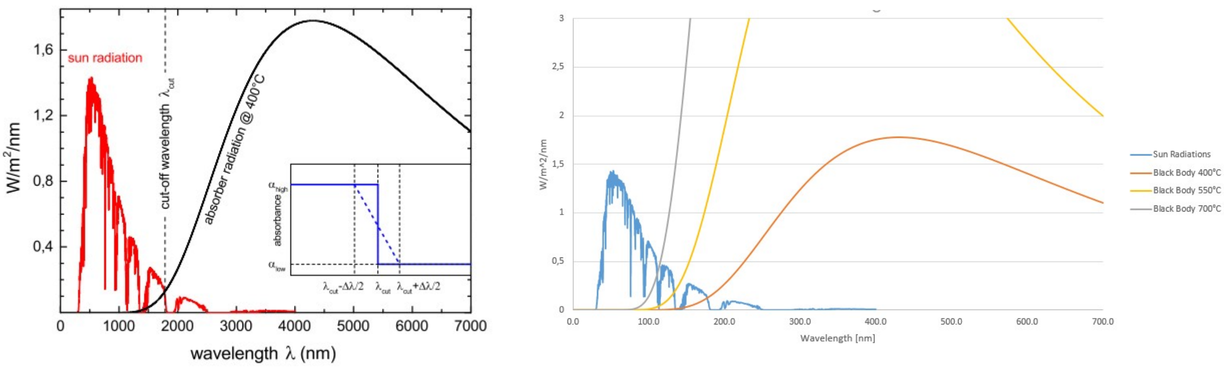

Figure 2.10: Distribution of the radiations between the sun ones and the ones from the absorber at a given temperature. The sun radiations are from a terrestrial reference spectra of type AM1.5 from the American Society for Testing Materials. At the left, plot of the cut-off wavelength and the absorbance function from [24] and at the right evidence of the dependence of the cut-off wavelength on the temperature of the black body from the black body equations.

This study then research the optimal temperature, which depends now on the optical properties of the absorber. The goal is to find, for a given concentration ratio, the ideal temperature and cut-off wavelength. The difference with the previous assumption are that the convection losses are taken into account here, with a convection factor of 10 W/m^2K. The model used to compute the efficiency is the same than before excepted that now the radiations emits by the receiver depends on the wavelength considered and its temperature according to the Planck law. As well, the energy absorbed depends on the wavelength.

$$P_{abs} = \int_0^\infty \alpha(\lambda)(CP_{sum}(\lambda) + P_{amb}(\lambda)d\lambda$$

From the optimal temperature and cut-off wavelength for each concentration ratio, the global efficiency is computed and the results are showed in 2.11.

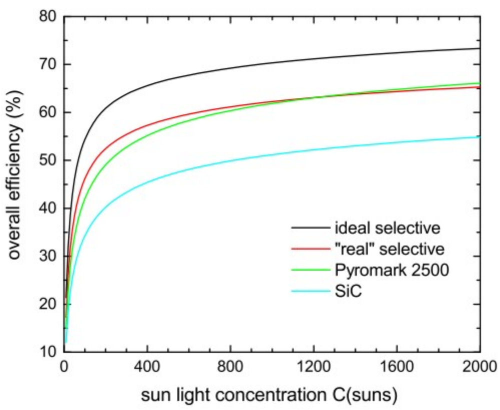

Figure 2.11: Results for the global efficiency using a perfect selective absorber and a Carnot machine. The field efficiency and storage cycle are set to one and the convective losses are considered, from Burlafinger et al. [24].

For a concentration ratio of 2000, the results show a difference around 200°C between the optimal efficiency of a normal black body and the one of the selective receiver which lead to a high efficiency of about 73%.

The previous development assumes that the solar rays are not affected by the mirrors and that all their properties are conserved which is not so natural since we know the light rays lose energy by the reflection. Indeed, the special CSP mirrors from AGC have an energy reflectivity of 94% [32]. The question is to know if the wavelength of the light is disturbed during reflection, which could query the previous development. It is the same as study the change of velocity or frequency since the wavelength is the ratio of these both quantity. We wonder how mirrors reflect photon which is the subject of an article granted to Pascotta, an optical physicist [33]. As explained, a mirror is generally composed of a layer of silver and an exterior layer of glass. Into the glass, the electrons are fixed and the velocity of the light decreases ; there is almost no reflection at the air-glass transition and almost no energy losses during the path of light through the glass. For a metal, the electrons are free to move but their movements are damped, when a photon encounter an electron, it is absorbed and the energy is converted into heat by the damped movement of the electrons. But, in a metal, the reflectivity is high which generates two cases: the photon is absorbed and its energy is lost or the photon is reflected and all these properties are conserved. The thin layer of glass does not impact the light beam properties, and the reflection, occurring in the glass-silver transition, returns a 100% similar beam ray in properties but not in quantity of photon (attenuation) which leads to a loss of total energy. To study the radiation beam reaching the receiver, applying wavelengths from the sun direct radiation is then accetable.

2.4.5 Which components to improve

The purpose of this section is to highlight the critical components to improve in a way of impacting the global efficiency of a SPT plant. The best way to achieve an improvement enlightenment on the different parts, is to perform an exergy analysis. The exergy analysis gives importance to the energy losses. So, knowing which part of the cycle most impacts the exergy leads to know which components is the most critical to improve in order to increase the global efficiency of the plant.
An exergy study was performed on a representative hypothetic SPT plant by Xu et al. [34]. The four subsystems composing the plant are the heliostat field, the central receiver, the steam generator and the power cycle. The main assumption is a steady state analyze which lead to not consider a potential TES system and to have a DNI constant. The others assumptions concern the heat losses and irreversibilities occurring in the pipe which are not taken into account. The plant use molten salt as HTF and the power cycle water/steam Rankine with a feed water heater to avoid too low temperature at the entry of the steam generator. The main parameters and a scheme of the plant, from the study, are presented in figure 2.12.

Subsystem	Properties	Values	Unit
Heliostat field	Beam radiation (DNI)	800	$W\,m^{-2}$
	Overall field efficiency	75%	–
	Total heliostat aperture area	10,000	m^2
Central receiver	Aperture area	12.5	m^2
	Inlet temperature of molten salt	290	°C
	Outlet temperature of molten salt	565	°C
	View factor	0.8	–
	Tube diameter	0.019	m
	Tube thickness	0.00165	m
	Emissivity	0.8	–
	Reflectivity	0.04	–
	Wind velocity	5.0	$m\,s^{-1}$
	Passes	20	–
SGSS	Inlet temperature of water	239	°C
	Outlet temperature of steam	552	°C
–	Ambient temperature	20	°C

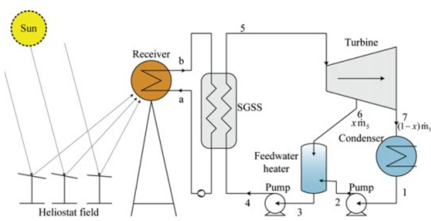

Figure 2.12: Main parameters and scheme of the plant that Xu et al. studied to perform an exergy analysis [34].

The overall field efficiency is quite high, in comparison with the values around 60% described previously. As well the DNI value is quite exaggerated since an average one on a day is about 250 $[W/m^2]$ ($2200 kWh/m^2$ on a year, see the map on figure 2.13), the value here would correspond

	Heliostats	Receiver	SG	Power Cycle
Energy Yield [%]	75	90	100	37.8
Energy Losses [%]	32.4	10	0	53
Energy Yield [%]	75	55.5	88.8	74.5
Energy Losses [%]	33.1	44.2	9	12.6

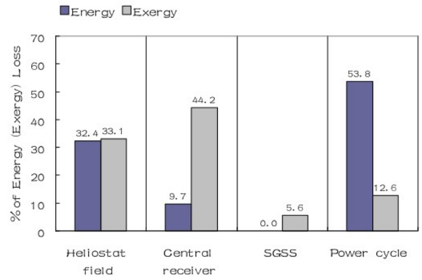

Figure 2.14: Exergy and energy efficiency of each part of the plant, by Xu et al [34].

to a pick in a good day. Anyway, the DNI impact on the efficiency is also analyzed.

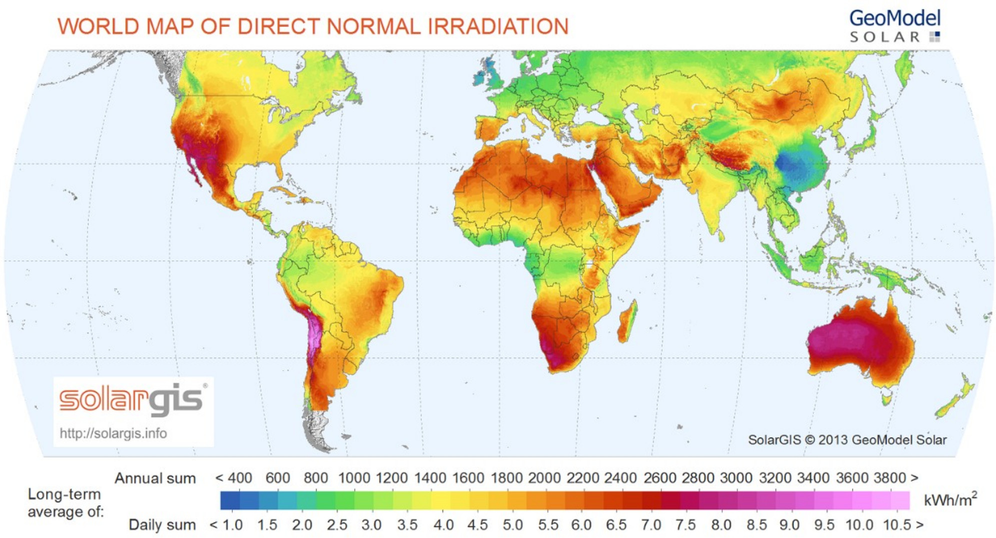

Figure 2.13: Map of the annual mean DNI on earth.

The energy results (see figure 2.14) lead to conclude that the biggest losses occur in the thermal cycle and that it is the critical component to improve to raise the global efficiency of the plant (which was computed as 22.9%). The exergy analysis highlight one fact: the energy in the receiver has a high quality and lose only a tiny quantity impacts more the global efficiency than in any other parts of the plant. The sun radiations concentrated in the receiver own a superior energy quality since they come from sun which has a temperature about 4500K. In the receiver, they are converted into heat at 700 to 900K, a way lower in temperature. So, the quality losses of the energy in the receiver generates high exergy waste, even for small ones. In the opposite, the power cycle has high energy losses but low exergy ones since the quality of energy is a way lower than in the receiver.

In the following subsection, a description of the effect of the concentration ratio, DNI values and the power cycle chosen is described. Before introducing these discussions, the model uses to describe the exergy efficiency of the receiver is briefly demonstrated, from the analysis of Xu et al [34]. It will allow to investigate the DNI and C impacts on the receiver efficiency. The exergy efficiency of the receiver is described as the ratio between the efficiency absorbed (ϕ_{abs}) and the one transmitted by the heliostat field (ϕ_{tot}).

$$\eta_{exe-receiver} = \frac{\phi_{abs}}{\phi_{tot}} = \frac{\dot{m}_{HTF}\ cp_{HTF}\left(T_{out} - T_{in} - T_0\ ln(\frac{T_{out}}{T_{in}})\right)}{\dot{Q}_{rec}\ (1\ -\ \frac{T0}{T^*})}$$

The denominator, the exergy received, could be written as the heat received decreased by a Carnot ratio (inevitable losses). The numerator, the exergy absorbed, is written as the exergy transferred to the HTF. It could be written as a function of the temperature of the HTF and its thermal properties. In the end, the exergy efficiency of the receiver could be written as a function of its energy efficiency (heat absorbed on the total heat transmitted by the heliostat field) and the inlet and outlet temperature of the HTF with T_0 the ambiance temperature and T^* the one of sol.

$$\eta_{exe-receiver} = \eta_{ene-receiver} * \frac{1 - \frac{T_0 \, ln(\frac{T_{out}}{T_{in}})}{T_{out} - T_{in}}}{1 - \frac{T0}{T^*}}$$

This equation leads to conclude that even with an energy efficiency of 100%, the maximum exergy efficiency achievable, with the temperature set (T_{in} = 290°C and T_{out} = 565°C) for the HTF, has a maximum of 54.4%. The only way to raise the exergy efficiency is to augment the outlet HTF temperature. With a temperature of 1000°C, the authors computed an exergy efficiency equals to 71% of the energy one. The losses by radiations and convection augment with the temperature and should be decrease also and moreover temperature is limited by the material constrains. So, for the moment, when a plant is running, the optimal temperature is set by the losses, and so, it is not always better to raise it from 565 to 590 degrees. But, designing a receiver, the main goal should be to: increase material performance to achieve high temperature and decrease losses by convection and overall radiations ($\propto T^4$).

The DNI effect on the efficiencies is really high. In fact, we should be careful that the average DNI on a year on earth is limited at about $400W/m^2$ (= $3500kWh/m^2year$) as showed on figure 2.13. Hence the values below take into account high DNI above the average. If we analyze the graph to have an overall idea on a year, the interesting values on the graph 2.15 are the ones who has a larger rate of change (derivative). The global trend of the efficiencies is dictated by the receiver, which is really impacted.

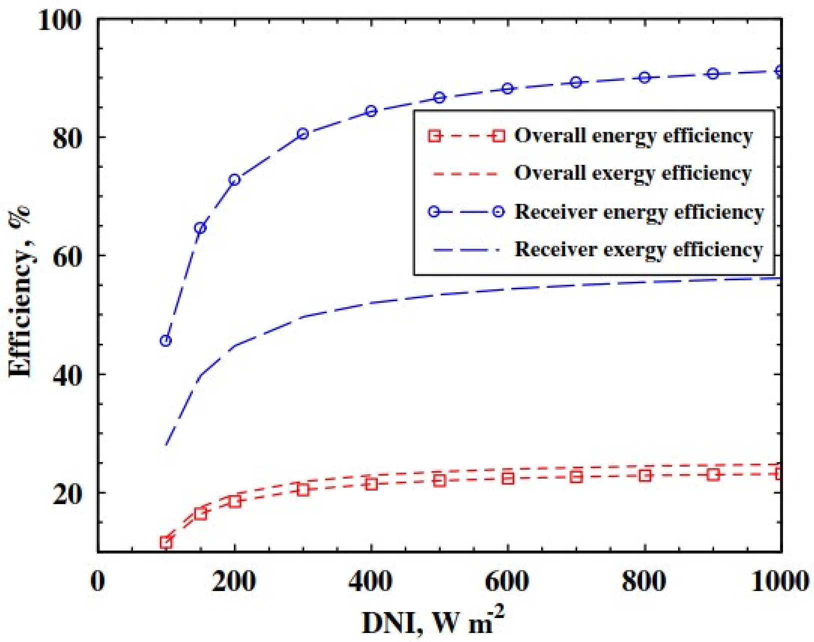

Figure 2.15: DNI influence on the exergy and energy efficiency of each part of the plant, by Xu et al [34].

It is normal that DNI factor has a huge role on the efficiency. The heat losses have an important role at the receiver but only the temperature (that the DNI does not change, +36°C if DNI values are multiplied by 10 according to the authors) and the absorber surface play a role, not the DNI. The output electricity increases linearly to the increase of the DNI. A critical point for CSP tower plant is then the localization.

The concentration impact on the efficiencies is not negligible. As the concentration ratio is defined as the total aperture area of the mirrors on the receiver area, the ratio is always quite high, generally comprised between 500 and 1500. To study its importance, Xu et al. fixed the heliostat field and play on the receiver area to change the value of the concentration ratio (see figure 2.16).

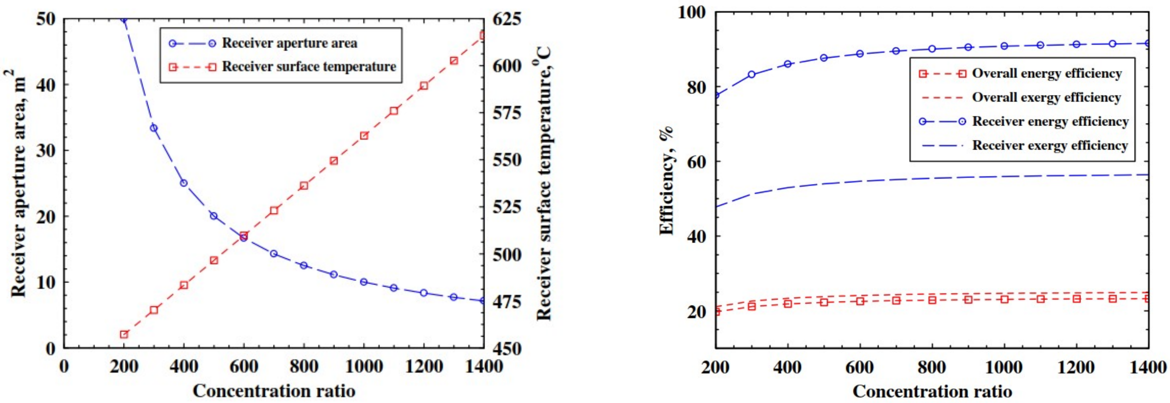

Figure 2.16: Concentration ratio importance in efficiency and influence on the temperature and area of the receiver, by Xu et al [34].

As C increases, since the aperture area of the heliostat field is fixed, the receiver area decreases, first rapidly and then more and more slowly. Then, quite logically the temperature of the surface composing the receiver (absorber) augments linearly. In terms of efficiency, see figure 2.16 right, the overall efficiency increases, but the derivative is less and less. The overall efficiency trend is dictated by the receiver one, the other components are not affected. The fact is that, on a theoretical study like this one, augment C is always beneficial since the surface area is smaller (less losses by convection and radiations) and the temperature rise. In reality, we should be careful that some heliostats are one kilometer away from the tower, meaning that pointing all the rays without any losses is quite challenging if the receiver surface is small. Moreover, depending on the mass flow, the receiver should be able to heat all the HTF quite rapidly, meaning that the surface should be large enough to achieve this goal.

To conclude this analyses of the exergy study of Xu et al., two other cycles are studied: one with a reheat path (system 2) and one with a reheat path and supercritical carbon cycle (system 3). The result of the efficiency are presented on figure 2.17.

The cycles were not optimally designed and then the results have to be taken as the potential of increasing the global efficiency by playing with other configurations of power cycle. The conclusion is that effectively changing the power cycle by a state of the art one increases the efficiency in non negligible way but still not so important.

A study proposed by Zare et al. [35] analyzed the energy and exergy performances of a tower plant with a closed Brayton cycle. The air is used as HTF and heat by the receiver. Then, the air transfer its heat to a helium cycle and two ORC cycles recover the waste heat: one after the cooler and one before the second compression. The air is heated up to 1000°C by an

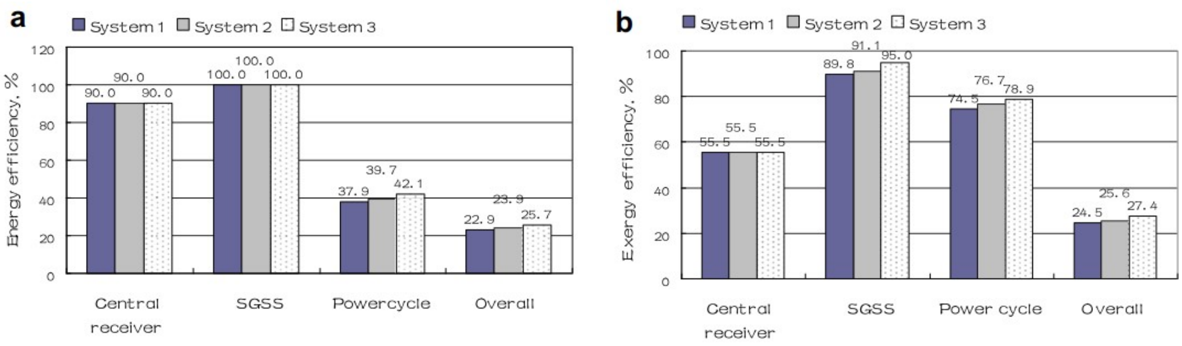

Figure 2.17: Results and comparison for the different plant configurations, by Xu et al [34].

open volumetric receiver. The mains parameters set to compute the efficiencies were: DNI of 850 W/m^2, optical efficiency of the field about 64% and a concentration ratio of 1111. The energy losses accounted to the receiver is only 20.9% but 32.65% for the power cycle. In the opposite, the exergy losses are greater for the receiver, 39.41%, and only 14.05% for the power cycle while the heliostat field has an efficiency of 46% for both energy and exergy point of view. The results for the energy and exergy efficiencies confirm the conclusion of the previous study: the receiver is the critical component to improve. As well, DNI impact was studied and a comparison between different values is showed in the figure 2.18 where we can observe the previous conclusion between receiver and cycles energy and exergy efficiencies. On the figure, we can observe that the DNI increase does not impact so much the receiver exergy losses but augment his energy ones as explained before.

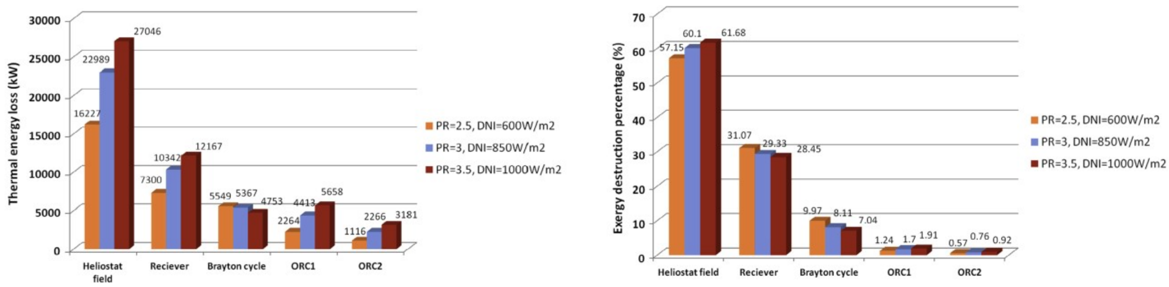

Figure 2.18: Exergy and energy, results and comparison for different DNI levels, by Zare et al [35].

In conclusion about performances, the real focus should be done on the location (DNI) and receiver properties (temperature max, surface of the absorber, design, etc.).

2.5 Summary and conclusion about CSP tower status

The CSP technology is new and consequently, only two countries (Spain and USA) own the majority of currently installed plants. On the other hand, numerous plants around the world are being built and many more projects are being studied.

The leading technology is currently parabolic trough concentrators but the tower system, mainly due to its high temperature achievement and improvement perspective, is at the heart of CSP projects interests.
The main parts of a CSP tower plant are the heliostat field, the tower-receiver and the power cycle. As well, the thermal energy storage and the nature of the heat transfer fluid (HTF) are important components. Numerous types of field layouts, receiver technologies and absorber materials, power cycles and HTF exist, and, non negligible perspectives of improvement are in view for all of these parts.
The current performance of a state of the art plant could be summarized as: 63 % for the heliostat field (see table 2.3), 90 % for the receiver (see graph 2.8), 98 % for the storage system and about 35-45 % for the power cycle (see table 2.5). Exergy analyses showed that the main energy losses happen at the power cycle but highlighted the exergy loss of the receiver which would be the most important part to concentrate improvements (in design and new materials). Moreover, it proves the critical impact of the irradiation level on the efficiency.

From these informations, an electricity production model of a CSP tower plant will be created. Nevertheless, in the following chapter, the focus is done on the Energy Return on Investment.

3 EROI and Life Cycle Assessment

This chapter introduces the Energy Return on Investment (EROI) factor and describes its contribution in the context of our study. Also, Life Cycle Assessments (LCA) are covered with a focus on the Cumulative Energy Demand (CED) for typical CSP tower plants. In fact, the LCA is the first step for the EROI analysis.

3.1 The EROI

3.1.1 General Use and definition

The primary energy is used, as seen in the first chapter, to produce electricity, heat and is also employs for some non-energy uses. The electricity and heat are then consumed by the industries and the transport and domestic sectors. In fact, a part of the primary energy is directly used by the energy sector. The energy sector produces energy and consumes energy. Therefore, it is logical that when analyzing this sector, the total energy cost for the creation of the energy park and its operations should be taken into account and compared to the energy production value. The same conclusions apply when designing a plant: the plant must produce more energy than the quantity consumed during its whole life. But, to be useful, a plant should produce more than one time the quantity of energy consumption. These considerations imply to analyze the Energy Returned on Investments (EROI) factor.

The EROI factor, for a plant, is a ratio of the total energy produced by the plant by the total energy consumed during the whole life cycle of this plant. Then, the EROI is a ratio representing the net energy a system could deliver to the society.
The EROI is computed as:

$$EROI = \frac{\text{Energy}_{\text{delivered}}}{\text{Energy}_{\text{consumed}}}$$

3.1.2 Why optimize the EROI

The main reasons to optimize a plant in terms of EROI is simply due to the importance of the net energy a technology could deliver to the society.
EROI studies are now more than ever subject of interests since we need to replace an energy mix based on fossil fuels, with a certain EROI, by a new mix based on renewable sources, with another EROI, which is lower. On the other hand, the EROI of the fossil fuel based technologies is decreasing. Now, the question is: is a renewable energy mix able to replace the current fossil based one? It is in order to answer this question that the EROI of new renewable technologies should be analyzed, at the scale required, and compared to the current ones of fossil technologies.

Society needs a certain minimum of global EROI to keep its trend and, a minimum one, to survive. According to Lambert et al. [36], the EROI is highly correlated to the life standards. This study highlights the improvement of life standards up to a EROI of 20. When this value is passed, no improvement of life standards are registered with an increase of EROI. It could mean that our society, based only on technologies with a global EROI below 20, shouldn't keep its current trend, and should adapt itself. Indeed, a decrease of EROI means that more energy should be used to produce the same amount of energy. So, less energy could be employed for certain areas (culture and art would be the first impacted). In this context, EROI studies should be performed to determine on which basis we can rely on renewable technologies.

3.1.3 Methodologies for an EROI study

Two different approaches are possible for an EROI study. A static one, to describe a plant, and a dynamic one, to describe the deployment of a technology for a territory. In this work, a static analysis is performed to optimize the EROI of each plant and, a dynamic one, to analyze the deployment of CSP tower plants. In the following paragraphs, both methods are described with a general point of view.

Static EROI study

The goal of the next chapter (Chapter 4) is to optimize a CSP tower plant in terms of its EROI, considering a given location. The optimization could have been done for the electricity production or the quantity of hours operating or the benefits, but for the reasons described previously (predominance of the net energy), the EROI was considered as the most relevant factor to optimize.

To compute the EROI, the electricity produced by the CSP tower plant is computed over a year. So, the quantity produced during its lifetime is known by multiplying this yearly production by the plant expected lifetime. The energy required by the plant is computed at a high level [37] taking into account internal energy consumption, external energy consumption, material consumption, labour consumption and auxiliary service consumption. In figure 3.1, the principle of the methodology is demonstrated over time. In the end, the EROI is the positive part on the graph, divided by the sum of all negative ones (energy consumed for the construction, operation and disassembling). The energy required by the plant to produce energy (negative part of the graph: construction, operation, disassembling) for all these steps are summarized in the next section of this chapter (3.2).

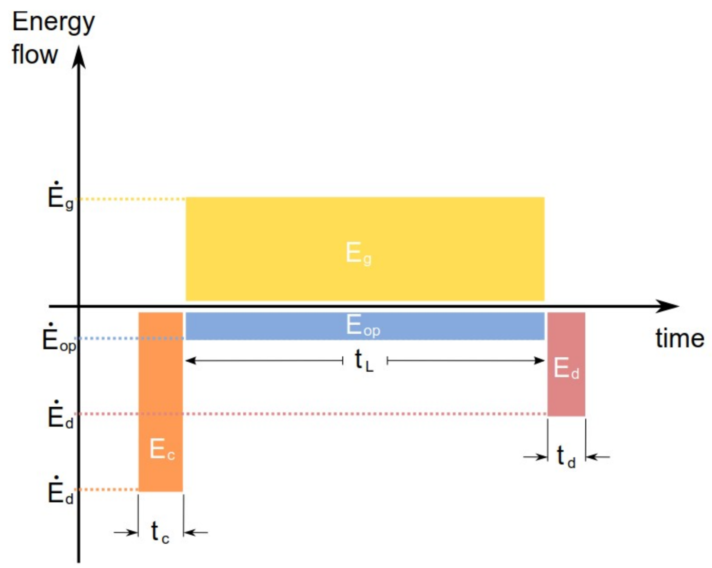

Figure 3.1: Static EROI analysis for a plant, as pursued in our study. The method was defined in the study of Murphy et al. [37] about EROI analyses methodologies.

The EROI, as seen, is computed from the energy consumed and produced by the plant during its life cycle. By comparing the EROI for different configurations of the plant, we will be able to choose the best configuration; i.e. the one that optimizes the EROI for the given plant location.

Dynamic EROI study

The EROI of the CSP technology is expected to rise and then decrease, the more plants are installed. As explained in the study about dynamic EROI analyses of Dale et al. [38], a physical decreasing depletion and increasing technological improvements form the dynamic EROI curve (see figure 3.2).

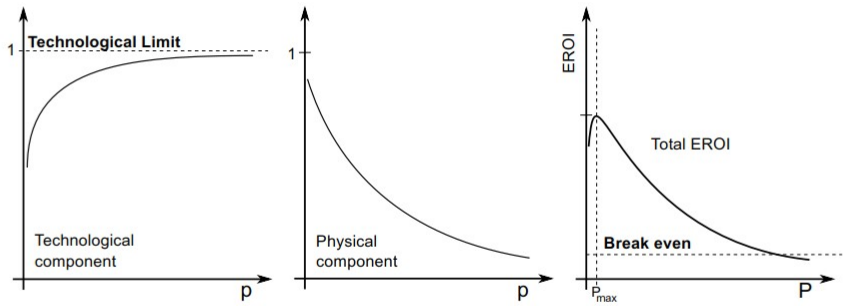

Figure 3.2: Dynamic EROI analysis method as pursued in this work. The method was defined in the study of Dale et al. [38] about EROI dynamics analyses. The x-axis represents the cumulative installed production.

The first curve indicates the growth of the EROI due to the amelioration of the production coming from technological improvement leading to better efficiency values. The potential improvement of CSP tower technology is quite high for each of the main part. The new solar field disposition and the new types of receivers and power cycles are expected to grow the global efficiency of CSP plants. As explained before, a physical limit constrains the increase of the components.

The second curve is linked with the depletion concept. The depletion for a fossil fuel source is described as the fact that the best spots, with easy and large quantities available, are exploited first. With time, it becomes more difficult to access the deeper reserves, and the energy used to extract the same quantity as before is greater. For our case, renewable sources, the curve expresses the abundance to scarcity evolution of sites to place the renewable sites. Indeed, the first CSP plants of Europe are located in Spain, near Sevilla, a highly sunny place. But if the deployment of CSP plants grows, other locations, with less and less average sun irradiations, would have to be investigated, which implies a smaller production.

In conclusion, the expected evolution for the EROI is first constituated of an increase since the current technology is not mature. Then, the scarcity of sites characterized by high sun irradiation values will affect the EROI. The technology begin to be stuck by the physical limit, meaning a decreasing rate of improvement. From this slow improvement and the land availability scarcity, the EROI value decreases. The goal of the last chapter is to take into account these effects to characterize a future potential deployment of CSP technology in Europe.

3.1.4 Example and values for some technologies

The tables 3.1 presents brief examples of some EROI values for current technologies. It allows to better understand an EROI analysis of a plant and have some ideas of EROI value for some technologies. It should be mentioned that the plants here are not configurated to be optimal in terms of EROI but to be representative of current plants in these different technologies. The table **??** presents some values for Fresnel and PTC CSP technologies, values from which CSP tower plants should be near.

Technology:	**Wind turbine**	**Hydro power plant**	**Hard coal**	**Nuclear**
Installed Capacity [MW]	1.5	90	509	1340
Location	Holstein, Ge	Waitaki Rive, NZ	-	-
Life Time [years]	20	100	50	60
Full-load Hours [h]	2000	3000	7500	8000
Energy Construction [TJeq]	12.9	1800	1970	4050
Energy Maintenance & Operation [TJeq]	0.3	75	21800	25700
Energy Decommissioning [TJeq]	-	60	91	1150
EROI	**16**	**50**	**29**	**75**

Table 3.1: Examples of EROI analysis for different technologies, from a study of Weissbach et al. [39] about EROI.

3.2 Life Cycle Analysis

As seen previously, to compute the EROI of a plant, we need to know its energy cost during its whole life cycle. The goal of this section is to understand the energy requirement of a typical CSP tower plant.

Whitaker et al. [40] performed a life cycle assessment of a CSP tower plant. They defined a typical plant for a given location (Tucson, USA) and analyzed the GHG emissions and cumulative energy demand (CED). The CSP tower plant has a 115 MW capacity, composed of a dry cooled system. The storage system is composed of a two tanks system, one hot and one cold, and has a capacity of six hours. The heat transfer fluid (HTF) is molten salt, heated from 288°C to 565°C in the tubular receiver.

The LCA analysis is composed of different phases (see the phases at table 3.2). The E&M phase considers the energy cost of the minerals extraction, transport to the facilities, process of manufacturing and the transports of the products to the regional storage. The construction phase regroups the energy costs of the transports of the material from the regional storage to the project site, components manufacturing processes and the energy used to assemble the plant. The O&M phase takes into account the projected manufacture of replacement material and transport to project site, the energy cost for the plant's water consumption and the maintenance vehicles fuel consumption. It also considers the electricity grid consumption of the plant and, if it is used, the propane consumption to melt the salt at the start-up. The D&D phase takes into account the energy needed to disassemble the plant, as well as the energy needed to incinerate or recycle demolition waste. From the results of the analysis, we can summarize the cumulative energy demand (CED) for the life cycle of the plant (see table 3.2).

LCA phases	CED [TJeq]	CED /CED_{total} [%]
Minerals extraction & Manufacturing (E&M)	1930.0	34.7
Construction (C)	204.3	3.7
Operation & Maintenance (O&M)	3292.6	**59.1**
Dismantling & Disposal (D&D)	138.5	2.5
Total	**5564.5**	100

Table 3.2: Cumulative energy demand for the different phases of the CSP tower plant of 115 MW according to Whitaker et al. [40].

The O&M phase is from far the most consuming phase. It is due to the auxiliary boiler consumption which is used to regulate the temperature of the molten salt and bring heat during start-up phases. The E&M phase requires also a lot of energy, which is mostly due to the heliostat field. Then, the construction phase and the D&D account as minor parts of the total. Whitaker et al. [40] proposed other configurations as a plant using synthetic salt as the HTF, a natural gas boiler instead of an electric one and a thermocline storage instead of a two tanks system. The synthetic salt configuration rises the CED by 7% (increase of the E&M phase) in comparison with the one with mined salt (reference plant). The authors concluded that the GHG emission also increased and that the benefits come only from the fact to not use mined salt, which is submitted to scarcity and controversial environmental consequences according to the authors. The auxiliary natural gas boiler allows to save 21% of the O&M phase without increasing the others. Another configuration using a thermocline storage energy system (one tank system, filled with concrete) was proved to not change the CED: the concrete used for the sensitive storage increase the CED but the fact to use only one tank decreases the quantity of HTF used. In the end, the CED is more or less the same than for the reference configuration. Since there is less salt used for this last configuration, the authors proved that using synthetic salt with a thermocline storage system was beneficial for the global CED, and even better if a natural gas boiler is used, allowing in total an average gain of 11% in comparison with the reference CED.

In the article [5], from Corona et al., the LCA of a CSP tower plant operating in base load, with a biomethane combined cycle, is studied. The plant has a classical configuration and the gas turbine is only used to bring heat to the heat recovery system of the plant when needed (because of bad weather, or during the evening and the night) in order to operate at full load during 24 hours. For our study, we will only focus on a plant operating solely by solar source. However, this article decrypts the E&M phase of the CED which is divided as shown in the table 3.3. The fact that the cycle used a gas turbine does not seem to affect these results since the power block only accounts for 2% of the total CED for the E&M phase. Then, for any CSP tower plant, the heliostats field makes up the major part of the CED for the E&M phase. The authors found that 50% of the CED of heliostat field for the E&M phase is dedicated to the use of steel and 15% for the mirrors itself (other part is due to the tracking system, foundations, etc.). The authors remind also that the TES CED is composed of the steel from the storage tanks but also the supplementary quantity of HTF the plant needs to operates. Consequently, if a TES is installed, more HTF is needed, and this quantity is directly linked to the storage capacity.

To conclude this part about the LCA of a CSP tower plant, we can compare these results with the ones of a PTC plant. Results from Rembrandt Koppelaar, IIER, demonstrated a CED for a 1 GW plant of about 31 PJeq and 117 PJeq with molten salt and 12h storage. If we compare

Subsystem of the plant	part of the CED in E&M [%]
Heliostat field	70
Central receiver	18
TES	7
Facilities	3
Power block	2

Table 3.3: Cumulative energy demand repartition for the E&M phases of the CSP tower plant with a biomethane CC according to Corona et al. [5].

to the 115MW plant exposed before (see table 3.2), we could multiply the numbers proposed by 0.115 (115 MW divided by 1000 MW) which gives a range of 3,565 to 13,455 PJeq. The 5.5 PJeq found before for the CSP plant of 6 hours storage capacity (see 3.2) is therefore in a good range. Two things should be notified between these CSP technologies: the PTC plant used much more HTF since the HTF flows in the whole field, but doesn't have a huge tower-receiver system. In our comparison, the PTC plant used 527 thousand tons of HTF (12h storage), which is about 61 thousand tons at 115 MW scale. The CSP tower plant uses 17 thousand tons of HTF [40] (6 hours storage). So, it seems normal to have a higher CED for PTC than for a CSP tower plant since the mining of the HTF requires 20.8 TJeq/tons according to the study of Rembrandt Koppelaar, IIER.

3.3 The EROI computation and the primary energy factor

This section analyses in details the computation of the EROI and the utility accorded to the primary energy factor (PEF, α in the equations) for the EROI computation.

3.3.1 The EROI computation

The EROI factor could simply be defined by:

$$EROI = \frac{\text{Energy}_{\text{delivered}}}{\text{Energy}_{\text{consumed}}} = \frac{\text{Out}}{\text{Inv}}$$

The units for the denominator (Inv, the energy consumed) are given in primary energy equivalent by the LCA analysis. The units for the numerator are initially given in electricity which represents the production of the plant (that will be given by the model).
Indeed, the EROI does not consider any other inputs as it is a net energy analysis, see the figure 3.3.

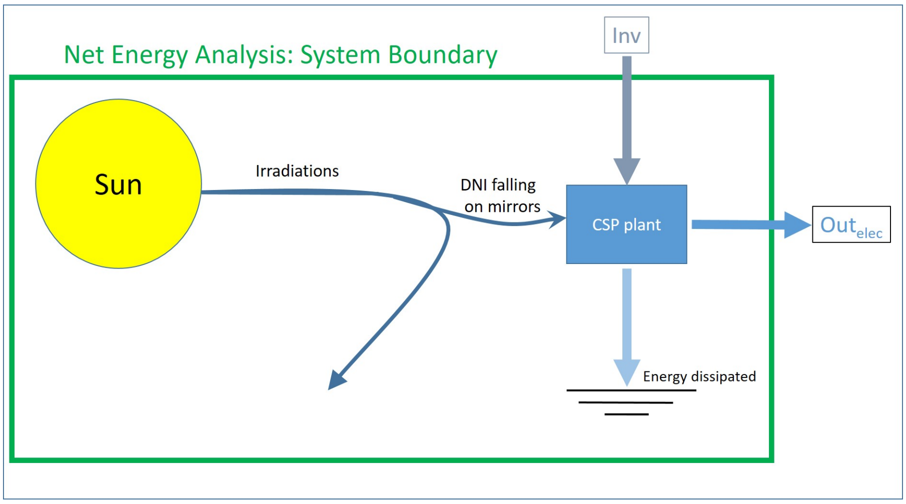

Figure 3.3: Definition of the system boundary for the EROI computation. Inspired from an IEA report of 2016 about guidelines and methodologies for net energy analysis [41].

Nevertheless, two major types of EROI exist: one considering the numerator as electricity and the other considering that the numerator should be transformed in primary equivalent energy.
It is in this context that the primary energy factor (PEF) appears, to convert the numerator in primary energy equivalent.

3.3.2 The Primary Energy Factor (PEF)

The PEF is defined as:

$$PEF = \alpha = \frac{\text{global electricity generated}}{\text{primary energy fuel inputs for electricity generation}} \tag{3.1}$$

and then, multiplied to an electricity quantity, gives the fossil fuel necessary to produce it. The PEF depends of the energy mix defined in the zone considered.

The computation of the EROI in the following tests is done by the equation 3.2, setting the primary energy factor at the current value of the Europe region which is 2.5 according to the EU legislation [42].

$$EROI = \frac{\text{Production}_{life\ time} * \alpha}{CED_{LCA}} \tag{3.2}$$

The utility of this factor in the EROI computation is described in the following.

3.3.3 Utility of this factor for the EROI

As explained, the EROI factor could simply be defined by:

$$EROI = \frac{\text{Energy}_{\text{delivered}}}{\text{Energy}_{\text{consumed}}} = \frac{\text{Out}}{\text{Inv}}$$

The units for the denominator (Inv, the energy consumed) are given in primary energy equivalent by the LCA analysis. The units for the numerator (primary equivalent or electricity) are subject to discussion and both could be computed, see the table from the IEA presented at figure 3.4.

Metric	$EROI_{el}$	$EROI_{PE\text{-}eq}$
Formula	$\frac{Out_{el}}{Inv}$	$\frac{Out_{PE\text{-}eq}}{Inv} = \frac{\left(Out_{el}/\eta_G\right)}{Inv}$
Units	[MJ / MJ]	[MJ / MJ]
Meaning of the numerator	Energy delivered ('returned') to society, in units of electricity	Energy delivered ('returned') to society, in units of *equivalent* primary energy
Meaning of the denominator	Sum of energy carriers diverted from other societal uses (excluding energy delivered to society), in terms of their total primary energy demand	

Figure 3.4: Two different methods to compute the EROI, as presented by the IEA report of 2016 about guidelines and methodologies for net energy analysis [41].

The IEA, in this report [41], analyses the PV technology and recommends to use the primary equivalence of the numerator:
"The approach that is recommended here follows a replacement logic akin to that used in LCA, whereby one unit of energy carrier delivered by any one technology is assumed to be equivalent to the primary energy that is cumulatively harvested from the environment by the current mix of technologies deployed in a given country or region in order to produce the exact same unit of energy carrier (e.g., that country's or region's grid mix in the case of electricity)" [41].

So, as explained in this study of IEA about guidelines for net energy analysis [41], the $EROI_{PE\text{-}eq}$, of the CSP technology in our case, evolves with the change of the technology itself, but also according to the gird evolution, which is assumed to be partly replaced.

Since this work study the integration and valorization of the CSP technology potential deployment in a grig being transformed, the fossil primary equivalent units (i.e. the use of the PEF) for the numerator will be chosen.

From the moment, we have:

$$EROI = \frac{\text{Production}_{life\ time}}{CED_{LCA}} \qquad \frac{\text{Final Energy}}{\text{Primary Energy}}$$

So, by using the PEF factor, we can compute the EROI as:

$$EROI = \frac{\text{Production}_{life\ time} * \alpha}{CED_{LCA}} \qquad \frac{\text{Primary Energy}}{\text{Primary Energy}}$$

3.3.4 Another vison of the PEF

We can in fact see the $EROI_{PE\text{-}eq}$ as a ratio of primary or final energy:

$$EROI_{PE\text{-}eq} = \frac{\text{Primary Energy}}{\text{Primary Energy}} \quad \text{or} \quad \frac{\text{Final Energy}}{\text{Final Energy}}$$

The EROI could be computed, splitting the CED in an electricity part and fossil part, using the PEF. Indeed, the PEF is used in the CED derived by LCA analysis.

For example, in the analysis of Rembrandt Koppelaar, IIER, which was used in the LCA part (see Section 3.2) the author points out that: "All energy values are expressed in primary equivalent with electricity corrected by a factor based on global electricity generated and primary energy fuel inputs for electricity generation", which is in other words the PEF.

By computing the EROI with this form of the CED, it becomes:

$$
\begin{aligned}
EROI &= \frac{Energy_{delivered}}{Energy_{consumed}} \\
&= \frac{\text{Production}_{life\ time}}{(CED_{LCA})_{electricity}} \\
&= \frac{\text{Production}_{life\ time}}{CED_{LCA} * \frac{1}{\alpha}} \\
&= \frac{\text{Production}_{life\ time}}{(\text{CED}_{\text{electricity}} * \ \alpha + \text{CED}_{\text{fossil fuels}}) * \frac{1}{\alpha}} \\
&= \frac{\text{Production}_{life\ time}}{\text{CED}_{\text{electricity}} + \text{CED}_{\text{fossil fuels}} * \frac{1}{\alpha}}
\end{aligned}
$$

Then, we can write:

$$
EROI = \frac{\text{Production}_{life\ time}}{\text{CED}_{\text{electricity}} + \text{CED}_{\text{fossil fuels}} * \frac{1}{\alpha}} \quad \frac{\text{Final Energy}}{\text{Final Energy}} = \frac{\text{Production}_{life\ time} \ * \ \alpha}{CED_{LCA}} \quad \frac{\text{Primary Energy}}{\text{Primary Energy}}
$$

So, using the PEF (α) is equivalent to simply transformed the fuel consumption of the plant (from construction, transports, etc.) into electricity, which allows to obtain a ratio of final energy.

3.4 Summary and conclusion about the EROI and LCA parts

The choice of this study is to optimize the plant according to the EROI factor. Indeed, it is more relevant to optimize the EROI, rather than the production, as the net energy has a higher importance in the context of an energy transition and scarcity of resources.
The EROI could be studied for the whole life cycle of a plant, considering its energy cost (construction, operation, dissembling) and energy production. This is a static analysis. The EROI could also be studied from a more global point of view, considering the technology's evolution and resources quality of lands. This is a dynamic analysis.
In the EROI computation, the primary energy factor is used to have a ratio of only primary equivalent energy. Indeed, we want to consider the EROI in the context of a grid evolution. The primary energy factor is set to 2.5 (official EU value [42]).
To complete the EROI analysis, it is necessary to be able to compute the energy cost of a plant, which was done in the previous LCA section. It was found that the Extraction & Manufacturing and the Operation & Maintenance parts have the highest energy cost. For the E&M phase, the heliostat field accounts for 70 % of its total. From there, we should be able to compute the energy cost of any plant. This methodology is explained in the next chapter about the plant simulation model.

4 Construction and validation of a model to evaluate the production of a CSP tower plant depending on its location

This chapter describes the methods used to implement a model able to compute the annual production of a plant for a given location on earth. Moreover, the model computes the EROI of the plant, depending on the configuration of this plant.
The location influences the direct irradiations (DNI) level received, and consequently, as seen in Chapter 2, critically impacts the production. The objective of the model is to compute the number of operating hours in a year, depending on the DNI level (and so the location) and the configuration of the plant. From there, the plant production and EROI, given the configuration of the plant, could be computed.
First, the model to compute the hourly DNI level for a given location is described, and then, the plant model is covered and the whole is validated.

4.1 The sun irradiations model

As we want to know the number of hours per year the plant is operating for a given location, we need to find hourly data of direct irradiations for any locations in the world. The usual data, easy to find and reliable, are given by monthly average of global radiations. The ones used here come from NASA and are an average of 22 years of measures [43]. These data are reliable (22 years average) and available for any location on earth at one degree of latitude and longitude accuracy. The goal is to transform these data into hourly average irradiations. This subsection presents the method implemented.

The method is inspired by the review of Zhang et al. [7] describing the design methodology of a plant and completed from Willian and Geyer book [44] and a course from KTH about solar engineering [45].

From the monthly average global irradiations (diffuse plus direct irradiations), from the NASA, we will retrieve the hourly average direct ones. The first step is to find the monthly average clearness index. This factor indicates the proportion of radiations that effectively reach Earth crust from the top of atmosphere. Then, the daily global irradiations are computed from a daily distribution of this clearness index. After that, we separate the direct and diffuse beams and spread them on a day.

4.1.1 step 1: Finding the average clearness index

The clearness index (K), is defined by the quantity of global irradiations reaching Earth crust (H) from atmosphere (H_0):

$$K = \frac{H}{H_0}$$

The average global irradiations reaching Earth is given by the data from NASA and the average global irradiations on the top of atmosphere is computable by [44] [45]:

$$H_0 = (24 * 3600/\pi)\, G_{sc}\, dr\, [cos\phi cos\delta sin w_s + w_s sin\phi sin\delta] \qquad [\text{J/m}^2\text{day}]$$

This expression depends on the day of the year and so H_0 evolves during the year. ϕ is the latitude angle (rad), δ the declination angle (rad), w_s the sunset hour angle (rad), G_{sc} the solar constant for irradiations received on top of atmosphere for a perpendicular surface: 1367 $[W/m^2]$ and dr the inverse relative distance sun-earth which is equivalent to: $1 + 0.033cos(2\pi n/365)$ with n the number of the day in the year.
From there, computing H_0 for the month to find the monthly average, we can retrieve K_{av} for the given month since H_{av} is known from the data.

4.1.2 step 2: Using the monthly average clearness index to find the daily irradiations

From Zhang et al. [7], the average monthly clearness index K_{av} is used to define a minium and maximum one on a day, allowing to define a distribution of an average daily clearness index. The method was established to fit for each region of the world as the location only really impact the monthly average and that the distribution of this latest is similar everywhere.
K_{min} is defined as 0.05 and $K_{max} = 0.613 + 0.267K_{av} - 11.9(K_{av} - 0.75)^8$. The daily clearness index is then computed by:

$$K_{daily} = \frac{1}{\gamma}\left[\ln\Big((1-\alpha)\, e^{\gamma K_{min}} + \alpha\, e^{\gamma K_{max}}\Big)\right]$$

with $\alpha = \frac{n_d - 0.5}{n_{dm}}$ knowing that n_{dm} is the number of days in the month and n_d the number of the specific day studied in this month ; $\epsilon = \frac{K_{max} - K_{min}}{K_{max} - K_{av}}$ and $\gamma = -1.498 + \frac{1.184\,\epsilon - 27.182e^{-1.5\epsilon}}{K_{max} - K_{min}}$.
From there, the daily irradiations is computed from the formula used in step one:

$$H_{daily} = K_{daily} * H_{0\ daily}$$

.

4.1.3 step 3: Estimation of the hourly diffuse and direct irradiations

The goal now is to compute the daily diffuse irradiations, to transform it on daily data, as the global one, and to obtain the direct hourly irradiations by subtracting the diffuse hourly to the global hourly irradiations.
To compute the daily part of diffuse on global irradiations, the following process proposed by Zhang et al. was implemented:

if $w_s < 81.4°$

$$\frac{H_{diffuse\ daily}}{H_{daily}} = 1 - 0.2727K + 2.4495K^2 - 11.951K^3 + 9.3879K^4 : \quad \text{if } K_{daily} < 0.715$$

$$\frac{H_{diffuse\ daily}}{H_{daily}} = 0.143 : \quad \text{if } K_{daily} > 0.715$$

if $w_s > 81.4°$

$$\frac{H_{diffuse\ daily}}{H_{daily}} = 1 + 0.2832K - 2.5557K^2 + 0.8448K^3 : \quad \text{if } K_{daily} < 0.715$$

$$\frac{H_{diffuse\ daily}}{H_{daily}} = 0.175 : \quad \text{if } K_{daily} > 0.715$$

From there, the method of Thamn et al.[46] allows to distribute the daily to hourly irradiations for the diffuse radiations:

$$I_{hourly\ diffuse} = H_{diffuse\ daily} * \text{ratio}_d = H_{diffuse\ daily} * \left[\frac{(\pi/24)(cosw - cosw_s)}{sinw_s - w_s cosw_s} \right]$$

and for the global radiations:

$$I_{hourly} = H_{\ daily} * \text{ratio}_g = H_{daily} * \left[(a + b\ cosw)\ * \left(\frac{(\pi/24)(cosw - cosw_s)}{sinw_s - w_s cosw_s} \right) \right]$$

with w the sun hour angle (rad) and $a = 0.409 + 0.5016\ sin(w_s - \frac{\pi 60}{180})$ and $b = 0.6609 - 0.4767\ sin(w_s - \frac{\pi 60}{180})$. Then direct hourly irradiations are simply computed by:

$$I_{hourly\ direct} = I_{hourly}\ - I_{hourly\ diffuse}$$

.

4.1.4 Results

Here are presented the results obtain for Tucson USA location. The direct irradiations falling on a tracking plane surface (beam irradiations) is represented for a year (see figure 4.1), a month (see figure 4.2) and a day (see figure 4.3).

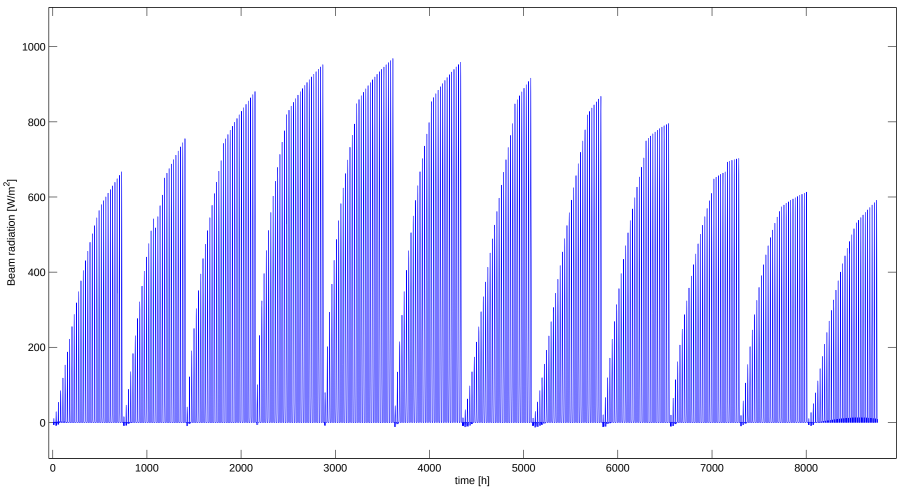

Figure 4.1: Beam radiations results for Tucson USA, on a year. The month values are ranked by the worst to the best day of the month. Each pick corresponds to one month.

On figure 4.1, the yearly variations are clearly visible. The summer occurs in mid-year (June-August), since Tucson is in the North hemisphere, and the direct irradiations is higher for this period.

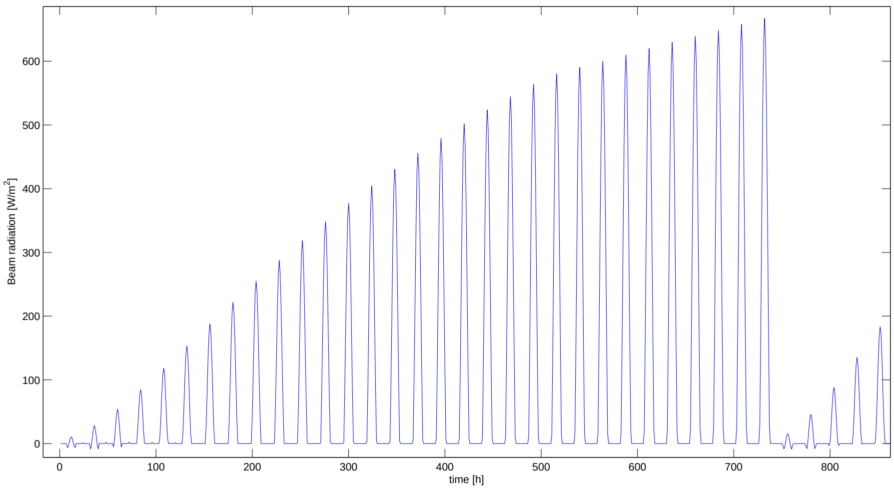

Figure 4.2: Beam radiations results for Tucson USA, on a month. The month values are ranked by the worst to the best day of the month. This plot is a zoom on the first pick of the radiations on a year, figure 4.1.

The month values, see figure4.2, for January (from h = 1 to 744), are ranked by the worst to the best day of the month. It could be seen that the amplitude differences between the best and worst day is quite high, meaning that clouds have a high impact on direct irradiations. This is why a clear sky model could not be implemented: these models take into account the year evolution (since they compute the distance earth-sun among others) but not the sky conditions (clouds) since they work with the atmosphere chemical composition. Here, these effects of clouds are taken into account thanks to the clearness index, which varies with the sunset hour angle and so, location and date.

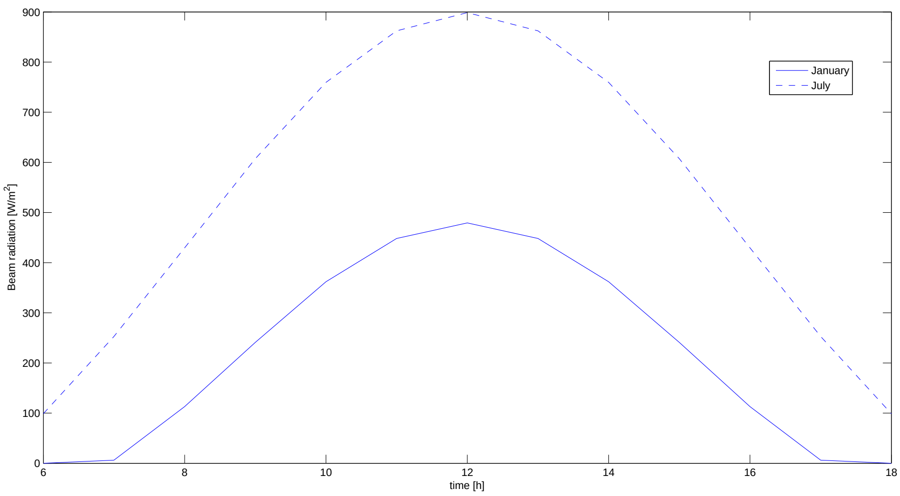

Figure 4.3: Beam radiations results for Tucson USA, on the 15th of January and July depending on the solar hour.

The figure 4.3 highlights the seasonal difference in a day between summer and winter. The distribution, in a day, reachs always its maximum at a solar hour equals to 12h00, meaning that the sun is at its highest position in the sky.

4.2 The plant model

4.2.1 Simulation: goal and parameters

The goal is to compute the electricity produced, as well as the EROI, for a plant of a given configuration and location. The plant is composed of a tower, a solar field, a storage system and a power cycle. The solar field is disposed around the tower as a circle. The HTF transfers the heat from the receiver to the power cycle and its energy is stored if needed. The model inputs are only the DNI data computed by the method previously described.

First, the solar field modelization is presented. Then, the technology considered, mainly about receiver and power cycles parts of the plant, are covered. Afterwards, the algorithm used to simulate the plant (i.e. compute the annual production) is explained. To conclude, the formula used to compute the EROI of a plant, depending on its configuration, is presented.

4.2.2 Characterization of the solar field

To characterize the plant, an important parameter is the total aperture area (total reflective surface), which is the number of heliostats multiplied by the surface of each of them. The goal number one is to determine the total aperture area of the plant necessary to, at conditions to discuss, reach an output power which is equal to the designed power.

First, it is necessary to define the DNI level at which the computation of the aperture area occurs: the DNI level varies during the day but the number of heliostats does not. From the mean DNI value in the year, the area of mirrors needed to achieve the power set could be found. Firstly, the total power transmitted to the heat transfer fluid (HTF) should be known. Then, knowing that this heat is transmitted to the power cycle, we can find the enthalpy expansion in the turbine and derived the total area.
The link between the area of mirrors and the energy transmitted to the HTF could be written by:

$$\text{Aperture}_{total}\ \eta_{field}\ \overline{DNI} = (\dot{m}_{HTF}\ \Delta T_{HTF}\ cp_{HTF})\ \frac{1}{\eta_{tower}}$$

We can retrieve the energy absorbed by the HTF by linking the energy used in the power cycle part, skipping the storage part (which anyway has a high energy efficiency):

$$\dot{m}_{HTF}\ \Delta h_{HTF} = \dot{m}_{steam}\ \Delta h_{steam\ generator}$$

and compute the mass flow of steam by linking it to the parameter of the plant, the designed power:

$$\dot{m}_{steam} = \frac{\text{Power}_{designed}}{\Delta h_{steam\ turbine}}$$

In the end, the equation to find the aperture area could be written by:

$$\text{Aperture}_{total} = \frac{\text{Power}_{designed}\ \Delta h_{steam\ generator}}{\eta_{tower}\ \eta_{field}\ \overline{DNI}\ \Delta h_{steam\ turbine}} \tag{4.1}$$

In the program, the enthalpy values are computed by the function *Janaf* if the cycle uses CO_2 and *XSteam* for the steam. The temperature and pressure levels of the power cycles are determined by the type of power cycle which are described further.

As it could be deduced from the equation 4.1, the aperture increases linearly with the power designed and decrease linearly with the mean DNI. In reality, the total field area is always higher than the one found to be able to produce the designed power. The real aperture area is equal to the one found multiplied by the Solar Multiple, which is, in general, comprised between 1.5 and 2.7 [47] and is a parameter to optimize.

The total area of the plant (space between mirror considered) is found by a rule of thumb: it is equal to the field aperture total area multiplied by 6. From the data of the NREL projects list [6], for the Gemasolar (20MW) and the Dune project (110MW), a ratio of 6.39 and 5.4 is found respectively and for the hypothetic project of the LCA analyses [40] the ratio is about 6.2. From the total area, the radius of the field, which is describing a circle around the tower, is computed by: radius = $(\frac{\text{Total field surface}}{\pi})^{\frac{1}{2}}$ since the field is assumed to have a circular layout. In the program, if the radius exceeds 1500m, the solar multiple is reduced in order to stay to the maximum radius of 1500m, which is a general rule [5]. In fact, if the field is bigger than with a radius limited at 1500m, the field efficiency decrease rapidly, not only because of the distance (and so higher atmospheric attenuation) but also due to the disposition of the mirrors, which is less optimized (see figure 4.4).

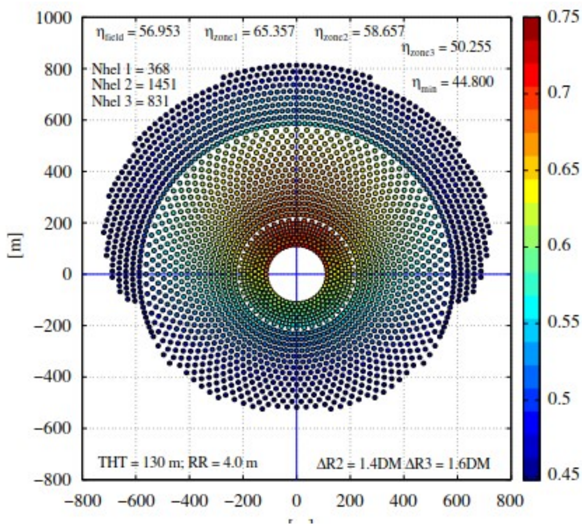

Figure 4.4: Representation of a heliostat field, see efficiency of zone 3, the furthest ; from Collado et al. [13].

In reality, the larger the solar field is, the less its optical efficiency. From the field analyses of [17], we can retrieve the distance impact on the optical efficiency from the diminution of the attenuation efficiency. As explained in this source, until 1000 m the attenuation efficiency decreases slowly and from 1000 to 1500 m decreased faster. The code calculates the impact of the distance depending on the radius of the field. A decrease of 3% is obtained for a radius of 1000 meters. A linear function decreases this ratio in the program from 500 to 1000 meters. If the field radius is higher than 1000 meters, the decrease is 3% (from the previous part, up to 1000m) plus another part, which is for example 5% for a radius of 1500 meters.

4.2.3 Technology and power cycle

The technology is based on the molten salt one with a tubular receiver. The salt is a mix of 60% Sodium Nitrate and 40% Potassium Nitrate. In the receiver, the salt is raised from 288°C to 565°C. The characteristics of the power cycle, steam Rankine cycle, are described in the first column of the table 4.1. The efficiency range is large since the model is built to use this technology combination to 2035. After this date, a switch is operated to the second cycle of the table: also steam cycle but which take into account an improvement of the receiver. The receiver is now able to heat solid particles and the outlet temperature would be up to 800°C. In this case the efficiency of the power cycle is higher. In the end, another cycle, also with solid particles receiver technology, is taken into account to follow the potential evolution of the design of a CSP tower plant. Each year, the efficiency of the solar field and tower receiver increase also according to a certain methodology. The different impacts about technology evolution according to time will be describe in the last chapter. The goal here was to describe the first type of plant from which the results and optimization are performed in the next chapter.

	$Steam\ Turbine$	$Steam\ Turbine$	CO_2
Technology	Molten Salt	Solid Particle Receiver	Solid Particle Receiver
High T [°C]	540	580	700
Low T [°C]	25	25	50
Pressure [MPa]	13	24.2	25.0
Yield range	35-45	40-50	45-55

Table 4.1: The three types of power cycles used in the model, adapted from the previous cycles presented at Chapter 2, see table 2.5. The values shown are the one of the working fluid in the power cycle (not the HTF).

4.2.4 Storage system implementation

The storage method used is based on the current technologies. The thermal storage system, used in combination with HTF, which is molten salt in our case, is composed of a hot and cold tank. The hot tank stores the fluid if its temperature exceeds the one needed at the heat exchanger between the HTF and the power cycle. The storage system is described by three important parameters:

- its maximum capacity
- its efficiency to deliver energy
- the heat losses, in function of time, during the storage

During the storage, thermal losses occur through the walls of the tank. In the model, we are interested to know the power losses by the molten salt stored in the hot tank, to know the energy degradation of the salt. A study of the Heat and Mass Transfer Technological Center of the UPC [48], analyzed by numerical modelling the heat flux and temperature loss occurring in the hot tank of the Andasol CSP plant. Their methodology consisted to consider separately the different elements of the storage system (the tank walls, the foundation, the molten salt media, etc.). They were solved separately and then linked to each other. The principal effects considered were the convection between the molten salt surface and the walls, the radiation between free surface of molten salt media and the surroundings and the natural/forced convection of the molten salt within the tank. At 288K (about 565°C, the temperature set for the molten salt in our case) they found a loss about 1K per hour. Knowing that the power loss in the storage is directly proportional to the temperature, lead to set a loss of:

$$\gamma_{losses} = (1 - \frac{287}{288}) * 100 = 0.34 \qquad [\%/h] \tag{4.2}$$

It seems quite low. But, if we imagine the tank as a big thermos, with walls of steel, two times 10 cm, and an interlayer of air, this result appears in a good range. Indeed, by computing the only conduction occurring in, we can found a temperature difference after one hour, imagining that one meter cube of salt has a surface contact of one meter square on the wall. The energy flow in one hour should be equal to the energy loss in the media ($c_p * \Delta T * mass$). The difference in temperature after one hour is a way smaller than one degree. By adding the convection and other losses by radiation and taking into account the foundation, we can imagine that achieving a one degree loss by hour is realistic. In a study from the National Renewable Energy laboratory [47], to modelize the TES system, they used a $\gamma_{losses} = 0.031$ [%/h] ; this value seems a bit too low and the reference does not seem really convincing. In the code, the value found with the equation 4.2 is implemented.

The maximum capacity is defined by the number of hours the storage system is able to provide energy to operate the power cycle at the designed power. This parameter is defined before executing the program and will be part of the optimization process as one of the most important parameters. The efficiency to deliver energy is about 98-99% for a thermal storage and is fixed in the program. The parameters used in the code are summarized in the table 4.2.

Storage Parameters	
Losses [%/h]	0.34
Maximum capacity [h]	0-40
Efficiency to deliver energy [%]	98

Table 4.2: The main parameters used to characterize the storage system in the code.

4.2.5 Electricity production computation

First, the data of the DNI are extracted from the previous model for the given location. The goal is then to compute the number of hours the plant is operating during the year. From there, the total produced electricity is computed. Thanks to the data on the production and the given configuration of the plant, the EROI could be computed. In the next paragraph, the methodology pursued is presented and could be followed on the scheme (see figure 4.5).

First the location is chosen, as well as the three configurations parameters, which are: the designed power, the storage capacity and the solar multiplicator.
The designed power set is taken into account to found the size of the solar field, following the methodology described before. As well, each hour of the year is linked to a DNI data (see *DNI Function* on the scheme 4.5). Then, from the solar field characteristics and its optical efficiency defined for the year chosen, the power reaching the tower is computed. Then, the efficiency of the receiver is taken into account to know the power that we are able to have at the heat exchanger, without regarding the conduction losses. If this power is greater than the designed power divided by the efficiency of the power cycle, then, the overage is sent to the hot tank to be stored (if the maximal capacity of the storage tank is not reached). If the power computed before is too low, but able to operate the turbine at minimum half of its full load, this power is sent to the turbine. Moreover, if the storage is not empty, a part of its power (or everything if needed) is sent with the other power flow to reach the full load turbine operation.

It is important to understand that at each iteration per hour, the storage is updated (see *Storage* on the scheme 4.5) since the degradation of its thermal energy should be taken into account. The program considers days of 24 hours. After 18h (hour solar), no DNI resources are available until five in the morning. Then the plant is able to run only if the storage is not empty during this period and that its capacity is able to run the turbine at a minimum of half of its full

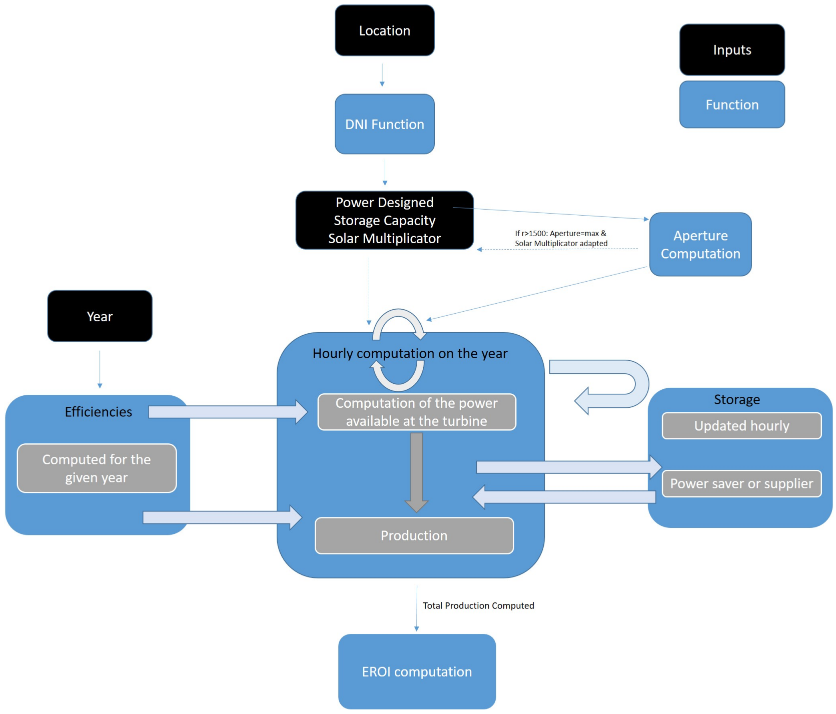

Figure 4.5: Representation of the main steps of the model. From the plant's parameters and location the total production and the EROI are computed.

load. The plant is then always operating as the molten salt was hot enough, even at the start. This assumption is allowed since in reality a gas or electricity boiler is used to warm the salt when needed. This electricity is taken into account in the LCA and so the method is viable.

In the end of the year, the total production is known by summing the number of hours at which the plant was operating. If the turbine was operating at 3/4 of its load, the hour during this iteration is set as 3/4 and the total sum of the vector on the year give the number of hours at which the turbine was operating at full load. Then, multiplying by the designed power, the electricity production is found.

4.2.6 EROI Computation

The model presented defines the energy production on a year. Nevertheless, to be able to compute the EROI, we need to define the total energy that was necessary to build and operate the plant during its whole life cycle (CED). Then, the data from the LCA (see Section 3.2) were used to compute the equivalent energy necessary. The goal is to adapt the energy cost of the plant to its characteristics.

In table 4.3, the different methods to compute the energy necessary for each phase of the LCA are presented. The method is based on the numbers found by the LCA study presented before [40] which applied to a 110 MW plant located in USA Tucson. From this study, we know the energy allocated to extraction & manufacturing (E&M), construction (C), operation & maintenance (O&M) and dismantling and decommissioning (D&D). The other LCA study [5] allows to decompose the CED part due to E&M between the different components of the plant. From there, in general, the CED applied to a specific plant is composed by linking it to a linear relation with the designed power characterizing the plant. This method is simple but logical: the plant design is based on the power to deliver and the design impose the size of the plant which is related to the quantity of energy needed which is here linked by a linear relation. This

LCA parts	distribution [5]	CED [MJeq], 110 MW plant [40]	adapted to other plant
	70% heliostat field	202202 / mirrors	$CED*$ number mirrors
	18% tower & receiver	347 429 433	$CED*(0.5+0.5*\frac{power_{designed}}{110\ MW})$
E&M	7% storage	22 518 574 / hour storage	$CED*(\frac{power_{designed}}{110\ MW})*n\ _{h\ storage}$
	3% facilities	57 904 905	$CED*(\frac{power_{designed}}{110\ MW})$
	2% power block	38 603 270	$CED*(\frac{power_{designed}}{110\ MW})$
C	100%	204 370 230	$CED*\frac{power_{designed}}{110MW})$
O&M	94% for boiler to regulate salt temperature	3 292 631 910	$CED*(2.5/3.4)*(\frac{power_{designed}}{110\ MW})$
D&D	100%	138 517 590	$CED*(\frac{power_{designed}}{110\ MW})$

Table 4.3: Summary of the formula used to compute the CED of a given plant, depending on its configuration. The EROI is then computed from this value and the total energy production of the plant. The CED increases lineraly with: the power designed, the storage capacity and the number of mirrors.

approximation is used for all parts, except for the heliostats field tower CED in the E&M. For this part, the size is computed by the number of heliostats which is defined by the previous part of the code. For the tower and receiver CED, half of the value is taken as a fixed value and the other varies with the size of the plant. The O&M phase considers the different values between the grid electricity between USA (3.4) and Europe (2.5). From there, we can retrieve the total CED for any specific CSP tower plant and so the EROI is computable for any plant at any location.

The lifetime considered to compute the EROI is the same as the one from the major LCA study [40]: 30 years. The factor (α) is set to 2.5 (value set by EU legislation [42]) and represents the primary energy factor. From there, the EROI is simply derived as:

$$EROI = \frac{\text{Production}_{life\ time}\ *\ \alpha}{CED_{LCA}}$$

4.2.7 Parameters

The table 4.4 summarized the important values considered in the simulation. The values in italic will be optimized in the next chapter. Moreover, these parameters, all the efficiencies (for the optical, receiver and power cycle parts) are set to normal value and will grow as explained before, depending on the year. For the simulation's results, the efficiencies considered (for the optic, receiver and power cycle) will be cited.

General ones	*Designed Power*	20-150	[MW]
	Parasitic load	7	[%]
	Radius max	1500	[m]
Field Parameters	*Solar Multiplicator*	1.5-3	[-]
	ratio mirrors/total surface	6	[-]
	Area of one mirror	13*11	[m^2]
Storage Parameters	*Maximum capacity*	0-40	[h]
	losses	0.34	[%/h]
	Efficiency to deliver energy	98	[%]
EROI	lifetime	30	[years]

Table 4.4: The main parameters and the fixed ones. The ones in italic are expected to be optimized.

4.3 Validation

The goal of this section is to compare the production resulting from the simulations with real plants production.

The idea is to enter the configuration data of the plant as well as its position, and then, compare the real and simulated production on a year. Indeed, from the power designed, the size of the heliostat field and the storage capacity, the simulation should give a near approximation of the real value produced. In fact, in the simulation program, there are still some unknow parameters as the effeciency of the different componenents. Classical values presented in Chapter 2 were tested.
If the simulation gives a good approximation of the real production with commonly observed efficiencies, the all simulation model is considered as validated.

Finding accurate data for operating CSP tower projects is not easy for numerous reasons. The main reasons are that:

- few commercial operating projects exist
- often, the expected electricity produced is given instead of the real current production
- precise information about the solar field should be given (aperture area)
- as well, the storage capacity and power designed should be given (but it is always the case if previous points are completed)

Thanks to the website of the US Renewable Energy Laboratory (NREL) [9], most of these informations could have been found for several projects. Three projects were selected (in fact, not many more could have been chosen) and the informations needed are summarized in the table 4.5. The current production of the US plant is (much) lower than the one expected by the owners. In fact, it is normal, since during the first years of operation, the calibration of all components and optimization process are performed. But, there is schedule set to reach the normally output power designed and for some projects the reality is currently lower than the expectations and only the future could say if the design was wrong or if it needed more time than expected to fully operate.

The Gemasolar plant, the first commercial CSP plant of the world, is a well-known project from which the detailed data are easy to find. It was then evident to choose it. Moreover, it will allow to validate the model for a small scale CSP plant.
The Ivanpah, a three towers project, started production in 2014. From 2014, the announced production was never reach, and, currently, the production is below one third of the expected one, mainly due to technical problems and design un-expectations [1]. This project is quite criticized for the non-use of storage capacities and utilization of natural gas. This plant allows to test the model on a-large plant without storage capacities.
The Huanghe project, in China, is one of the numerous CSP projects of China. This two towers project is the first part of a large scale project: six towers will be constructed in total, for an equivalent surface of 27 km^2 [2]. This project does not produce electricity yet, but will start to produce at the end of 2017. It will allow to test the model for another continent, on a large scale plant and with few storage capacities.

	Gemasolar	Ivanpah	Huanghe Qinghai
Location	Sevilla, SP	California, USA	Qinghai, China
Number of Towers	1	3	2
Start production year	2011	2014	end 2017
Power designed [MW]	19.9	125 (*3)	135 (*2)
Aperture [m^2]	304 750	2 600 000 (/3)	unkn., 13 km^2 (/2) total area
Storage capacity [h]	15	none, gas backup	3.7
Electricity production [GWh/y]	80	1079.232 (/3), expected	628.448 (/2), expected

Table 4.5: Information of current operating CSP tower plants and one Chinese project in construction. The data were taken from the website of the US Renewable Energy Laboratory (NREL) [9] and values are given for one tower or for the total project.

	Gemasolar	Ivanpah	Huanghe Qinghai
Operating time at full load [h/year]	3836	1580	2300
Electricity production [GWh/y]	79	205 w/o backup, 259 w/ (*3)	310 (*2)
Optical eff [%]	67.19	64.37	63.48
Receiver eff [%]	90	90	90
Power cycle eff [%]	35	40	39

Table 4.6: Results obtained by the model according to certain efficiency settings.

The optical efficiency is computed by the program, from a basic value (70%) which then varies (is reduced) with the size of the solar field, as explained in the previous section. For the

[1] see, among others: https://www.greentechmedia.com/articles/read/ivanpah-solar-plant-falling-short-of-expected-

[2] And this is only a part of China CSP program, see https://www.nrel.gov/csp/solarpaces/by_country_detail.cfm/country=CN.

recent projects, higher power cycle efficiency could be accorded because of the utilization of a hybrid cooling system, or a higher pressure of the working fluid or depending of its size. The best suited values were set for the tests. From there, if the value of the simulated production is highly different, a discussion should be perform to understand from where it comes.

The results obtained for the Gemasolar plant are in good agreement with the real plant. Indeed, the optical efficiency is high (since the field is small) and the power cycle efficiency has an appropriated value for a first CSP plant.
The power produced by the model, for the Ivanpah project, is smaller than the 359 GWh expected per plant. Indeed, without any backup and storage system, it is normal to find a low value. The backup system was simulated by authorizing the turbine to run, even if the power at its entry was not enough to operate it at half load (as constrained normally) and, moreover, the turbine operates at full load, considering a power supplied, to the HTF, by the gas turbine. From there, 260 GWh could be produced. The 359 MWH are not reached, but, by optimizing the gas utilization in the program (which normally do not consider backup systems), a higher value could certainly be found. Anyway, the real production for the moment at Ivanpah central is lower than the expected one, and, it is difficult to know if the expected production announced was exaggerated.
For the Chinese project, the aperture is found from the total surface, with the same ratio, 6, that is used in the program. The Chinese project is for its part really well simulated, since the parameters for the efficiencies are common values, and the exact power is found.

In conclusion, the model produced about 27% less than the expected value for the Ivanpah plants. In contrary, the correct production is reached for the Chinese and Gemasolar plants with good settings for the efficiencies parameters.

4.4 Summary and conclusion about the plant model

The construction of a model, able to compute the electricity production and EROI, for a specific CSP tower plant, was constructed and validated.

The model is based on the analysis of monthly average data from the NASA. From there, hourly DNI average values are computed. Then, the electricity production is calculated by simulating the plant comportment for each hour of a year.
The model has some hypothesis to keep in mind, as the simplified method using the efficiency for the conversion and not a thermodynamic simulation. As well, the simple storage implementation used and the highly used linear relation between the size and CED of the plant in the EROI computation should be remembered.

In the following chapter, static (no evolution of efficiency, study of one location) results are described, and the importance of each parameters is deeply analyzed.

5 EROI Static analysis: optimization of a plant depending on the location

In the previous chapter, the construction of a model, able to compute the electricity production and EROI of a specific plant, was presented. The model considers the location of the plant. The goal of this part is to optimize the EROI of the plant depending on its location.

First the importance of each parameters is studied and then an optimization process is proposed.

5.1 Analysing the results on a year

On figure 5.1, some results for a plant of 130 MW in Sevilla are shown. The number of hours operating at designed power and the DNI average are expressed per day. The DNI plot (curve with larger amplitude on the graph 5.1) is similar to the one presented previously (see figure 4.1) except that the day in the month were spread according to a realistic order, which is important for the storage evolution as we will see later. The pick appears in the middle of the year during summer as the first day corresponds to the first January, which is quite logical since we speak about direct radiations and a location above the equator. As it is demonstrated here, the number of hours per day producing at full load (lower amplitude on the graph 5.1) is completely dependent on the radiation level and follows its shape. For this plant configuration, the number of operating hours per day are about 10 hours in high season (summer) and 5 hours in low season (winter).

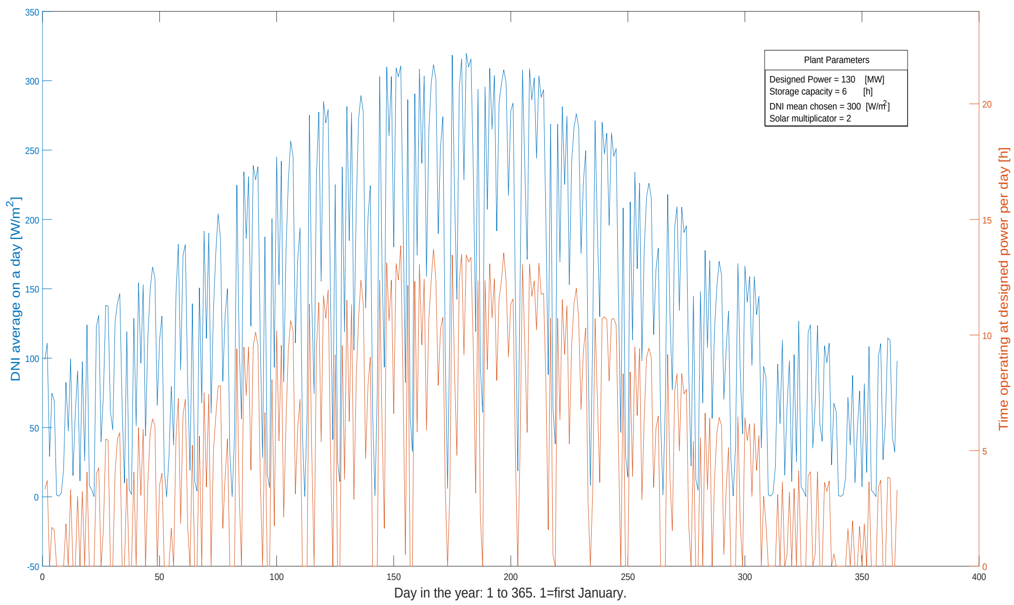

Figure 5.1: Time operating at designed power per day (lower amplitude, right axis and red curve on the graph) in hours in comparison with the average DNI on a day (higher amplitude, left axis and blue curve on the graph), for all days in a year in Sevilla.

In the following figures, the energy produced in one hour is plotted over a year for the same plant, in comparison with the one received and the one stored for the same hour.
In the figure 5.2, we can see that in average the energy produced is 5 times lower than the one supplied by the radiations. It would mean that the average energy efficiency is about 20% which is in accordance with the values seen in the previous chapters. The plant never produces more than the designed power (of the turbine) but sometimes less or not at all. In the summer, we can see that quite a lot of energy is stored. It would mean higher number of operating hours since the plant can operate with low DNI level and even without sun at all (evening). Regarding the previous plot 5.1, we can in fact confirm it. Moreover, looking at the energy production (red), we see that the production is more compact in summer, during high storage values. These results clearly highlight the importance of a storage system.

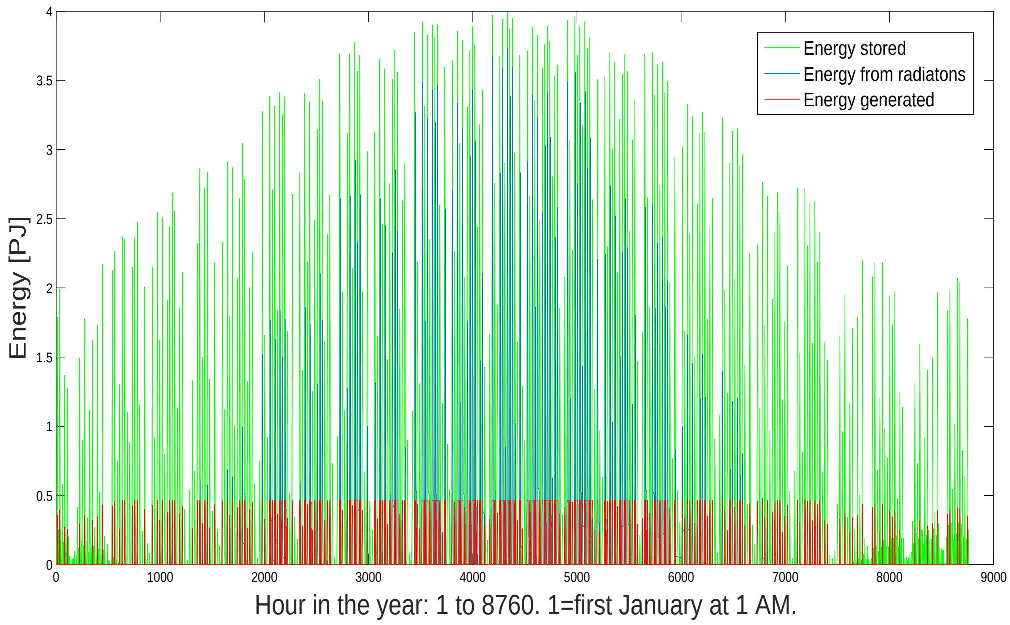

Figure 5.2: Energy produced in one hour (red), in comparison with the one received (green) and the one stored (blue) for the same hour, represented on a year. The plant is 130 MW in Sevilla with the same characteristics as in the figure 5.1.

As seen, the storage is an important factor to maximize the production. In the following, a focus is done to understand deeply the evolution and parameter influencing the TES system. The figure 5.3, a zoom of the previous plot which was on a year (figure 5.2), allows to highlight the storage evolution. As it could be seen, the model never store energy if the energy produced is smaller than the one designed (see the plateau of the red curve and compare it with the evolution of the blue curve). If this level is reached, the surplus of energy is stored and the total energy stored could reach high values, in the order of the one supply by radiations in one hours in this case. We can also conclude that the production is not smooth at all.

The figure 5.4 presents different typical comportments possible for the energy stored. Each pick represents a day. The first day allows to store energy after some hours of daylight and the energy stored increases from 1 am to the middle of the afternoon. After that, this energy is needed to reach the designed energy in one hour (designed power * 3600). At the end of the day the energy stored left is not high enough to operate the turbine during one hour at least half designed power. Then the energy is stored during all the night, decrease a bit since the isolation is not perfect, and is used with the first radiations of the next days. This next day is not so shinny and the production could not reach the condition to store energy. The third and fifth days prove the efficacity of the storage, which allows a constant production at full load during long hours. The central operates more as a on/off plant for these days, in the sense that, if there is production, it is at full load.

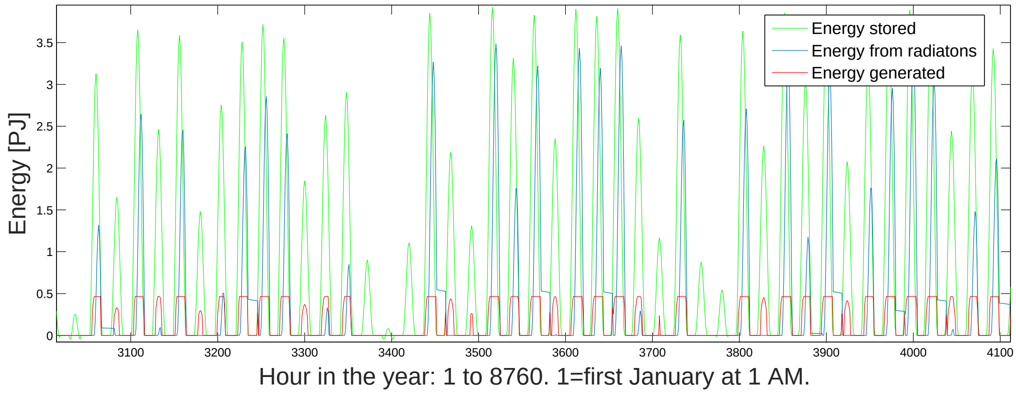

Figure 5.3: Energy produced in one hour (red), in comparison with the one received (green) and the one stored (blue) for the same hour, represented on a month scale. The plant is 130 MW in Sevilla with the same characteristics as in the figure 5.1.

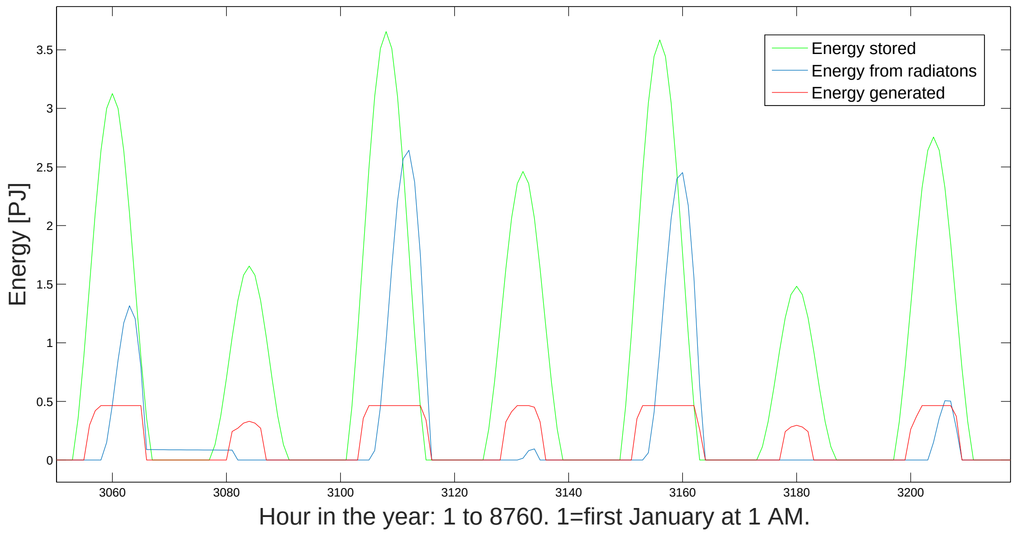

Figure 5.4: Energy produced in one hour (red), in comparison with the one received (green) and the one stored (blue) for the same hour, represented on a day scale. The plant is 130 MW in Sevilla with the same characteristics as in the figure 5.1.

5.2 Configuration for a base load plant

In the Chapter 3, we saw that the advantage of the tower technology was to be able to produce almost as a base load plant: 24h per day, for a capacity factor about 70% for the year. Indeed, if we configure a plant as a base load one, it is possible achieve high numbers of production hours keeping realistic parameters. As example, the configurations described in table 5.1 gave a high capacity factor.

Storage Parameters		
Designed Power	30	[MW]
Maximum storage capacity	24	[h]
DNI average	110	[W/m^2]
Solar multiplicator	2	[-]

Table 5.1: The parameters used to configure the plant as a base load one.

The idea is to reduce the designed power in a way to store a maximum and being able to use the stored energy during the night. The storage capacity is then set to high value (but not so high since the hours refers to the designed power which is low). The DNI average is used to computed the mirrors field surface to produce the designed power. This value of 110 W/m^2 is low and then field is relatively big since we imposed to produce the power for low irradiations value [1]. Since the irradiations value is often higher than the average set, the plant will be able to store a lot of energy.
The results gave a total operating time on a year of 6142 hours, which corresponds to almost 71% as a capacity factor. As it could be seen on the figure 5.5, the time operating at full load is 24 hours for consecutive days, on a basis of an intermittent sun energy. In comparison with the previous configuration, which as a number on a year of 1816 hours and capacity factor of about 20%, the difference is high. On the figure 5.6, the energy stored appear as really high and the production in summer is almost constant, reaching almost a 100% capacity factor during this period.

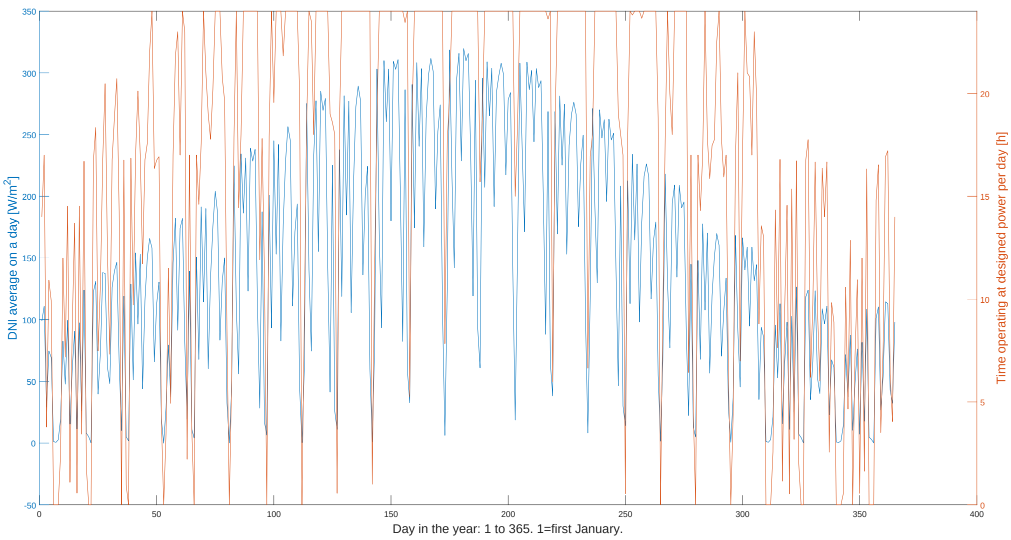

Figure 5.5: Time operating at designed power per day, in hours, in comparison with the average DNI on a day, for all days on a year in Sevilla with plant characteristics presented in table 5.1.

[1]We could have kept the same mean DNI level as before and increase the Solar Multiplicator to reach a great aperture.

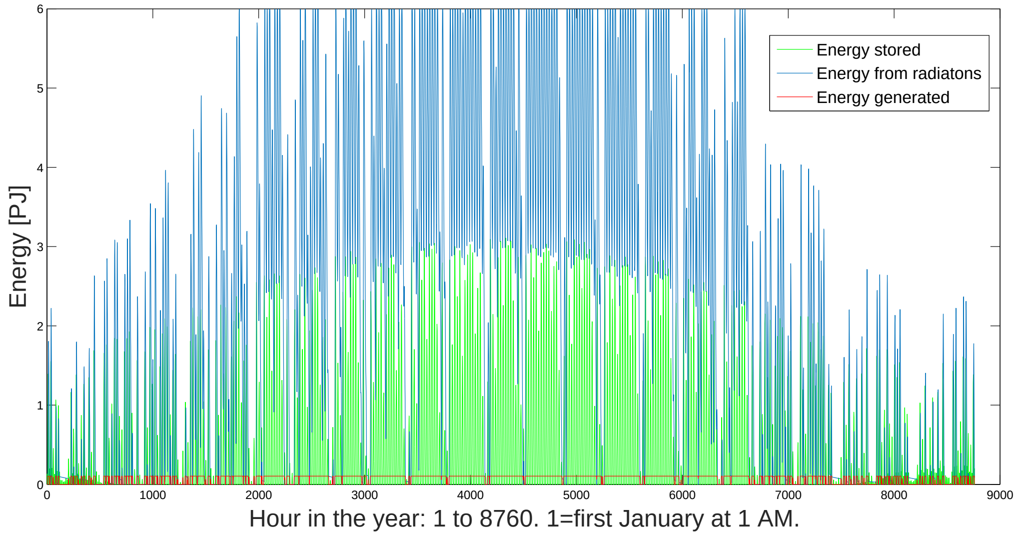

Figure 5.6: Energy produced in one hour (red), in comparison with the one received (green) and the one stored (blue) for the same hour, represented for a year. The plant is 30 MW in Sevilla with the characteristics presented in table 5.1.

The drawback of this configuration is that the total production is smaller than the one of the previous configuration studied (the one at 130 MW and 6 hours storage capacity) and that the total area needed is more or less the same. The first configuration produced 237 GWh but the base load one 178 Gwh in a year. It could have been guessed since the designed power of the first plant is more than fourth times the one of the baseload plant. So, to achieve this annual production, the base load one should have operated during, more than four times (3.38 is reached in our case), the number of hours (1816) of the first plant.

This example showed that we can do a distinction between two criteria: the number of operating hours in a year (better capacity ratio) and the annual total production. In the following, the impacts of all parameters are studied to better understand which configuration is optimal, in terms of EROI.

5.3 Impacts of the different parameters

Before presenting the optimal plant configuration, given a location, the influence of the parameters should be understood. The parameters to optimize are, as already presented in the last chapter, the designed power, the capacity of the storage system and the solar multiplicator. Let's summarize what's these parameters imply:

- Variations of the *storage capacity* for a given *(power designed ; solar multiplicator)*:
  - the more the storage capacity, the more the CED (which is the denominator of the EROI), because the tanks are bigger and quantity of HTF increase, which implies energy costs. But, the more the possible quantity of energy stored.
  - the less the storage capacity, the less the CED and the less the possible quantity of energy stored.
- Variations of the *solar multiplicator* for a given *(power designed ; storage capacity)*:

- the more the solar multiplicator, the more the size of heliostat field in comparison with the production output. It means more energy than necessarily in general at the receiver, and so, a need of storage. It also means more mirrors, and so, a higher CED.
- the less the solar multiplicator, the less the size of the solar field. The field is near the necessarily size it needs and so the energy sent to the receiver is in general smaller, or a bit higher, than the one required, meaning that the storage would not be used a lot and that a high capacity is not necessarily. In the other hand, the number of mirrors is small and so the CED is quite low.

• Variations of the *power designed* for a given *(solar multiplicator ; storage capacity)*:

- A weak designed power would mean, a smaller plant and so smaller CED. It does not necessarily implies a low production on the year since the number of hours could be higher than for a plant with a greater designed power (which would require higher hourly DNI level to operate).
- A high designed power would mean a bigger plant in general (higher CED), but this affirmation depends on the solar multiplicator. Since it consumes more energy to feed the power cycle, the storage capacity should not be so large. In consequence, the number of hours operating at full load on a year are not expected to be high.

As a remark, we could also mention that if the power designed is low, increase the storage capacity of some hours does not necessarily imply a high increase of the CED. For example, if the power designed is 20 MW, for the same CED increase, we could add 2 hours of storage capacity but only 1 for a plant with a power designed at 40 MW.

The storage capacity is a critical factor to optimize. On the graph figure 5.7, different plant configurations were plotted. The power designed is growing from 20 to 150 MW, a realistic range for CSP tower plants. For each different power, a range from 1 to 13 hours of storage capacity is computed. On this graph, the annual production, total hours operating in the year and the EROI value of the plant are plotted for all configurations. These configurations have the same solar multiplicator but different powers designed and storage capacities.

The first thing we realize is that all curves decrease suddenly at the same point for this graph. This point, when it occurs, represents the fact that the field surface required by the plant is too high (radius field > 1500m) and is then blocked to the maximum authorized surface. As explained before, if we add more mirrors to such a field, they will not serve the EROI since their contributions to the optical efficiency is really bad and the energy transferred low. Since the power needed in one hour increases but the mirrors surface does not follow, the number of production hours (less stored energy) drops and the production decrease, in this configuration. The EROI, in this case, follows the production and decreases also.

As we can see on the graph, the number of operating hours is decreasing with the power designed. It is logical, since more energy are necessarily to operate the turbine of the power cycle, and in consequence, the energy source being the same (given by the location in Sevilla) then less energy could be stored. Moreover, the total aperture area is increasing with the power designed (linearly), so, as explained previously, the optical efficiency of the field decreases since the mirrors are further and further from the tower. When the maximum size of the field is reached, as explained before, the energy provided by the field is lower and lower and could less and less comply with the energy required by the power cycle. So, only high DNI picks in the day could run the cycle, and the operating hours in the year decrease.

From the graph, we can conclude that the maximum of operating hours is always achieved, for any power designed, with the highest storage capacity. As well, the maximum annual production, for any power designed, is achieved with high storage capacity number. There is a

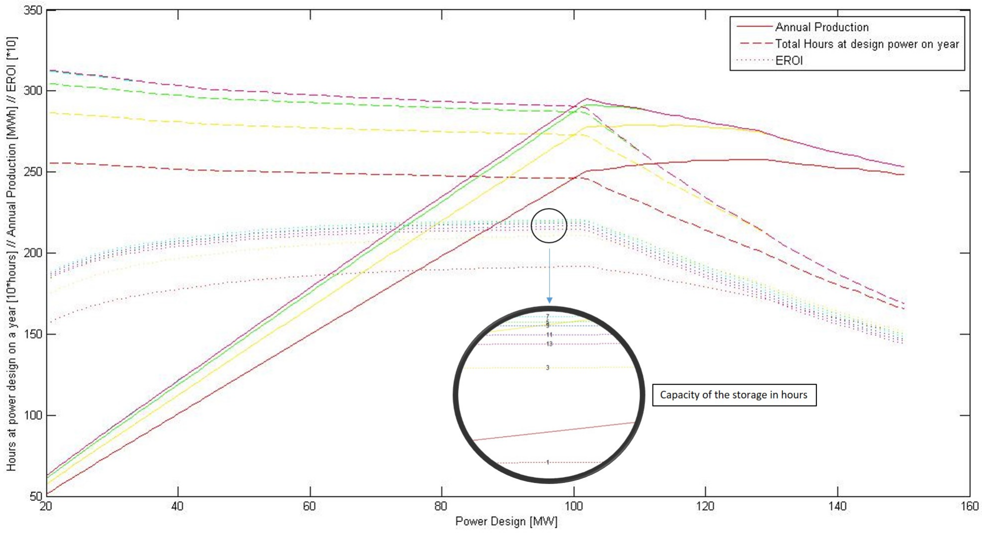

Figure 5.7: EROI, production and operating time evolution according to the power designed for different storage capacities. The zoom highlights the fact that the highest storage factor does not give the best EROI. The different colors correspond to different storage capacity.

high difference between a configuration with 1 hour storage and 3 hours storage for any power designed in terms of operating hours and production. On the other hand, the amelioration by increasing the storage capacity is smaller and smaller and the curves overlapped already after about 5 hours of storage capacity. For the EROI, as showed on the zoom in the figure 5.7, the highest value is not achieved for 13 but 7 hours of capacity. Indeed, for the point in the region of the maximum, adding storage capacity is not useful since the surplus of energy is never really high since the power designed is quite important (about 100 MW). Then, more storage capacity means only more material (steel, HTF, etc.), and a higher CED for the plant. Evaluating the EROI for all storage capacity should always be done in order to find the one giving the highest EROI.

It should be noticed that all these conclusion applied for this specific solar factor. In what follows, we wonder what is the impact of this parameter by plotting the same graph but for a solar factor of 2.7 (which is high according to the litterature), see figure 5.8. The EROI, annual production, total hours operating at full load, the aperture area, the LCA (CED) are plotted together for different power designed but all with a six hours storage capacity and solar factor of 2.7.

As it could be seen from the purple (lowest curve on the graph) curve on the graph, the surface of the field is stuck at a power designed of about 47 MW. The number of operating hours (light blue dotted curve on the graph) is then falling. In the contrary of the previous graph, the annual production continues to growth even after the fall of the operating hours. It means that the increase of the power designed counters the decrease of operating hours, in terms of annual power. The production reaches its maximum at about 90 MW and then decreases since the power required by the power cycle is too high.

The CED (LCA) is increasing linearly with the power designed and the number of mirrors (from its implementation, see table 4.3). It could be seen that two different derivatives shape its evolution: the first is higher since the number of mirrors grows and the power designed grows and then the maximum radius is reached (at about 47 MW) and the number of mirrors is stuck. So, from this stage, only the increase in designed power intervenes in the evolution.

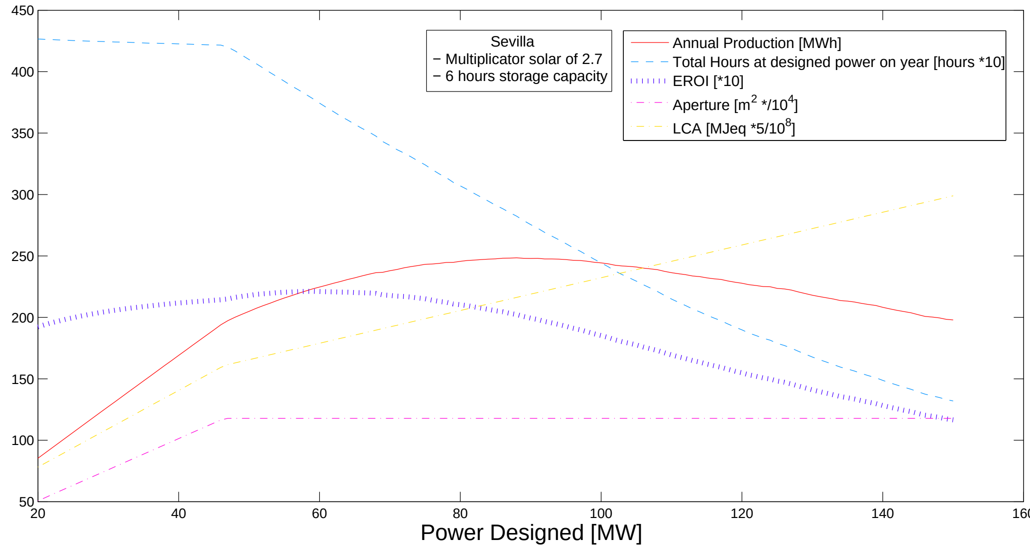

Figure 5.8: Evolution of the EROI and the annual production, LCA, aperture area, operating hours in function of the power designed, in Sevilla, with a storage capacity of 6 hours and multiplicator solar of 2.7.

The most interesting fact comes from the EROI evolution: its maximum, in this case, is not achieved for the same designed power than for the maximum of the annual production. Indeed, the EROI would be high if the CED is low and the production high. So, the maximum should be for low power designed (in this case), to avoid a too great CED but not for too low power designed since the production should be high enough (numerator of the EROI). In our case, the maximum is reached for 58 MW and the EROI value is 22.12.

In conclusion, we could predict that for a high solar factor, the power designed leading to the highest EROI is low (about 58 MW here, figure 5.8) and the one for a low solar factor would be higher (about 110 MW here, figure 5.7). But, it is really hard to predict which configuration will give the highest EROI since all parameters interfere and that for these two examples, the maximum EROI reached was the same, about 22. In the next subsection, the plant is optimized according to the three parameters and the unique optimal configuration is found and described.

5.4 Finding the optimal plant

The optimal plant is defined as the one optimizing the EROI for the given location. As explained previously, the EROI achieves a maximum for a certain designed power and capacity of storage. Moreover, the EROI value, for the same storage capacity and designed power evolves also with the solar multiplicator. To find the one and only one plant achieving the best EROI value for a given location, the simulation operates all the possible configurations. It is the same process as the one used to plot the graph before, except that the solar multiplicator is not fixed but evolves for each couple (power designed ; capacity of storage).

The table 5.2 presents the results of the optimization for Sevilla. The designed power is relatively low but the storage capacity and the solar multiplicator are high. It means that the optimized plant is quite small in power capacity but owns a big solar field and then have a high potential to store energy and in consequence have a high number of operating hours (5231 hours) on a year.

Sevilla	DNI average at this location	206	[W/m^2]
Optimized Parameters	Designed Power	49	[MW]
	Storage capacity	20	[h]
	Solar multiplicator	2.84	[-]
Results	Production on a year	2.51	[GWh]
	Number of operating hours at full load	5231	[h]
	CED	$3.35 * 10^9$	[MJeq]
	EROI	**26.32**	[-]

Table 5.2: The parameters describing the optimal plant in terms of EROI for Sevilla.

The plant is a mix between a base load and a high production configuration (see both example presented before). It means that the best EROI is achieved for a sufficient production and sufficient storage potential.

In this case, achieving a high number of operating hours is only possible with a high storage capacity as it could be seen on the figure 5.9. The maximum EROI is not achieved with the maximum production but at the power which reach the maximum total surface allowed first.

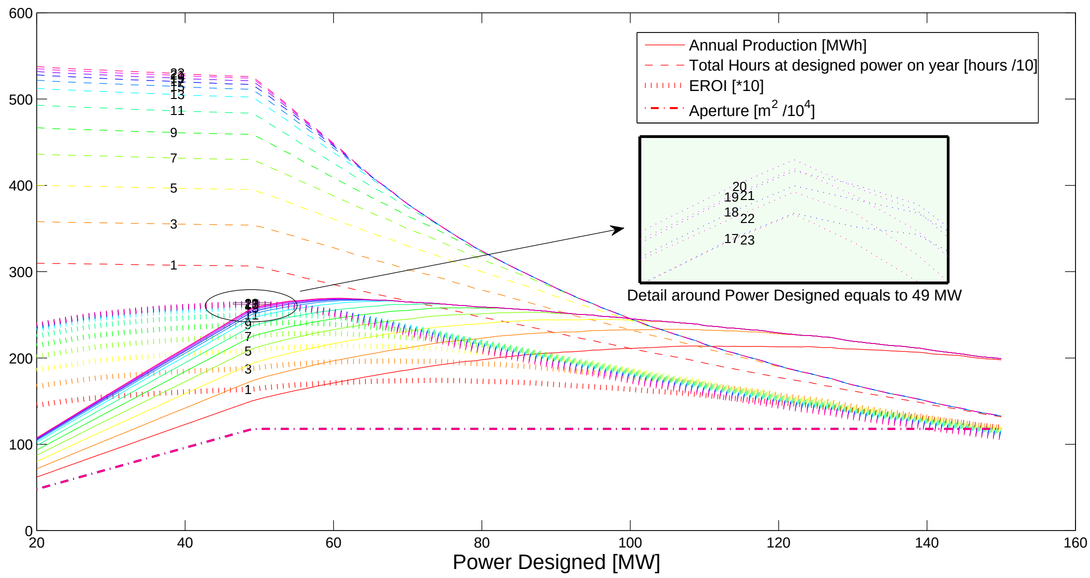

Figure 5.9: Evolution of the EROI and the annual production, LCA, aperture area, operating hours in function of the power designed, in Sevilla, for different storage capacities and for the configuration giving the highest EROI (see parameters at table 5.2). The numbers indicate the capacity of the storage system, in hours.

On figure 5.9, the detail demonstrates the inefficiency of increasing the storage capacity.

Indeed, a 18 hours storage system is more efficient, in terms of EROI, than another one with 22 hours of storage capacities. Moreover, the detail shows that after the EROI pick, the ranking of the curve is changing. Indeed, after the pick, the capacity of 20 hours is not the maximum anymore.

5.5 Impact of the location on the optimal plant configuration

The optimal configuration found before is linked to the location: Sevilla. Now the goal is to determine the difference between the optimal configuration of different locations. Three different locations with a highly different mean annual DNI will be studied. The better location, in terms of irradiations, is Sevilla in Spain, then Bilbao was chosen as a medium location and Brussels, in Belgium, as the worst one. The results are presented in the table 5.3 and discussed below.

Location Region		*Sevilla, Sp*	*Bilbao, Sp*	*Brussels, Be*
	Annual mean Irradiation [W/m^2]	206	162	27
Optimal Parameters	Designed Power [MW]	49	37	27
	Storage Capacity [h]	20	29	38
	Solar Multiplicator	2.840	2.964	2.960
Results	EROI	26.320	19.028	11.970
Details	CED [PJeq]	3.35	3.13	2.86
	Production Annual [GWh]	2.51	1.69	0.97
	Annual time at full load [h]	5231	4566	3611
	Total Surface [km^2]	7.0376	7.0376	7.0376

Table 5.3: Results of the optimization for the locations in the region of Sevilla, high irradiations, in the region of Bilbao, medium irradiations, and in the region of Brussels, low irradiations.

From the table 5.3, we can conclude that the optimal configuration is adapted to the location. The designed power is less and less as the mean irradiation decreases. It is logical since, as seen before, the optimal EROI is achieved for a plant which has a quite large number of operating hour. Since the power from sun is weaker, the power required to drive the turbine should be lower to have the possibility to store at certain moments.

The storage capacity increases (in hours) with a worst location since the power designed decreases. In fact, we can notice that the capacity of the storage in MWh is more or less constant: $49 * 20 \approx 37 * 29 \approx 38 * 27$[MWh] (see table 5.3). The solar multiplicator does not evolve logically at first view.

	Solar Multiplicator	Pd at $Area_{max}$ [MW]	Pd at $EROI_{max}$ [MW]	$EROI_{max}$ for all Pd
Bilbao	1.5	**73**	**73**	15.27
	2.2	**50**	**50**	18.08
	3	**37**	**37**	*18.90*
	5	22	36	18.56
	7	16	35	18.31
Sevilla	1.5	**93**	**93**	19.48
	2.2	**63**	**63**	24.81
	3	47	49	*26.30*
	5	28	47	25.92
	7	20	46	25.59

Table 5.4: Different optimization results from the variation of the designed power (Pd) according to different solar multiplicator value and a storage capacity of 20 hours. Bold characters show the link between the maximum EROI and area of the plant.

In the table 5.4, different optimization results are proposed, according to different solar multiplicators and a storage capacity of 20 hours. Bold characters show the link between the maximum EROI, at the given solar multiplicator, and area of the plant. In fact, for the different configurations (Pd ; solar multiplicator) at the storage capacity of 20 hours, we can notice a link between the power at which the optimal EROI (for this configuration) is achieved and the maximum area allowed. Indeed, in the first example (Bilbao), the maximum EROI is, in a first time, reached at the power designed which is the first to achieve the maximum area allowed: see solar multiplicator of 1.5, 2.2 and 3. To visualize it, see figure 5.9: the maximum EROI is reached when the area begin to be stuck.

In fact, the more the solar multiplicator, the more the area of the field. But, at one moment, the field is stuck ($radius_{max}$ = 1500 m). In fact, the solar multiplicator, when we compute the configuration for all designed power, only changes the rate at which the maximum area is reached: for low solar multiplicator, the area could be reached for high power designed (see in the table 5.4 Bilbao first row: 73 MW) and for high value the maximum area is reached sooner (see in the table 5.4 Bilbao third row: 35 MW).

After a certain value, the maximum EROI is not achieved at the same power that the maximum area but for higher value of the power designed (see in the table 5.4 Bilbao from fourth row). Indeed, the power at the maximum area is too low to achieved a great production on a year and so a great EROI. From the different value proposed, the highest is the one, linked to the solar multiplicator, which configures the plant so that the maximum EROI is reached at the maximum area but also at a solar multiplicator that allows this to arrive at the greatest designed power possible (to have a sufficient production).

From this maximum EROI for a (Solar multiplicator, Power designed) optimization (storage capacity fixed), keeping these parameters and computing to find the storage capacity giving the highest EROI does not allow us to have the real optimal EROI for the location. Indeed, the power designed and solar multiplicator are different for the real optimal configuration (compare both table 5.4 and 5.3). Because, the storage capacity impacts the all results and the three parameters should be optimized together. But, the real optimal parameters, as it could be seen on figure 5.9, is also achieved for the first configuration giving the maximum area. This explain why all these optimal configurations do have the same surface area, which is in fact the maximum one, even if the optical efficiency decreases with the area (as the distance from the mirrors to the tower increases).

5.6 Summary and conclusion for the static analysis

In conclusion, the configuration giving the highest EROI value varies with the location. The plants have a medium designed power, which decreases with the quality reduction of sites. Moreover, the optimal plant always has the maximum area allowed.
In the next chapter, the optimization results are used to complete a dynamic EROI analysis.

6 EROI Dynamic analysis: application of the model and optimization process to analyze a deployment of the CSP tower technology in OECD Europe from now to 2050

This chapter proposes to applicate the model, presented in the previous sections, to the deployment of the CSP technology, described by Greenpeace scenarios, for OECD Europe.
First, the method to consider the land availability is explained. Then, the methodology to simulate the technology improvement is covered. Finally, the global process is applied to OECD Europe.

6.1 The land availabitlity

The weakness of renewable energy is the highly dependence on the location and particularly for the CSP technology, as seen before. This section explains the method used to compute and exploit the land availability.

As seen in the model section, solar data from NASA are employed and have a one degree accuracy in latitude and longitude. In the following, the land availability is defined from the European Space Agency GlobCover Portal, ESA GlobCover 2009 Project [49]. The land cover is defined from different categories (23 in total) which allow to distinguish the areas covered by different types of vegetation (grassland, cropland, broadleaved deciduous forest, shrubland, etc.), urban and water bodies for example. These data are analyzed for each cell of 1/25 degree latitude-longitude edge length. So, 625 of them composed each cell of one degree latitude-longitude (solar data). Then, we know precisely the land occupancy in parallel with the solar data.

Two types of covered land are interesting for CSP tower applications: bare areas (see figure 6.1, left) and areas covered with a sparse vegetation (<15%, see figure 6.1, right). From there, the program browses all possible locations, for each one degree latitude-longitude, computes the area of type bare and sparse availability and ranks them from the highest to the lowest mean DNI.

The program selects the first area of the ranking, checks the mean DNI of this location, attributes a configuration on this basis and simulates the installation of this CSP tower plant on a year from the location solar data. Then, when all available areas are covered for this one degree latitude-longitude cell, the program will fill the next one, with the optimal configuration suited, until it is full, and so on until the end of available locations for the constrained geography (country or group of countries). A summary of this process is proposed at the figure 6.2.

Example of bare area. Ivanpah CSP tower construction (USA), source `http://www.powerengineeringint.com`

Example of sparse vegetation area. Solnova CSP tower pants (Spain), source `http://informeanual.abengoa.com`

Figure 6.1: Types of area suited to CSP tower applications.

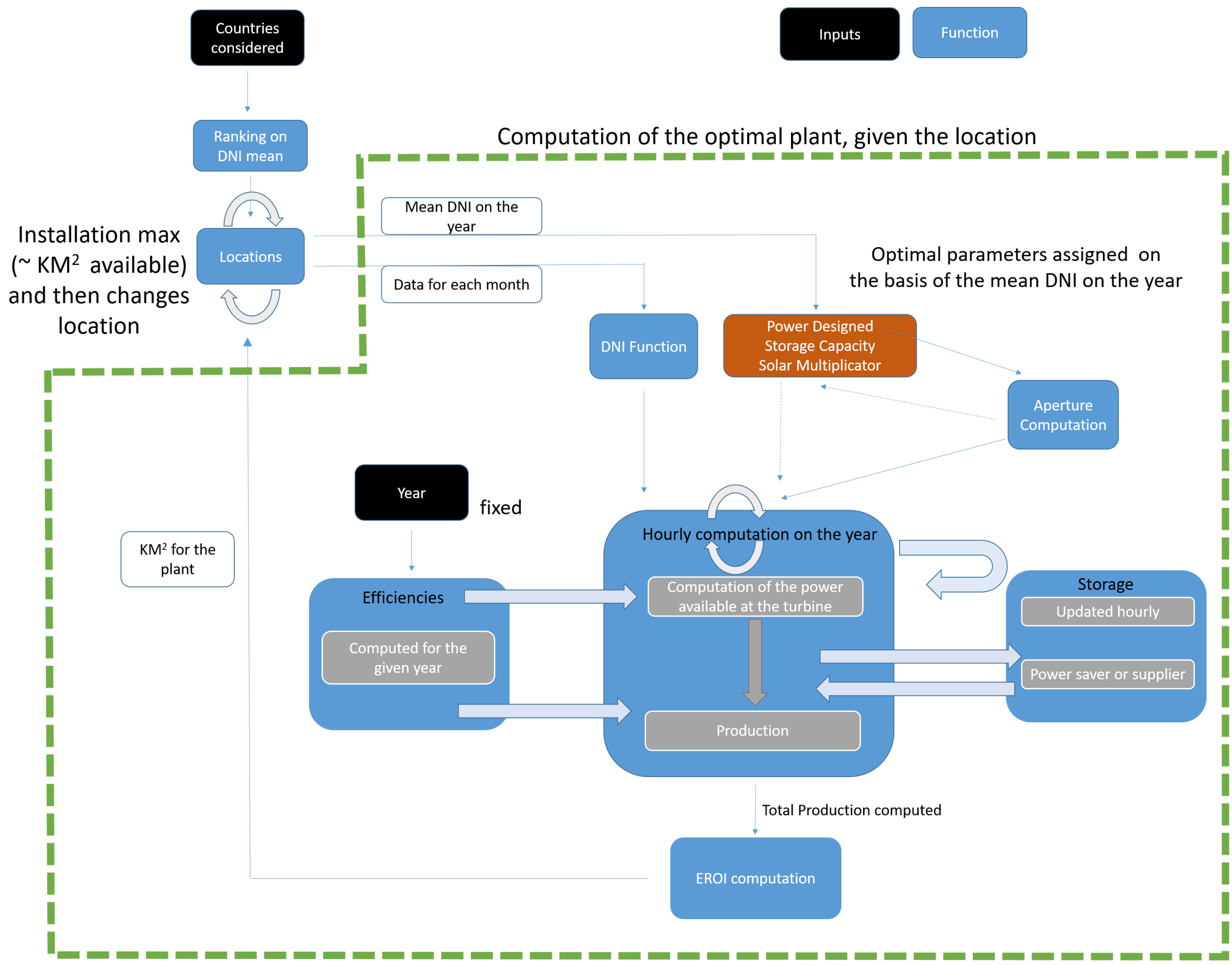

Figure 6.2: Process implemented to compute the CSP potential of a territory.

Optimal configurations are delivered given defined levels of average DNI on the year (step of about 10 W/m^2). The optimization process was done before the computation described in the method presented (figure 6.2), for given areas with certain DNI level. Even with a similar mean DNI on a year and same plant configuration, results for two locations could be different since monthly data are different. So, in the process, the comportment of a given configuration (chosen on the basis of the DNI mean) is computed for the current location; not on the basis of the results (EROI, production,...) from where the configuration was found to be the best.

The selection is done for a country or a group of countries. In a first time, there is no evolution in technology and all possible (bare and sparse vegetation) areas are covered. The result lead to the maximum potential of CSP tower technology in the defined location.

In the following, some results are presented for different countries, see table 6.1 and for OECD Europe region, see table 6.2.

Maximal Potential	Italy	Spain	Turkey	France	Morocco	Chile	Australia
Number of plant [-]	923	6641	10405	584	41220	24236	>189313
Power installed [GW]	25	179	280	16	1113	654	>5111
Annual production [PWh]	0.12	1.01	1,57	0.07	7,85	5,35	>40
EROI drop [-]	21 to 12	24 to 13	20 to 13	17 to 10	26 to 20	28 to 5	27 to 24

Table 6.1: Results for a total filling of available lands (bare and sparse vegetation) with optimization of plants in terms of EROI.

In Europe, the countries with the most potential (see table 6.1) are Spain and Turkey: because of their size and sunny weather. Acceptable EROI is reached during the installation even if the last one are not so good. Chile's drop of EROI is due to the particular shape of the country: the country owns really good spots in the North (best of the world) but the country is narrow and install more significate go down, to the South, so, to cold and rainy places (as we are in the South of the Hemisphere South).
Australia potential is huge, but the deserts are in the center of the country and cities near the coast, meaning sometimes long transportation lines and then high losses of energy. But still the EROI is high and even after installed so much plant (>189000) the EROI still reached 24, which is near the best values in Europe. The results show also a huge potential in china with as much plant as in Australia and a EROI drop from 27 to 20.
In other words, Europe is not the most suitable place for CSP plants in comparison with other countries. But, the EROI values are quite good and the future mix is not based only on the CSP technology, so a deeper analysis should be done.

The EROI evolution of Italy is shown at the figure 6.3. The drop is, as mentioned in table 6.1, from 21 to 12 and, since there is not a lot of available cells, we can see the different steps of the EROI. A different value is reached when the program change the location since the previous cell was full. Then, the EROI is lower, since the new cell has a lower DNI mean, and until the cell is full, the EROI has always the same value, as the optimal configuration is set depending on the DNI mean which is a property of the cell. Sometimes, some next cells could have a better EROI. It is due to the fact that the value of the mean EROI is not the perfect method to rank the sites. If a site have a bigger pick of irradiations in summer but lower in winter, in comparison with another one, even with the same DNI mean, it could have better results.

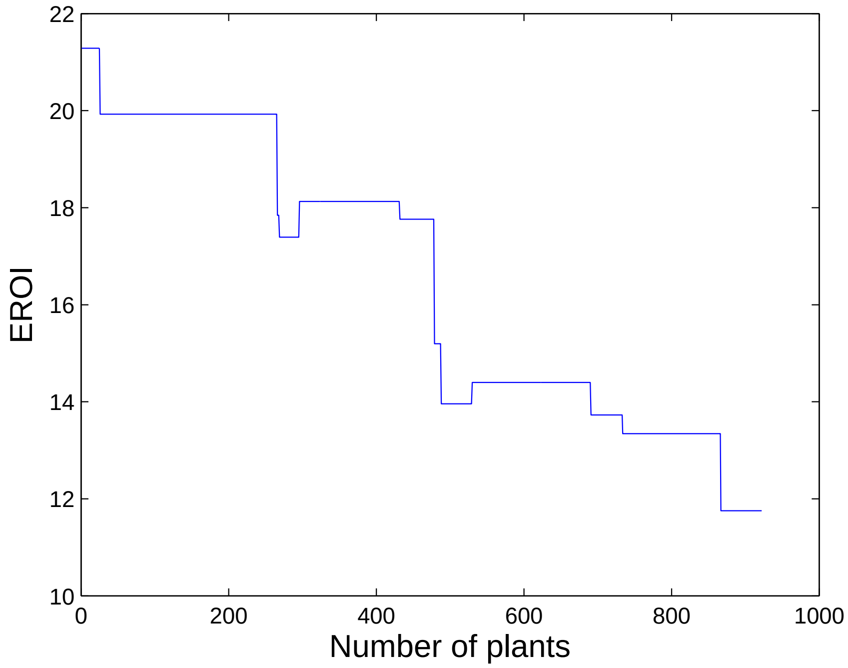

Figure 6.3: EROI evolution of Italy for a total filling of available lands (bare and sparse vegetation) with optimization of plants in terms of EROI.

OECD Europe	Type optimizing EROI	Plant type A	Plant type B	Plant type C
number of plant [-]	45374	45374	367182	58534
Power installed [GW]	1225	4537	3672	2341
Annual production [PWh]	4.49	3.54	4.30	4.64
EROI drop [-]	25 to 5	16 to 1	7.5 to 3	17 to 4

Table 6.2: Results for different types of plants, available areas entirely covered. *Type A*: 100 MW, solar multiplicator: 1.7, 7 hours storage. *Type B*: 10 MW, solar multiplicator: 1, 20 hours storage. *Type C*: 40 MW, solar multiplicator: 1.7, 20 hours storage

If we compute the maximum potential, with the same method as before, for OECD Europe region, we obtain the results shown in the first column of the table 6.2. The potential is quite high and, in comparison from the Greenpeace scenarios (advanced energy revolution) it seems we have the potential to apply it, but we will cover this in the next part with the technological evolution.

The comparison with the same methodology allow us to see the good effect of the optimization phase on the EROI. Indeed, the other tests, with only one type of plant reach highest production level for type C but lower EROI. The type B proposed to install a huge number of plants with a really small surface of mirrors, but the EROI and production are not efficient. The type A proposed a plant of 100 MW but the production and EROI results are not good. It should be mentioned than these plants adpat the size of their solar field to the mean DNI of the localization, as for the optimal EROI process. The only difference comes from the fact that the configuration target is not the optimum EROI.

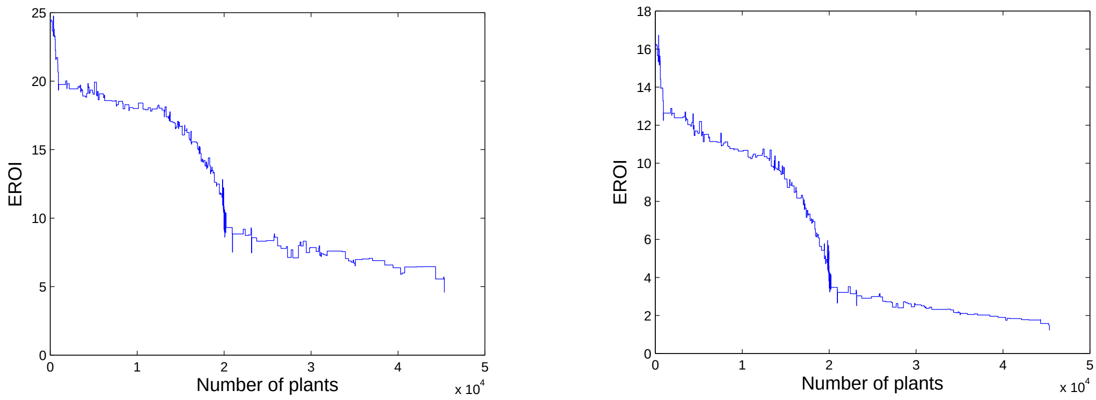

EROI optimized　　　　Type A

Figure 6.4: EROI evolution for OECD Europe region.

The EROI evolution for the optimal process and the type A (100 MW plants) is shown in figure 6.4. The evolution has the same trends, it seems that there is only a shift towards lower EROI values for the Type A plant, of about 5.

As demonstrated, CSP has a potential in Europe to be part of the energy transition and a greater in many others countries in the world. In fact, the decrease of the EROI could be balanced by the increase of the technology efficiency. This point is studied in the following section.

6.2 The technology evolution

The technology evolution represents the improvement in the design and implementation of new discoveries. Since the perspective is from now to 2050, most of future improvements are already known but need to be scaled up and improved from the laboratory to a commercial scale.

Major improvement on short to long terms are[1]:

- Improvement in design of the receiver (less heat loss by convection) and field layout at short terms.
- Amelioration of the absorber at medium terms (particles absorbers) or receiver with a selective comportement (photonic crystals) to highly reduce the emission losses.
- Change of the cycle to a CO_2 supercritical one, if the temperature delivered by the receiver could reach high values (particles or selective receiver). Long terms vision.

These improvements are not considered as a fiction at all. For example, the Sunshot plan was settled by the U.S. Department of Energy in 2011 [14]. The initial objective was to make possible the solar production of electricity at a competitive cost by 2020. The table 6.5, summarizes the goals set by the initial report in 2011. In 2016, they published a report on the progress of the Sunshot initiative and set new goals which are about the same but a bit spread on a time scale.

[1] See in Chapter 3, the technological review and performances part.

Solar Field	Receiver	Heat Transfer Fluid	Thermal Storage	Power Block
Cost ≤ $75/m² (Beyond SunShot: ≤ $50/m²)	Cost ≤ $150/kW$_{th}$	Cost ≤ $1/kg	Cost ≤ $15/kWh$_{th}$	Cost ≤ $900/kW$_{e}$
- Optical error (calm) ≤ 3.0 mrad - Optical error (windy) ≤ 4.0 mrad - Max operational wind speed ≥ 35 mph - Max survivable wind speed ≥ 85 mph - Lifetime ≥ 30 yrs	- Thermal efficiency ≥ 90% - HTF fluid exit temp ≥ 720 °C - Lifetime ≥ 10,000 cycles	- Thermal stability ≥ 800 °C - Melting point ≤ 250 °C	- Power-cycle inlet temp ≥ 720 °C - Exergetic efficiency ≥ 95%	- Net thermal-to-electric cycle efficiency ≥ 50% - Dry-cooled at 40 °C ambient temp

Figure 6.5: Sunshot inniative (USA) goals for the CSP technology (see [14]).

Here, the implementation considers an evolution in three parts. The optical efficiency of the mirrors field evolves from a value in 2015 to a value in 2050, the receiver and power cycles efficiencies follow the same scheme. Their evolution is stuck by a physical limit which gives the trends of the curve as presented in first chapter, at figure 1.4.

The figure 6.6, represents the EROI evolution for OECD Europe region from 2015 to 2050. No land restriction was set, so, it means that an infinite space was accorded to the first cell. The Greenpeace energy revolution need were installed. It means that each year, new plants were built to follow the need (in annual production) that was imposed by this scenario (more details at the next section).
Two types of technology evolution were imposed: an optimistic (but realistic) and a moderate one. The results show a good improvement of the EROI, which follows the trend of the evolution of the efficiency curve (compare with figure 1.4).

The two bumps on the optimistic curve represent the change of technology occuring. The first represents the transition between the steam power cycle linked to a normal receiver to another steam power cycle but linked to a solid particle receiver. The other bump represents the transition between this latter and a CO_2 supercritical cycle. In fact, these changes only impact the method to compute the size of the solar field. During the transition period (about 5 years), a random variable assigned the type of the power cycle to the plants, which give the variations, previously named bumps.

At figure 6.7, an improvement of 5%, between 2015 and 2050 is proposed for each part of the plant: the receiver, the mirrors field and the power cycle. In comparison the EROI without evolution is represented, and, since there is no land restriction and neither improvement, is constant.
The power cycle seems the most interesting part to improve in terms of EROI. In fact, the improvement for this part required an improvement of the temperature maximum of the HTF and then an improvement of the receiver.

As seen, the EROI of future installation could be better than the one of current plans, and at an non negligible way, even for a non optimistic evolution. It proves that the technology is not mature.
In the following, EROI evolution is studied from a technolgy improvement view in relation with the land constraint.

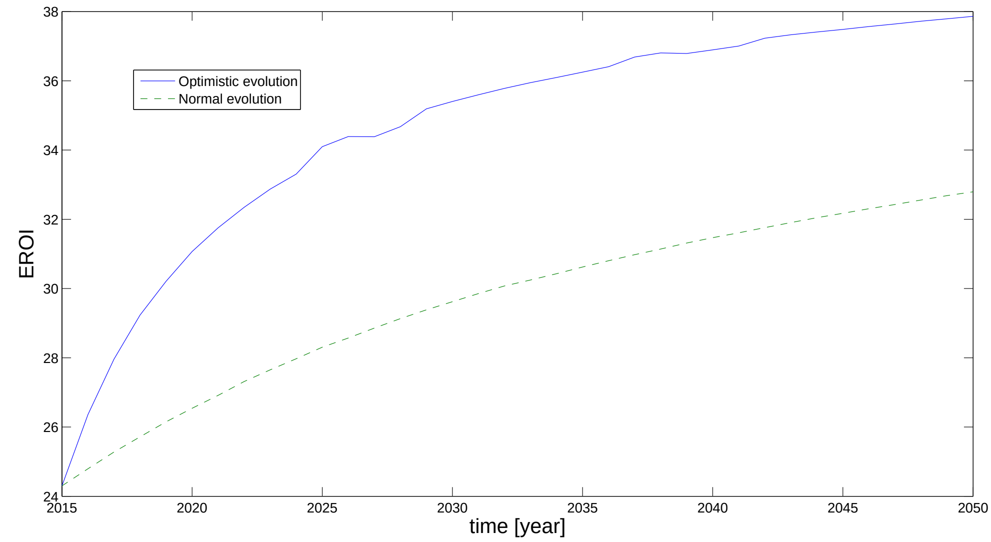

Figure 6.6: EROI evolution for OECD Europe region from 2015 to 2050, no land restriction (infinite space for the first cell) and technology evolution, Greenpeace energy revolution need installed.
- normal evolution: low improvement of the technology (efficiency 2015-2050 in [%]): power cycle 35-45, receiver: 90-95, mirrors field: 60-65.
- optimistic evolution: all type of power cycles and receiver with good results (efficiency 2015-2050 in [%]): power cycle 35-55, receiver: 90-97, mirrors field: 60-70.

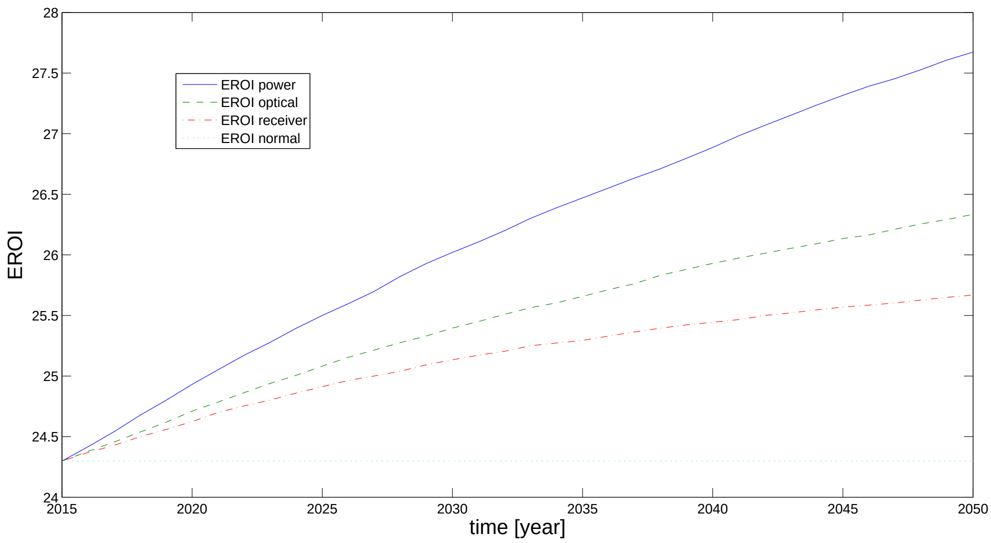

Figure 6.7: Comparison of the impact on the EROI of technology components evolution for 5% improvement for each. Done for OECD Europe region from 2015 to 2050, no land restriction (infinite space for the first cell), Greenpeace energy revolution need installed.

6.3 CSP deployment for OECD Europe

The goal of this part is to decrypt if it is relevant to installed CSP tower plants in OECD Europe. CSP technology could be a pillar for the future energy transition. Indeed, we saw that the efficiency is already interesting and is promissed to evolve. Moreover, there is available space in OECD Europe. The question is now: is it relevant to install plants in Europe and is it relevant to rely on this technology to face the future energy challenge?

As it could be expected, the question of the relevance could be approached by the EROI factor. Indeed, if we have a certain quantity of production to reach, if the EROI of the plants should reach low values, the deployment would be useless from a net energy point of view.

In the following, the program is used to install each year the number of required plants to reach the yearly production needed according to the evolution of the CSP electricity production of the Greenpeace Advanced Energy Revolution [3], see figure 6.8. These values are computed from the Chapter 1.

The program first fills the best spots, as previously and each year the efficiency of the field, receiver and power cycle evolves. The process is the same as the one of figure 6.2 except that the year value evolves from 2015 to 2050 and that a year is completed only if the install required capacity of this year is reached. So, we still optimize each plant configuration according to the location.
The land availability is also updated to relevant values. Not 100% of free bare areas are relevant to place a CSP plant: the soil should be flat, not too far from current lines, if far it should be large enough to receive a lot of plants so that a transmission line will worth it to be built,... and in the end 30% of bare area are kept and 5% of area with sparse vegetation.

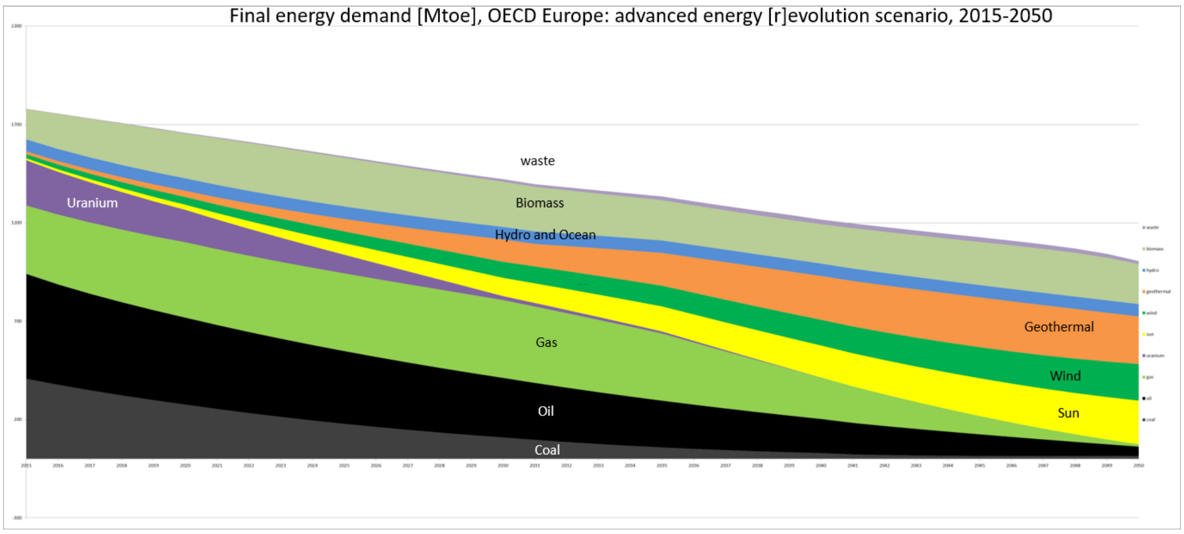

Figure 6.8: Evolution of the primary energy demand from 2015 to 2050, Advanced Energy Revolution, from the computations of Chapter 1.

Three types of technology evolution were simulated: no evolution, moderate evolution and optimistic evolution.
The more optimistic evolution propose an improvement of the different parts which are greater than for the moderate scenario, see table 6.3 and three types of power cycles are implemented, as explained in previous section.

Evolution parameters	efficiency 2015-2050 in [%]		
	Solar Field	Receiver	Power Cycle
no-evolution	60	90	35
Moderate	60-65	90-95	35-45
Optimistic	60-70	90-97	35-55

Table 6.3: Parameters used for the different technology evolution scenarios.

Space left blank for an easiest reading of the following graphics ans their description.

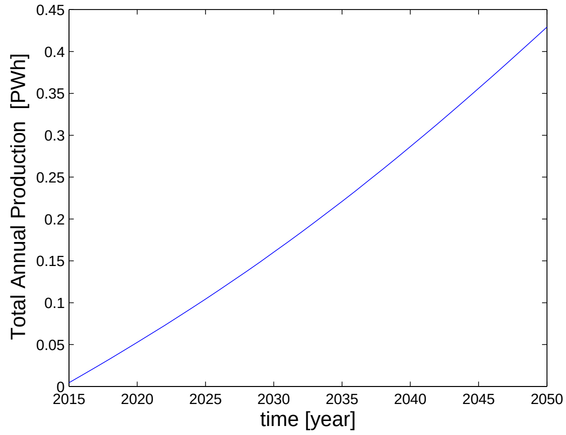

a) Evolution of the annual production of the installed capacity

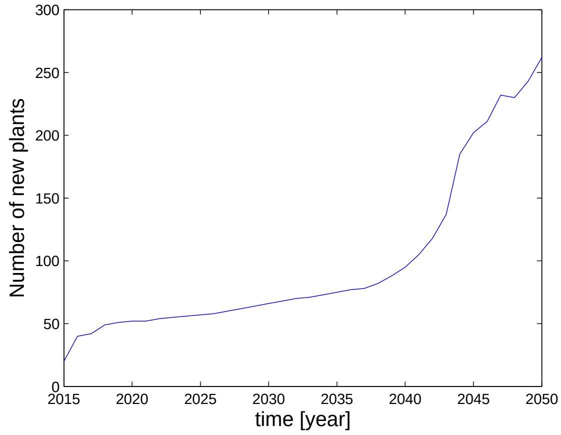

b) Evolution of new plant installations per year.

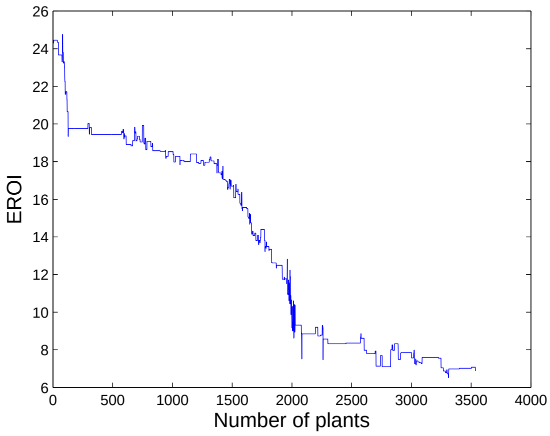

c) Evolution of the current EROI installed per number of plants.

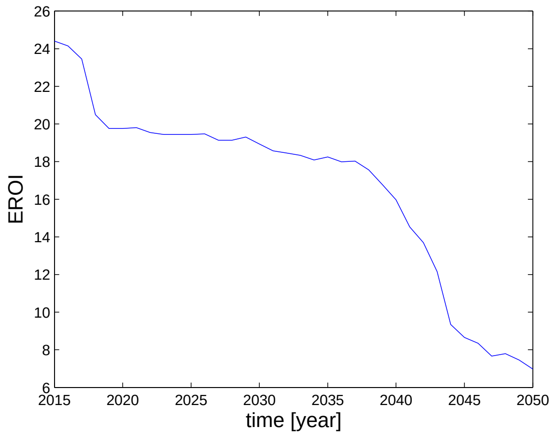

d) Evolution of the current EROI installed per year.

Figure 6.9: OECD Europe, GP Advanced Energy Revolution CSP yearly need installed. Test A: no evolution of the technology from now. Results in 2050: 126.5 GW installed capacity, 3540 plants, 431.9 TWh/year, 286 cells used, 24780 km^2.

First, the installation is computed with no evolution of the technology (see parameters at the table 6.3).

As it could be seen on figure 6.9.a, the production of the installed capacity should be greater each year and does not follow a linear evolution. In 2050, the production is set to reach 430 TWh, as programmed in the GP scenario. In the figure 6.9.b, we can notice that the number of plant explosed from 2040 to 2050. Indeed, from about a constant 50-60 installations of new plants per year, the new plants number for the last years should be about 200. This is due to the scarcity of available places and this effect is correlated to the fall of the EROI at the same years, see figure 6.9.d.

The installed capacity has a global average capacity factor of 38.9%. In consequence the installed capacity is high (126.5 GW) as well as the number of plant (3540) and the surface required (24780 km^2).

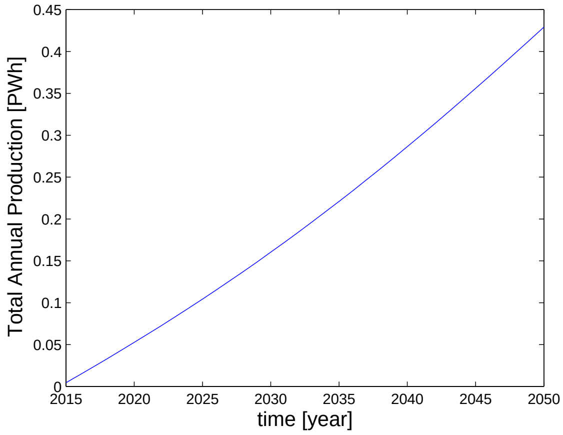

a) Evolution of the annual production of the installed capacity

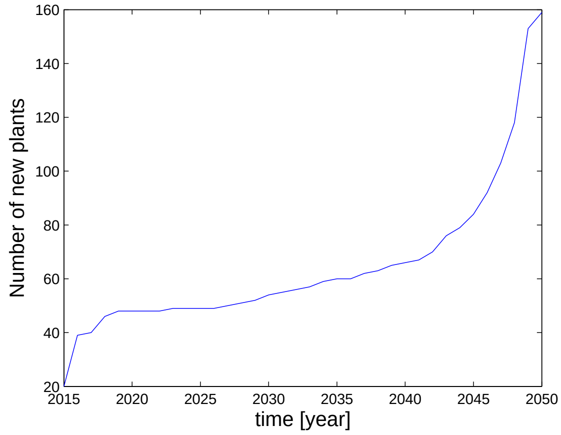

b) Evolution of new plant installations per year.

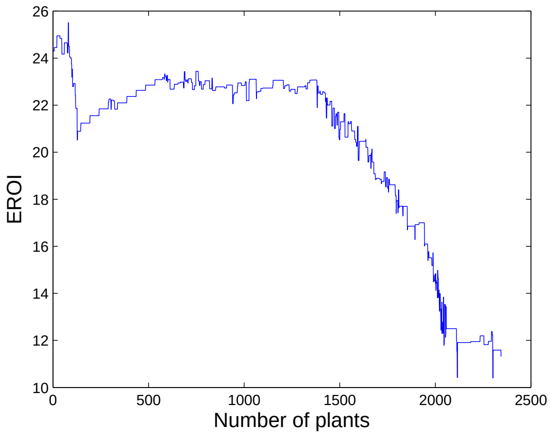

c) Evolution of the current EROI installed per number of plants.

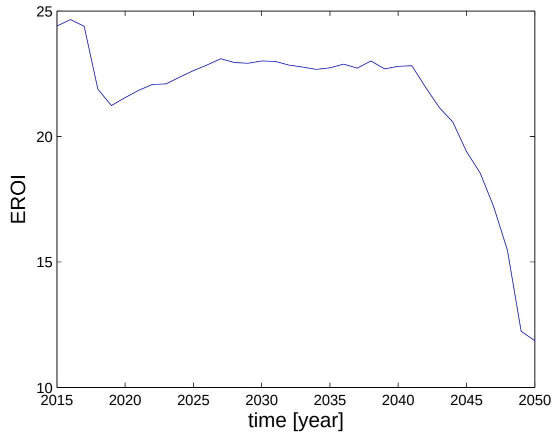

d) Evolution of the current EROI installed per year.

Figure 6.10: OECD Europe, GP Advanced Energy Revolution CSP yearly need installed. Test B: moderate evolution of the technology from now. Results in 2050: 94.5 GW installed capacity, 2344 plants, 433.4 TWh/year, 220 cells used, 16408 km^2.

Secondly, the installation is computed with a moderate evolution of the technology as presented at the table 6.3.

As it could be seen on figure 6.10.a, the production of the installed capacity is the same as previously, following the GP scenario instructions. The maximum number of new plants per year (see figure 6.10.b) is 160, which is lower than before, with 250. The number of new plant per year also increase a lot from 2040 to 2050. Indeed, the EROI falls at this moment, due to the lack of good spots, see figure 6.10.d. On the other hand, the EROI first decreases and then increases (see figure 6.10.c). Indeed, the first cells have a huge potential compared to the following ones, in the ranking, and this fall was already visible before (see figure 6.9.c) ; but, after a while, the technology improvement balances the lack of good spots and the EROI almost reachs is previous value, and stabilizes during a while (1000 installations, about 20 years). Even the fall in the end reached a lowest value of 10, which is low but not as low as before.

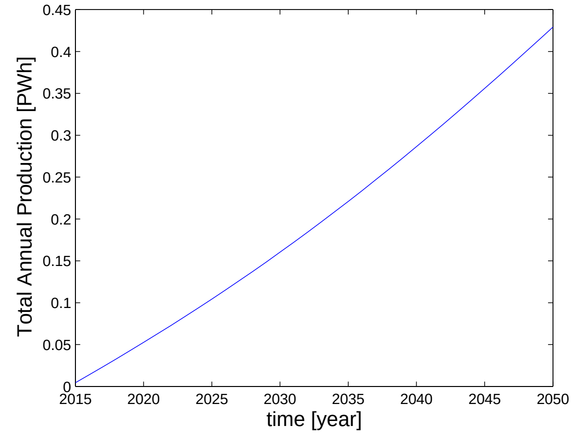

a) Evolution of the annual production of the installed capacity.

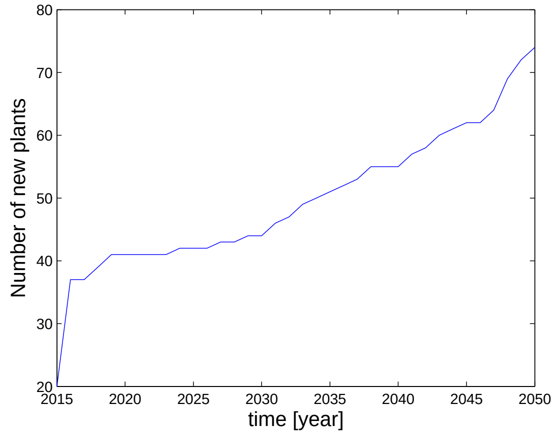

b) Evolution of new plant installations per year.

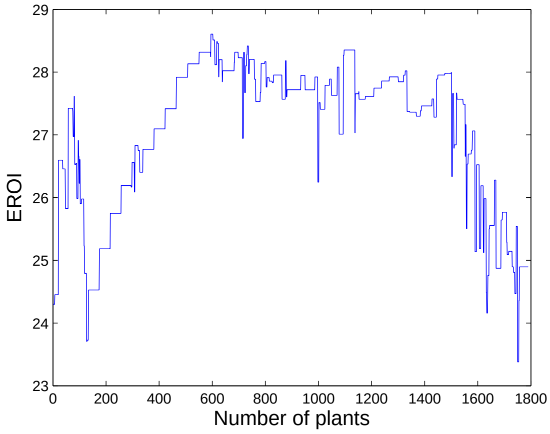

c) Evolution of the current EROI installed per number of plants.

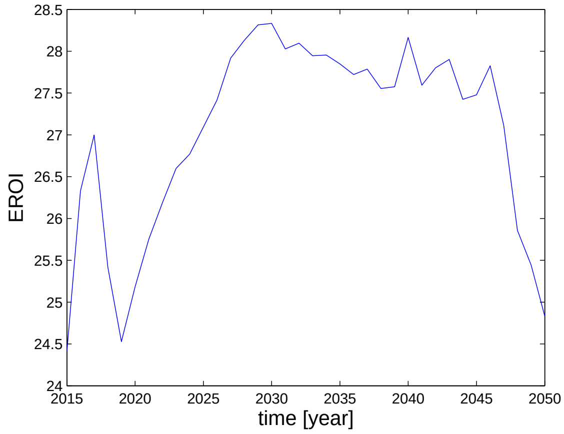

d) Evolution of the current EROI installed per year.

Figure 6.11: OECD Europe, GP Advanced Energy Revolution CSP yearly need installed. Test C: optimistic evolution of the technology from now. Results in 2050: 80.5 GW installed capacity, 1807 plants, 434.8 TWh/year, 117 cells used, 12649 km^2.

In the end, the installation is computed with a more optimistic evolution of the technology as presented at the table 6.3.

The maximum number of new plants per year (see figure 6.11.b) is low, and its evolution linear with the years. The number of new plants per year also does not increase between 2040 and 2050, since the technological improvement balances the lack of good spots, even for these final years. Indeed, the EROI decreases is reduced to the order of the first drop, see figure 6.11.d and 6.11.d, passing only from 27 to 24.

In final, in 2050, the installed CSP tower park, able to complete the GP demand (so producing about 430 TWh), has an installed capacity of 80.5 GW, owns 1807 plants, used 12649 km^2 and has a mean global capacity factor of 61.6%.

The geography of the deployment

Figure 6.12: The 119 sites of installations for the 1807 plants representing 80.5 GW installed, test C.
Done with Google and itouchmap.com.

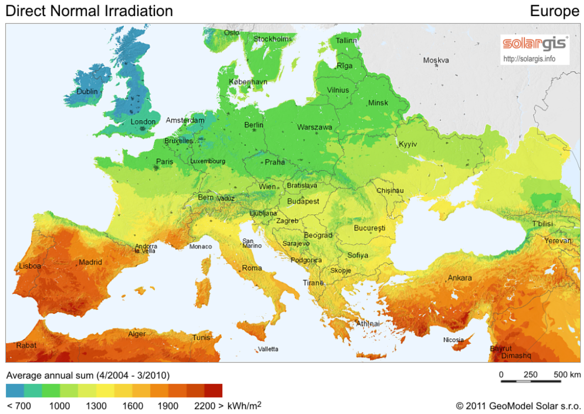

Figure 6.13: DNI levels, map of Europe.
Source:`https://tunedracers.com/uk/uk-energy-source-map`

The distribution of the installed capacity is, as expected, in accordance with the DNI repartition in Europe (see figure 6.13).
We can notice the lack of installations in Portugal, though the country has a high average irradiations. In fact, from looking into the data containing the availability of land, it was noticed that, no available land of bare type exists. Moreover, lands covered by sparse vegetation has a small surface and since the constraint of 5% is quite strong, no areas could be used to install a plant.
In fact, the early pick of all EROI evolution plot (see plots c of figures 6.9, 6.10 and 6.11) is partly due to the Canary Islands. Indeed, from all spots of OECD Europe, their irradiation level is the highest and denotes a bit from the other spots, due to their location.

6.3.1 Considering the evolution of the mix

Until here, the EROI was computed as follow:

$$EROI = \frac{\text{Production}_{life\ time} * \alpha}{CED_{LCA}} \tag{6.1}$$

$$PEF = \alpha = \frac{\text{global electricity generated}}{\text{primary energy fuel inputs for electricity generation}}$$

The primary energy factor is 2.5 according to the EU legislation [42]. And the previous computation were done with this value.
In fact, the PEF depends on the energy mix defined in the zone considered and its values should evolve since the energy mix changes.

Value of the primary energy factor (PEF)

A deeper analysis reveals that the value of the PEF factor should in fact evolve during the progression of the computation through the years.

The value of the PEF, for Europe, given by the EU legislation is 2.5 [42]. "In other words, the current PEF assumes that all power generation in the EU is delivered at 40% efficiency (100% divided by 2.5 = 40%)." [42].

A study of the Fraunhofer Institute [50] evaluates approaches to calculate the PEF. Four approaches were performed. They showed, amongs other conclusions, that:

- the 2.5 value for the European PEF should be updated
- a considerable decrease of the PEF is expected due to the renewable increase in the energy mix

Method	2000	2005	2010	2015	2020	2025	2030
Method 1	2.41	2.37	2.26	2.08	1.87	1.79	1.74
Method 2	2.41	2.36	2.14	1.90	1.59	1.46	1.35
Method 3	2.52	2.49	2.38	2.21	2.01	1.93	1.87
Method 4	2.65	2.61	2.49	2.30	2.09	2.00	1.93

Figure 6.14: Decrease of the PEF, for all methods of computation, as demonstrated by a study of the Fraunhofer Institute [50].

As we followed the Greenpeace advanced energy revolution scenario to evaluate the EROI evolution deployment, we should considered the evolution (expansion) of the other renewables energy as well.

So, in the energy mix, since the part of the renewable is larger and larger, the PEF should decrease since less and less fossil fuels are used to produce electricity. In 2050, the electricity production, considering this Greenpeace scenario, will be totally provided by renewables sources and the PEF factor should reach the unit value.

Computation with a decreasing PEF

The PEF value is then set to a linear function which is equal to 2.5 in 2015 and 1 in 2050. So, we have a value dependent on time: $PEF = \alpha(t)$.

In our study, the LCA already used the PEF factor since in the computation of the CED, the electricity needed had to be converted into primary energy as the global CED is given in terms of primary equivalent:

$$CED = CED_{\text{from electricity}} + CED_{\text{from fossil fuels}} \qquad \text{[Primary Energy]}$$

In fact, the part of the electricity in the LCA should be converted into primary energy with the updated PEF. With α_{LCA}, the value of the PEF used by the authors of the LCA analysis, this gives:

$$CED = CED_{\text{from electricity}} * (\alpha(t)/\alpha_{LCA}) + CED_{\text{from fossil fuels}} \qquad \text{[Primary Energy]}$$

Dividing by α_{LCA} allows to recover the electricity value that was computed during the LCA analysis. Then, this electricity is converted to the right amount of primary energy by the updated PEF: $\alpha(t)$.

The major parts of the electricity in the LCA comes from the O&M phase, which is almost only composed of electricity that the central consumes to heat the molten salt and control heliostats during all the days of the life cycle. This part accounts for 59.1% of the LCA, see table 3.2.

So we have:

$$\begin{aligned}
\text{EROI} &= \frac{Energy_{delivered}}{Energy_{consumed}} \\
&= \frac{\text{Production}_{life\ time} * \alpha(t)}{CED_{LCA}} \\
&= \frac{\text{Production}_{life\ time} * \alpha(t)}{(\text{CED}_{\text{from electricity}} + \text{CED}_{\text{from fossil fuels}})} \\
&= \frac{\text{Production}_{life\ time} * \alpha(t)}{\text{CED}_{\text{from electricity}} * (\alpha(t)/\alpha_{LCA}) + \text{CED}_{\text{from fossil fuels}}} \\
&= \frac{\text{Production}_{life\ time} * \alpha(t)}{\text{CED}_{\text{total}} * 0.591 * (\alpha(t)/\alpha_{LCA}) + \text{CED}_{\text{total}} * 0.409}
\end{aligned}$$

Results with a decreasing PEF

The results found before, as the installed capacity, number of plants, locations of these plants, etc., are not question by the PEF evolution. Only the EROI value is affected, since the deployment was performed according to the production need.

The adapted EROI is lower than the previous one, since the PEF decrease form 2.5 in 2015 to 1 in 2050.

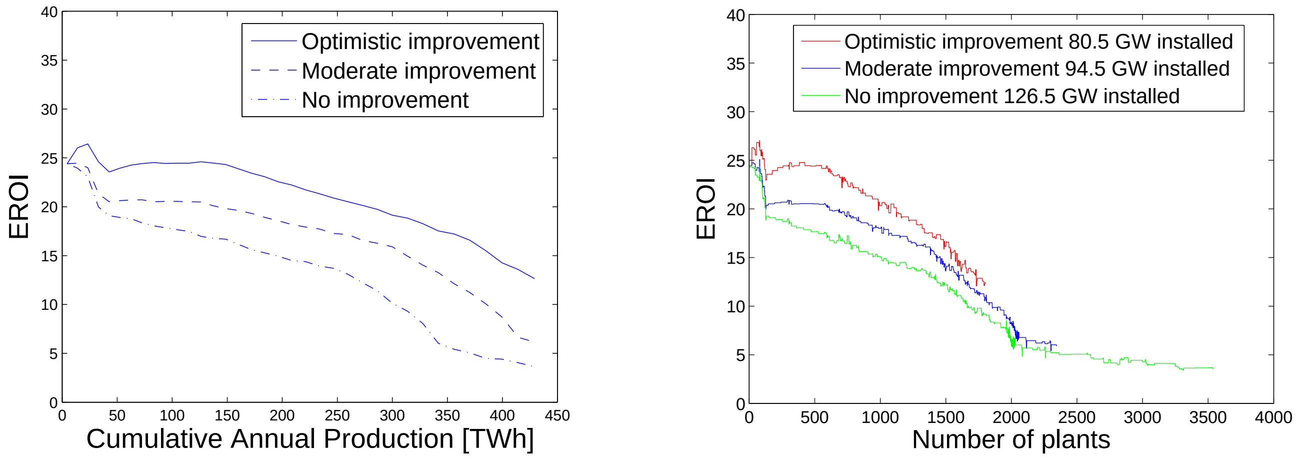

Figure 6.15: Primary energy factor decreasing (from 2.5 to 1 in 2050). OECD Europe, GP Advanced Energy Revolution CSP yearly need installed, from 2015 to 2050.

From these EROI values, we can characterized the deployment of the CSP according to these three different scenarios of the technology evolution (see table 6.3 for details about the optimistic, moderate and no-evolution scenarios).

We should keep in mind that the EROI computed consider the multiplication of the numerator (electricity produced) by the PEF. So, even if the PEF is reduced to one for the end of the delpoyment (2050), the previous values are higher than for other analysis which does not consider the primary equivalence of the electricity produced.

We can conclude from figure 6.15 that:

- For each scenarios the EROI decreases

- For a EROI considered acceptable, between 20 and 30, even the optimistic scenario could not complete the deployment
- Considering the values of EROI below 20 as unacceptable:
  - None of the scenarios is viable
  - The optimistic evolution should stop the deployment at an installed park able to produce 300 TWh. According to the scenario, this capacity is reached in 2041. This parks would account about 1200 plants, with an installed capacity of 56.9 GW installed.
  - The moderate evolution should stop at a park able to produce about 150 TWh, reached in 2027, accounting 750 plants, with 33.6 GW installed.
  - The non-evolution scenario should stop at about 40 TWh of annual production, reached in 2018, accounting 200 plants, with 9 GW installed.
- For a EROI considered acceptable between 15 and 30, only the optimistic scenario completes the deployment
- Considering the values of EROI below 15 as unacceptable:
  - Any other deployement than the optimistic one is viable
  - The moderate evolution should stop at a park able to produce about 300 TWh, reached in 2041, accounting 1500 plants, with 64.7 GW installed.
  - The non-evolution scenario should stop at about 200 TWh of annual production, reached in 2032, accounting 1000 plants, with 52.7 GW installed.

Results without accounting the PEF

In the past analysis we derived the EROI as:

$$\mathrm{EROI}_{\mathrm{elec,\ adapted}} = \frac{\mathrm{Production}_{life\ time} \ * \alpha(t)}{\mathrm{CED}_{\mathrm{total}} * 0.591 * (\alpha(t)/\alpha_{LCA}) + \ \mathrm{CED}_{\mathrm{total}} * 0.409} \qquad \left[\frac{\text{Primary equivalent fossil energy}}{\text{Primary equivalent fossil energy}}\right]$$

For a detail analysis of the deployment, we can defined two more value for the EROI:

- $\mathrm{EROI}_{\mathrm{elec,\ adapted}}$ without the PEF (α) factor at the numerator.

$$\mathrm{EROI}_{\mathrm{elec,\ adapted}} = \frac{\mathrm{Production}_{life\ time}}{\mathrm{CED}_{\mathrm{total}} * 0.591 * (\alpha(t)/\alpha_{LCA}) + \ \mathrm{CED}_{\mathrm{total}} * 0.409} \qquad \left[\frac{\text{Final Energy, elec}}{\text{Primary equivalent fossil energy}}\right]$$

- $\mathrm{EROI}_{\mathrm{elec}}$ without the PEF (α) factor at the numerator and without adapting the PEF factor used in the LCA analysis to the transformation of the grid.

$$\mathrm{EROI}_{\mathrm{elec}} = \frac{\mathrm{Production}_{life\ time}}{\mathrm{CED}_{\mathrm{total}}} \qquad \left[\frac{\text{Final Energy, elec}}{\text{Primary equivalent fossil energy}}\right]$$

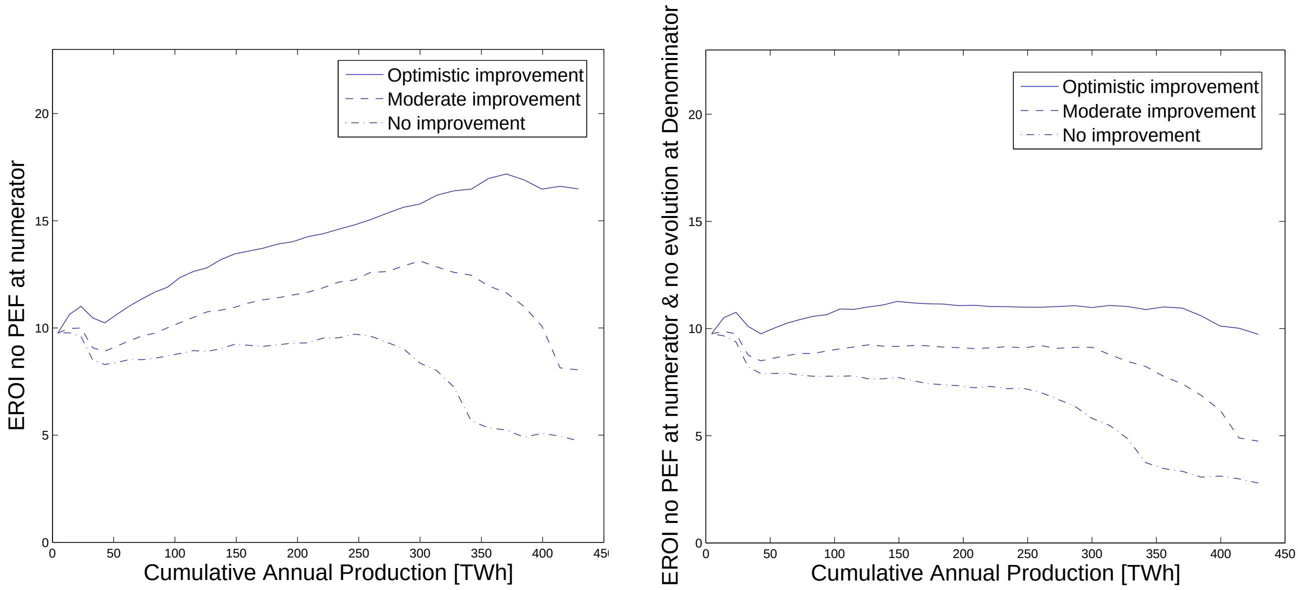

$EROI_{elec,\ adapted}$ $EROI_{elec}$

Figure 6.16: Primary energy factor not include at the numerator of the EROI. OECD Europe, GP Advanced Energy Revolution CSP yearly need installed, from 2015 to 2050.

For the $EROI_{elec,\ adapted}$:

- The EROI increases for the optmistic scenario since less fossil primary energy is consumed for the LCA which is lower and lower.
- For the moderate and no-evolution scenario the EROI increases for the same reason and then decreases fast since the locations are too bad.

For the $EROI_{elec}$:

- The EROI is stable for the optmistic scenario since the technological improvement balance the land scarcity.
- For the moderate and no-evolution scenario the EROI stabilized period is shorter and, since more plants are built, the land scarcity prevails over the technological improvement.

It is not a nonsense to reevaluate the energy cost of a plant (i.e. use $\alpha(t)$ instead of α_{LCA} in the CED computation for the LCA) over the years since the fossil contribution to the electricity production on the grid is lower and lower.
Nevertheless, it boosts the EROI. If we want to compare the EROI of CSP to another technology we should be aware that this technology will have the same boost.
So, it is better to use the $EROI_{elec}$ to compare EROI values to existing ones of other technologies.

From the table 3.1, we have an approximated value of a $EROI_{elec}$ which is set to 16. It gives an idea of the order of the value for wind turbines.
A real comparison with wind turbines technology could be done thanks to the article of Dupont et al. [4]. For a 430 TWh (1.548 EJ) optimal installation of annual production with wind turbines, the minimum EROI could be about 16.
In our case, for the same annual production, with an optimistic improvement growth for the technoly, the mean EROI is about 10. It then demonstrates that the CSP tower technology, considering the hypothesis made, is not as effecient as the wind turbines technology in terms of net energy returns.

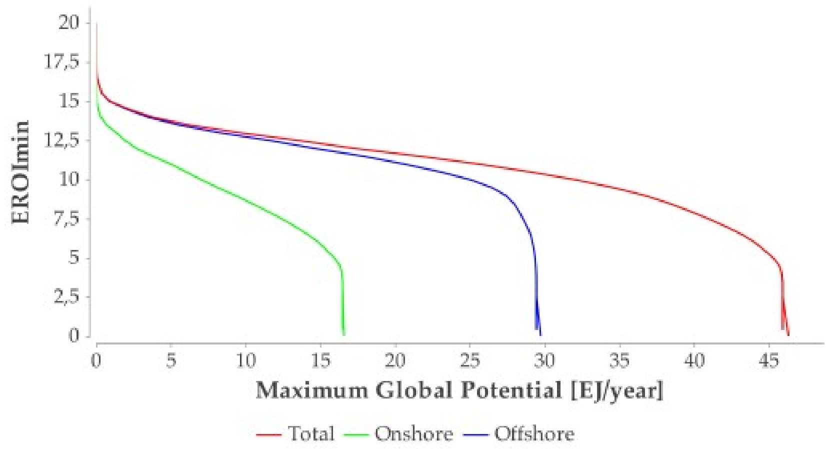

Figure 6.17: $EROI_{min}$ for wind turbines deployment for Europe, with optimal installed capacities, from Dupont et al. [4].

6.4 Summary of the different assumptions and possible improvements

These results are not so accurate since the EROI was set to a plant life cycle of 30 years. In these example, the plants built in 2015 for example, are not replaced by new one in 2015+30=2045. It means that from 2045, new spots, from the top of the ranking are available to install new state of the art plants.
This change is minor and would then improve the EROI since good spots are recovered.

We should also take care about the percentage of bare land (30%) and areas with sparse vegetation taken (5%). It is impossible to know exctacly which are available or not, but a more profound analysis on these parameters could improve the accuracy of this study.

An important assumption is the consideration of always usefull production. Indeed, the curve of electricity demand by region was not taken into account. It would mean that sometimes, the electricity produced could not be use at the same time it was produced. But, in our case, CSP tower are always equipped with TES and could adapt the storage to deliver the electricity at different time. It could be interesting to implement such a constraint and compare the result.

Another assumption is the non-consideration of the wind, which reduces the optical and receiver efficiency, from a place to another, but with a quite low impact.

6.5 Conclusion about CSP deployment in OECD Europe

The model demonstrates that implementing CSP tower technology in OECD Europe, even with the assumption that the technology evolves is not so interesting. Indeed, the net energy returns delivered by CSP plants is lower than the one of current technologies and wind turbines for the same production required.

The Greenpeace Advanced Revolution scenario plans to reach the goal of 430 TWH in 2050. In their scenario, they propose a 85 GW installed capacity of CSP technology (not mentioned if it is tower or not), with a solar multiple of 3 and 12 hours storage.
With optimistic assumptions about the technology improvement, our study proposed, to reach

this goal, to install 80.5 GW, representing 1807 plants, spread among the location showed in figure 6.12. The land required is about 12649 km^2 and the mean global capacity factor is 61.6 [%], see table 6.4.

Nevertheless, the EROI factor is low. Considering the values of the primary equivalent EROI (so with PEF evolution) below 20 as unacceptable: none of the scenarios is viable. The optimistic evolution should stop the deployment at an installed park able to produce 300 TWh. According to the scenario, this capacity is reached in 2041. This parks would account about 1200 plants, with an installed capacity of 56.9 GW installed, see table 6.4.
For the $EROI_{elec}$, the optimistic scenario has a mean of about 10 with quite stable values. This value seems low in comparison with wind turbines deployment values (15-20) (see figure 6.17).

Evolution parameters	efficiency 2015-2050 in [%]		
	no-evolution	Moderate	Optimistic
Solar Field	60	60-65	60-70
Receiver	90	90-95	90-97
Power Cycle	35	35-45	35-55
Deployment OECD Eu.	To produce 430 TWh/year by 2050		
Installed capacity [GW]	126.5	94.5	80.5
Number of plants	3540	2344	1807
Land occupancy [km^2]	24780	16408	12649
Primary equivalent EROI	from 25 to 4	from 25 to7	from 25 to 15
$EROI_{elec}$	< 10, decreasing	< 10, decreasing	plateau at 10
Installation chara.	40 TWh, 9 GW,	150 TWh, 33.6 GW,	300 TWh, 56.9 GW,
... at Pr-eq EROI = 20	2018, 200 plants	2027, 750 plants	2041, 1200 plants

Table 6.4: Summary of the results for OECD Europe Deployment. Notice that results always correspond to a year since the technology development evolves from 2015 to 2050.

As seen in the table 6.1, Morocco, as the other countries of North-Africa, has a huge potential for CSP applications, meaning that studies analyzing the electrification of North-Africa should deeply integrate CSP applications in their scenarios.

The figure 6.18 presents the $EROI_{elec}$ evolution for the countries of North-Africa with access to the mediteranean sea (Nigeria, Morocco, Egypt, Tunisia and Lybia). The installation from 2015 to 2050 was set as 5 times the one presented before for Europe, in terms of annual production in 2050. The land availability is huge, so the EROI grows with the evolution of the technology and reaches interesting values.

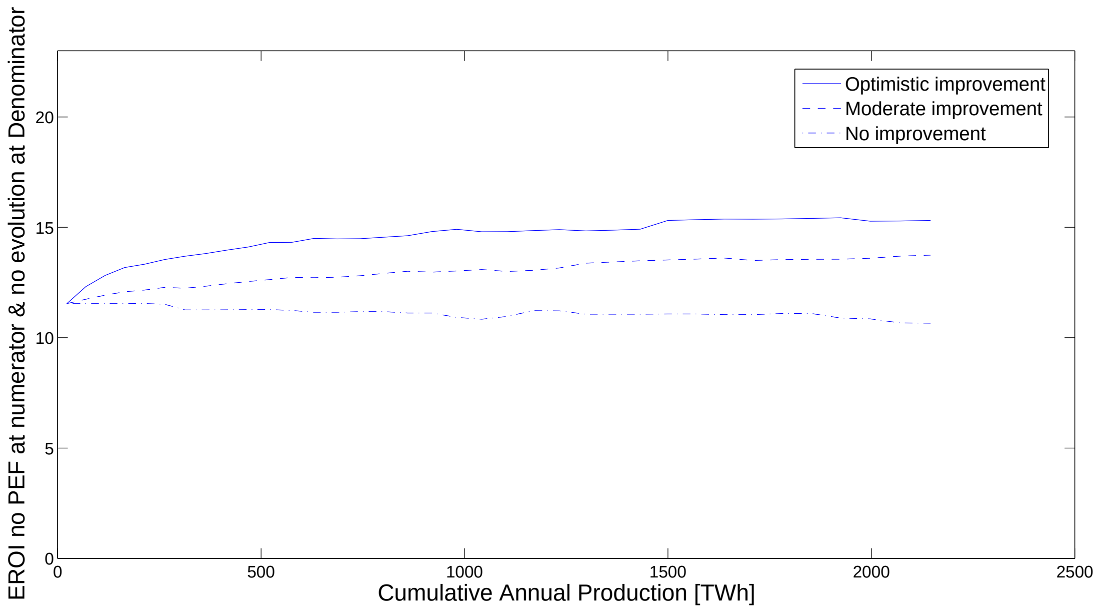

Figure 6.18: $EROI_{elec}$ evolution for North Africa (Nigeria, Morocco, Egypt, Tunisia and Lybia). The installation goal is a 5*430 TWh/year in 2050, 5 times the one defined for Europe before.

The transportation of stored hydrogen or electricity from there to Europe, as the Desertec plan, is reinforced from this analysis since Europe does not have the spots available but North-Africa does. Though, the energy security and the transportation cost and viability are strong challenges to face.

Conclusion

A model able to compute the electricity production and the Energy Return on Investment (EROI), for a specific CSP tower plant, was described and implemented. The model is based on the analysis of monthly average irradiation data from the NASA. From there, hourly direct average irradiation values are computed. The electricity production is calculated by simulating the plant behaviour for each hour of a year. Three main parameters distinguished themselves to characterize a CSP tower plant configuration: the power designed for the turbine of the power cycle, the size of the heliostat field and the storage capacity.
The EROI of the plant was concluded as the most relevant factor to optimize since it leads to the maximum net energy delivered by the plant. An optimization process, on the three main parameters (power designed, storage capacity and size of the heliostat field), allowed to compute the configuration giving the highest EROI factor for any location and plant configuration. To complete the EROI computation of a given plant, it was necessary to decrypt LCA analyzes. The energy cost of a plant, found for the plant's configuration considered by the authors, had to be adapted to any kind of plant configuration. A function was implemented to compute the energy cost of a plant given its configuration. The energy cost was set to increase linearly with the number of heliostats (mirrors), the power designed and the storage capacity.

The optimization process proves that the configuration giving the highest EROI value varies according to its location. In general, the optimal plants have a medium designed power, about 45 MW, which is reduced if the irradiation level of the site decreases. All the optimal plants always reach the maximum area allowed for the size of the heliostat field.

The optimization results were then used to complete a dynamic EROI analysis. A program ranks the available sites of OECD Europe from the best to the worst in terms of mean yearly irradiation. From there, implementing an improvement of the efficiency of the heliostat field, receiver and power cycle, it was possible to simulate the EROI evolution for a future CSP tower deployment.

The program was used to simulate different deployment scenarios of the CSP tower technology in OECD Europe. Different evolutions of the technology improvement were implemented. The evolution of the EROI factor was analyze to characterized the results.
The model had to install optimal plants in terms of EROI, at available sites, to supply enough power to follow the Greenpeace Advanced Energy Revolution scenario, i.e. to reach the goal of 430 TWH in 2050. Considering an optimistic improvement of the efficiency, 80.5 GW should be installed. It would represent 1807 plants, spread over Southern Europe. The land required is about 12649 km^2 and the mean global capacity factor is 61.6 [%].

The EROI ($= \frac{\text{Energy}_{\text{delivered}}}{\text{Energy}_{\text{consumed}}}$) was computed by two methods, leading to the primary equivalent EROI (EROI$_{pr-eq}$) and the electric one, EROI$_{elec}$. The first method, giving the EROI$_{pr-eq}$, converts the electricity produced by the plants (the numerator of the EROI) as a primary fossil equivalent energy. The conversion factor is adapted to the evolution of the energy mix in Europe and is also used to update the primary value of the electricity consumed by the plant for its operation (in the denominator of the EROI).
The second method, giving the EROI$_{elec}$, keeps the numerator, the energy production of the

plant, as an energy vector (electricity) and does not adapt the denominator to the energy mix.

Both EROI methods have advantages (the first is adapted to the energy mix evolution and the second is easier to compare to other technologies). For an optimistic improvement of the CSP tower technology:

- if the minimum $EROI_{pr-eq}$ is set to 20, which is not so strict, this scenario should stop the deployment at a yearly production of 300 TWh (over the 430 planned), representing 1200 plants and an installed capacity of 56.9 GW.
- the $EROI_{elec}$, during the complete deployment, has a stagnant value around 10, representing a plateau. In comparison with an optimal wind turbines deployment in Europe for the same yearly production, reaching $EROI_{elec}$ around 15-20 (from Dupont et al. [4]), the result seems quite low.

These results confirm the low net energy return of CSP technology for a deployment in OECD Europe, though the technological improvement was optimistic. With a value around 10 for the electric equivalent EROI, the energy sector scale would need to more than double, as the value of the current energy mix for the electric equivalent EROI is much higher than 10. Therefore, operating an energy transition in OECD Europe, with CSP technology as the main pillar, would change the way in which the energy is allocated in the society since the energy sector would need much more energy to produce the same quantity than currently.

However, the study also demonstrates that the countries of North-Africa have a great potential for CSP applications. They own a huge lands availability at good irradiation levels. The $EROI_{elec}$, for an installation able to produce more than 2000 TWh/year in 2050, increases from 11 in 2015 to values around 15 in 2050, thanks to the technology improvements linked to a high lands availability.
Studies analyzing the electrification of North-Africa should integrate possible CSP applications in their scenarios. The transportation of stored hydrogen or electricity from there to Europe, as the Desertec plan, is reinforced from this analysis. Nevertheless, the energy security and the transportation cost and viability are strong challenges to face.

The model has some hypothesis to keep in mind, as the simplified method using the efficiency for the energy conversion and not a thermodynamic simulation. As well, the simple storage implementation used and the highly used linear relation between the size and energy cost of the plant, in the EROI computation, should be remembered. Moreover, a deeper analysis of available areas would confer more weight to this kind of analysis.

To conclude, the CSP evolution perspective is highly linked to a continuous improvement of the technology. The review presented prove that the evolution of CSP tower technology is in a good way. Moreover, the CSP has the possibility to store energy, which could be used to control the rate at which the electricity is delivered, giving an advantage over the other renewable technologies. However, the high price of CSP plants and its large scale, in a new context of low-cost photovoltaic panels and decentralisation are serious drawbacks. The future real installations of new model of CSP plants, as for example ones with a solid particle receiver and a supercritical CO_2 cycle, will tell us if the technological improvement is strong enough to sustain a possible CSP development in certain regions of the world, or not.

Appendices

A Definitions of the terms used for the balance energy model

A.1 Resources

The different resources considered in the model are the ones below in accordance with the IEA. The resources are the natural elements, considered as primary energy. They are directly consumed as primary energy or transform into final energy as electricity or heat.

A.1.1 Coal

Coal suitable to support a blast furnace. Anthracite in this category too. Both with a gross calorific value above 24 000 kJ/kg.

A.1.2 Crude oil

Mineral of oil of natural origin. It comprises also refinery feedstock and addtitives as well as other hydrocarbons.

A.1.3 Oil products

Refinery gas, gasoline, kerosene, diesel, bitumen, lubricants, naphta, jet fuel,... and other type of products from refineries treatments.

A.1.4 Natural gas

Underground natural gas composed mainly of methane.

A.1.5 Uranium

Mineral accounted as primary heat equivalent for the electricity production.

A.1.6 Sun

Energy as heat and light from the sun.

A.1.7 Wind

Kinetic energy of wind.

A.1.8 Hydro and Ocean

Mechanical energy from the tidal movement and potential energy from lakes with damps.

A.1.9 Geothermal

Energy available as heat emitted within the earth's crust.

A.1.10 Biomass

All biomass sources except organic municipal wastes

A.1.11 Biomass wastes

Organic municipal wastes

A.1.12 Hydrogen

Thanks to the energy released while burning the hydrogen, it enables to use it as a fuel.

A.2 Technologies definition

A.2.1 Electricity plants

Designed the plants dedicated to produce only electricity except nuclear ones.

A.2.2 CHP plants

Plants producing both heat and electricity (equivalent to cogeneration).

A.2.3 Heat plants and direct heating

Refers to plants and devices (including heat pumps and electric boiler) designed to produce heat only.

A.2.4 Oil refineries

Refineries transforming crude oil in oil products.

A.2.5 Nuclear plants

Nuclear plants.

A.2.6 Photovoltaic

Refers to technologies converting light from sun to electricity.

A.2.7 Solar thermal

Refers to technologies converting heat from sun to electricity (CSP) and using the heat directly (solar panels).

A.2.8 Wind turbines

Refers to off-shore and on-shore wind farms.

A.2.9 Hydroelectric damps

Turbines producing electricity from potential energy contains in the water.

A.2.10 Tidal energy converters

Technologies producing electricity from tidal energy.

B Defining the current and limiting values for each technologies

In the following, the values of conversion for different technologies and sources are analysed. Sometimes the classification is done per source type or technology type, depending on the most suitable point of view. Firstly, direct heating is covered and followed by CHP technologies, described for all kind of sources. After that, a focus is done on geothermal and biomass for the heat and electricity plants only, because CHP plants were analysed in previous point for all sources. To finish, hydroelectric processes are described and their efficiencies analysed. A value is forecasted for the efficiency in 2050 for each case studied. In general, the rigth current efficiencies are quite difficult to defined since it should be an overall value of the efficiency for a certain technology-source tandem on all OECD Europe region and not only the best value achieved.

Direct heating

Heat from electricity generation and heat pumps. Heat pumps are made up of a condenser, an expansion valve, an evaporator and a compressor [51]

The COP, heat generated on the electricity consumed (by the compressor), has a range of about 1.8 to 5 [52]. The average COP for all applications could be approximated to 3. The COP value depends mainly of the temperature of the heat source needed and the one of the cold source. The theoretical Carnot cycle for a cold source at 10°C is from 12.3 (heat at 35°C) to 4.8 (heat 85°C) [52]. The average physical limit is about 7.5 for the same range of temperature.

Heat pumps system are used in industry processes as drying and also domestical heat systems. It exists different types as ground source heat pump, solar heat pump, photovoltaic-thermal heat pump, chemical heat pump (see [51]). The technology is promising to evolve. For example the author presents a hybrid system composed of PVT and heat pump combined. The system achieves an experimental COP value of 6.45 which is quite high for a drying application (drying temperature was 50°C).

Heat from fossil fuels. Most of thermal heating from fossil fuels can be summarize as boiler application. Boiler efficiency value is commonly set to 92% and is not really prone to evolve a lot.

direct heating efficiency values [%]	Current	Physical Limit	Prospection, 2050
Heat pumps	300	750	350
boiler with fossil fuels	92	100	93

Table B.1: Efficiency values used in the model to convert energy in heat from boilers and heat pumps. No real improvement is expected for boiler technology. The values for heat pumps depends a lot of the conditions of applications, then the average total efficiency can't grow so fast.

CHP

The main advantage of CHP technologies comes from the saving of energy resources by comparison to produce the same amount of useful energy (electricity and heat) from two separated systems. The overall efficiency of CHP plants is expressed as the sum of the electricity and heat production efficiency : $\eta_{overall} = \alpha_e + \alpha_Q = \frac{P_e}{\dot{m}_{fuel}LHV} + \frac{P_Q}{\dot{m}_{fuel}LHV}$. So, a high value of $\eta_{overall}$ doesn't mean a good thermodynamic efficiency since two flows of different nature are added and electricity is more valuable than heat. Then, the only losses are the one from the chimney and therefore this efficiency is always really high. A better thermodynamic variable is ϕ: the ratio between the heat production and the electricty one. Replacing it in the definiton of α_e and α_Q we obtain:

$\alpha_e = \eta_{overall}\frac{1}{1+\phi}$ and $\alpha_Q = \eta_{overall}\frac{\phi}{1+\phi}$. Here is the thing: the more we produce heat in CHP unit, the less the efficiency of the power production is. So, if the heat produce is not really well used, it is better to produce the electricity in a classical TGV central for example. Moreover, as explained in [53], the maximum economy of primary energy (EPE), so mathematically its limit, when compare to a power generation from a TGV production ($\eta = 0.58$) and a heat generation from a boiler ($\eta = 0.92$), is about 0.28 and occurs for a ϕ of 0.64. So, the saving of primary energy, using a CHP unit, exists but is not so high and really depends of the amount of heat compare to the quantity of electricity produce. Moreover, when the design is done and the production start, the heat is characterized by a constant flow and temperature, and can't be change easily or adapt. A CHP unit production is useful when it can be located in a place linked to a grid and not so far from the consumption of the heat, the calorific need should be enough so that the efficiency is high and stable in temperature and mass flow.
For the moment the global CHP production "remains stagnant at around 10% of the global world production"[54] and according to this book from IEA about energy technology perspectives, 26% are used for industries needs and the global average efficiency is was about 58% in 2011. Often the use of CHP processes is more reserved to industries but in some countries a big part of the population benefits from it as in Denmark, Sweden, and Estonia among others.
CHP technology is composed of a quite large number of different solutions, adapted to the electrical/heat output needed. This panel is composed of ICE(otto,Diesel), GT, ST, CC mostly plus all particular biogas processes.

Coal. Example of a Counter Pressure Steam Turbine from a manual about thermal machines [53]: EPE= 0.11, $\alpha_e = 21\%$ and $\alpha_Q = 69\%$

Natural Gas. Example of a Gas Turbine with postcombustion and Steam Turbine from the same manual: EPE= 0.202, $\alpha_e = 40\%$ and $\alpha_Q = 47\%$. for only heat recovering after the GT: EPE= 0.15, $\alpha_e = 37\%$ and $\alpha_Q = 47\%$.

Oil products. ICE: recovery of parietal losses and mechanical losses to produce heat with moderate temperature (district heating for example). Example [53]: EPE= 0.15, $\alpha_e = 39\%$ and $\alpha_Q = 45\%$.

Geothermal. Under certain conditions, geothermal source can be used to produce both heat and electricity. In general, it is done if the "waste" water from the electricity process has still a interesting temperature as for district heating or fish pond heating or another useful purpose not so far from the plants [55]. Nowadays, some low temperature geothermal CHP binary plants (ORC-WHR) appears and allows to use medium enthalpy. Some European region have potential to install such technology as the north and south of Alps region, Pannonian basin of Hungary and borders areas of the country, the Paris bassin, Northem Germany among others [56]. According to this article, this technology could theoretically rise the utilization efficiency of geothermal to 39-48 % (about +20%).

Biomass and wastes. Decentralized biomass CHP seems to be a good future solution. According to a review from the Biomass Gasification Group of Denmark[57], biomass gasification CHP, and especially for small units (<10MW) are good alternatives to biomass combustion. In effect, it could be possible to reach efficiency of $35-40\%$. So, decentralized CHP Biomass is already viable solution. Moreover, converting natural gas CHP units in biomass one is possible and not so expensive since the gas engine is already set up; and converting the CHP firing plants to efficient CHP plants with biogas is also easy.
The flexibility of this kind small units of biomass CHP plants were tested by a Denmark study from DTU in 2003. The "Viking project", explained in [57] is a two stages concept (pyrolysing and gasification separated). It proves a flexibility of this kind of gasification plants. Simulating demand curves for consumption of heat and electricity they reached a level of $\approx 70-100\%$ of following fluctuations (district heat and power) as well as supplying a calorific flow at the same temperature: all of this thanks to a gas composition staying more or less constant. And with an electrical efficiency of 25%. The article also mentioned a biofuel-heat-power cogenerating plants. They used the unconverted gas to produce electricity, and the heat of the fuel-process as useful heat, reaching an overall efficiency of 90%.

But the topics of biomass is more complex since the biomass itself, varies in nature and quality. All these results before were done for a good quality wood biomass. From the others type of biomass, the same article presents the low temperature circulation fluid bed (LT-CFB). This technology is able to use organic wastes and sewage sludge among others. Some test proves an efficiency for small units of 87-93% and it is attended to reach more than 95% for bigger projects. The drawback is that the gas produced during the process is unsuitable to produce electricity but it exists projects to couple this kind of plants next to a coal firing one and fire both coal and gas together. Now some researches try to clean the gas in the goal of using it directly to produce electricity.

Gasification Platform	Platform ad-on	$\eta_{electrical}(\%)$	$\eta_{thermal}(\%)$	$\eta_{total}(\%)$	Misc.
$Updraft$	Gas engine	28	55	83	-
$FICB$	Gas engine	25	56	81	-
$TwoStages_{Viking}$	Gas engine	25	46	71	small scale
$LT-CFB$	Steam Cycle	38	52	90	Fertilizer production

Table B.2: Technologies of biomass CHP units and their efficiencies [57].

The drawback of biomass CHP units are the lack of flexibility and efficiency. The Biomass CHP plants, if well implanted, are a sustainable way to pursue the energetic transition. For example, a case study in Lutvia show that it's load on environment is low as the emergy indicators indicates it [58].
But, as a study from Holland [59] demonstrated, the scaling up of biofuel plants does not necessarily incease performances and the environemental indicators are often lower. Moreover, the fear of feedstock problems and the high transport costs are two more factors that disadvantage big facilities.
In the Green Peace scenario revolution there is a transition from the traditional used of biomass to the state of the art CHP technology. Some other, in a short time period, imagine small CHP units as Stirling engines or Organic Rankine Cycle for personal house heating. This requires smart grid and storage supplies so a political support from governments for example. And the leading UK companies in this sector planned a strategy vision to enhance the micro CHP as a "key component of emerging smarter energy sector"[60]. According to this same article of the Fuel Cells Bulletin, the Japan launched in 2010 a support strategy to encouraged public to adopt this technology, with success.
In comparison with the use of biomass in incineration, gasification units or biofuel creation, the used of biomass for biogas used in CHP plants is more efficient. In the article [61], we learned that some future improvements are in studies as the improvement of the thermal processing using CFD optimization and the particle and ashes separation from the gas with the use of a cyclone gasifier with a vortex collector pocket.

Hydrogen. Hydrogen could be used as a fuel to deliver heat and power at housing characteristics. Used in a fuel cell, it can cogenerate heat at around 50°C and electricity, supplying a family or a district. More than attracting the attention, the technology is already in application in Corea and Japan with more than 80.000 applications for the latter [62]. A study from the universities of Ghent and Antwerpen [63], analyzed an alkaline fuel cell system as a micro-CHP. The system provides a heat at around 50°C. They found than for a heat-ratio below one, this technology is already better than all the others (Stirling, micro-turbine, diesel engines,etc.) in terms of efficiency. The electricity generation efficiency is particularly higher than for other technologies and the heat one below, but with a superior total. In average, for a low heat ratio (0.2-1) the electricity generation efficiency is about 43%, and very stable, and for heat generation about 30%. This technology is then promised to be more and more implemented as the electricity consumption for habitations is growing and the heat consumption expected to fall.

General forecast for CHP. Some are arguing that micro-CHP is not suitable since the heat delivery impacts the electricity production efficiency and could be better to use TGV to produce the electricity and heat pump to produce the heat, from the electricity of the grid, created with higher efficiency [64]. The major arguments are that non flexible of CHP units if the ϕ changes from the design one, the efficiency decrease and if their is an excess of electricity production the job on the grid would be really poor.

Still, everybody agrees than for Norway and Denmark among other countries, CHP is useful as district heating and useful for industries too [65]. The district heating in Denmark is about 46%. Most of it from Natural gas and a part from biomass solution. In the future, by connecting furthest buildings (1km around) to district heating areas this number could raise to 70% [66]. This study found out that Micro-CHP (like hydrogen cells based) have a too high cost and too low afficiency to be part of a real 100 per cent renewable energy system. It concludes that micro-CHP with natural gas, electric heating doesn't convince neither and that heat pumps more or less equal to district heating in a future 100 per cent renewable energy system from an energy and economy view, highly depending on the distance from buildings to heating grids.

CHP efficiency values according to sources [%]	Current	Physical Limit	Prospection, 2050
Biomass_{elec}	34	50	45
Biomass_{heat}	36	50	45
Geothermal_{elec}	6	35	11
Geothermal_{heat}	45	65	51
Waste_{elec}	22	50	28
Waste_{heat}	30	50	48
Hydrogen_{elec}	43	55	52
Hydrogen_{heat}	30	45	42
$\text{Natural Gas}_{elec}$	37	45	42
$\text{Natural Gas}_{heat}$	47	55	50
Coal_{elec}	21	25	22
Coal_{heat}	69	75	70
$\text{Oil products}_{elec}$	37	50	40
$\text{Oil products}_{heat}$	42	50	45

Table B.3: Summary of the efficiency values used in the model to convert energy by CHP technologies into electricity or heat.

Geothermal Processes

The geothermal processes thermal efficiency is lower than thermal ones for the power production. The evaluation of the efficiency is based on the enthalpy of the geofluid. It varies with heat losses, ambient condition, non-condensable gas content (NCG: H_2S, CO_2,...) and dissolved minerals quantity in the geofluid, the size of the power plants, the design, and the parasitic loads (fans, pumps,...). Those are the main parameters.
The main power plants designs are: dry steam, single flash, double flash and binary plants. All designs use the geofluid as calorific fluid except the binary one. The dry steam design use a particles remover while the single flash use a cyclone separator and the double flash a low and high pressure separator. It is an improvement of the single flash design, so its efficiency is higher. Actually the dry steam and single flash design are really close and can be set together. The binary plants transfer the heat of the geofluid to another low boiling point working fluid. Its efficiency is lower than the other concepts but its use is reserved for really weak geofluid potential. The review from the geothermics journal[67] studied 94 geothermal plants and realize an average efficiency by technologies (see table B.4) and an overall one.

Geothermal technologies	data approach	efficiency range [%]	$h_{geofluid}$ [kJ/kg]
dry steam/single flash	$\eta = 8.7007ln(h) - 52.335$	6-16	800-2550
double flash	$\eta = 10.166ln(h) - 61.68$	6-14	800-1800
binary plants	$\eta = 6.6869ln(h) - 37.929$	2-8	300-1050

Table B.4: Efficiency based on the enthalpy of the geofluid according to a review from the geothermics journal [67], based on a published data list and utilization efficiency from [68].

So, according to this review, the world average efficiency for the power generation, is about 12%, in compliance with the 94 plants studied. It is a bit bigger than the generally international 10% efficiency used and recommended by IEA. In the other hand, the efficiency of district heat supply from geothermal sources really depends on the location and the average efficiency of 50% suggested by IEA will be use.

The efficiency of the geothermal dry steam plants increased of 2.2 times from 1913-2000; mostly due to components improved [69]. The efficiency for the geothermal technology, in average, won't grow a lot in the future. The potential to enhance it is situated in the combined solar/biomass and geothermal cycles. Then the temperature of the geofluid could be raised to a hotter point. A study analyzing the role of district heating in future renewable systems [70], analyzed the solar-chimney and geothermal combined cycle and concluded that it is benefical to combined them. But still we saw than biomass need to be of high quality and local to be really efficient and I doubt there are a lot of place for combined thermal-solar and geothermal plants. Since both technologies really depend on their locations. But the installation is growing. In 2015, a capacity of 18.5 GW_e from geothermal plants were installed in the all world. It represents a raise of 73% from 2010 [67]. Moreover, the district heat supply from geothermal source (from "low energy source") is increasing and already well implanted in some regions of France [71].

geothermal efficiency values [%]	Current	Physical Limit	Prospection, 2050
Electricity plants	12	54	16
Heat plants	50	100	52

Table B.5: Efficiency values used in the model to convert geothermal energy in electricity or heat.

The physical limit for the electricity plant (see table B.5) is established from a Carnot limit with a hot source considered as a geofluid with characterisitc of water and an enthalpy of 1500 kJ/kg. Since the efficiency depends a lot of the geofluid characteristics, the forecasted value is not expected to reach high level in 2050. The heat losses incurred for heat plants aren't expected to vanish in the future and so the forecasted value is quite similar to the current one.

Biomass

Heat generation. Housing heating fireplace can be replace by catalytic stoves who can reach efficiencies of up to 83% but typically have an efficiency about 65-75% HHV [72], which could be about 30-40% LHV efficiency.

Electricity generation. The most effective way to generate power with biomass is to fire it with coal. If the amount of biomass exceeds a certain value ($\approx$ 10%), then the co-firing (separated firing) of coal and biomass take place. This process have an efficiency up to 45% for the really recent units[73].
Another way for power generation is to use a combined cycle: from biogas burning in a gas turbine combined with a steam cycle. The total efficiency is about 38-40% [74] and [65], depending on the parameters of the installations. But this kind of unit are an order smaller than the co-firing ones due to the lack of feedstock and transports costs mainly. This technology is not really installed yet and is promised to evolve.

From a power generation point of view, the CHP plants using biogas[1] have an efficiency about 34% from biomass and 22% from solid waste, according to a study of IEA [73] and the Eurelectric working group [65] with an "overall efficiency" of 85-90%.
Stirling engines CHP exist also, but for really small units, with an efficiency from 11 to 20% [73].

The co-firing process could be one of the most efficient way to use efficiently the biomass in a way of producing electricity and reduce CO_2 emissions. Under an article from IEA[73], since coal is used to produced 40% of electricity in the world, for each percentage point replaced by biomass, the gain is 8GW of installed biomass capacity (and should be around 60Mt of CO_2 avoided per year). The main advantage of this strategy is that the coal power plants already exist. Moreover, the investment needed to upgrade a coal plant to a co-firing one is quite low and the payback really fast, approximately two years according to the study of the IEA [73]. The drawbacks are the lack of good local biomass and big amount of it near the central. This strategy is realistic only for a short term vision because it is still based on coal. The future scenarios that Europe could follow to reach the objectives it engaged for at the COP21 can't lie down on coal. For example, according to the energy revolution scenario of GreenPeace [3], which the goal is to avoid CO_2 emissions to stay under a global warming of 2°C, coal will not be use anymore in OECD-Europe from 2040; and it is the same for their advanced energy revolution scenario. Only the reference scenario of GreenPeace [3] still used coal for the power generation. The common point of all these scenarios is that the amount of biomass used for power generation will approximately double from 2012 to 2040 but in the revolution case, will decrease a bit from 2040 to 2050. The same trends are remarquable in IEA's scenarios. For example, in 2040 for the European Union, the share of the coal to generate power decrease dramatically for the new policies scenario and the 450 scenario and is decreasing a bit for the reference one. In conclusion, to produce electricity from biomass, the co-firing process and it's expansion could happen only in the reference scenarios.
In opposition from power generation, in all these scenarios from both IEA and GreenPeace, the quantity of biomass use to produce heat is increasing a lot. In parallel as explained above, the quantity use for power generation increase (but not so much) and then decrease a bit. It's due to the fact that the biomass will be used in CHP plants and not at all in electricity plants. So, except in the reference scenario who will use mostly co-firing process and some BIG/GT processes, no electricity plants using biomass will exist. The electrical power product from biomass will only come from CHP plants. In summary, for the reference scenario power generation would be mainly co-firing process, increasing in time with BIG and also CHP. For energy revolution scenarios, CBCC/GT technologies disappear and only electricity production from CHP is left.

biomass efficiency values [%]	Current	Physical Limit	Prospection, 2050
Heat plants and direct heating	40	100	48
Electricity generation	42	60	45

Table B.6: Efficiency values used in the model to convert biomass in heat or electricity.

Hydroelectric damps

Hydroelectric is the first renewable source for power generation. It exists three different types: run of rivers, reservoir, pump/storage. The run of rivers is dedicated to small hydro, the reservoir ones to medium and large hydro projects and pump/storage are a particular kind of storage system. At the end of this section a table summarized the values defined in the model (see tableB.8).

	overall efficiciency [%]
small hydro	80-85
large hydro	90-95

Table B.7: Overall efficiencies of hydroelectric projects from a work of the Eurelectric Working Group [65].

[1] the losses occurring during the thermochemical transformation of biomass into biogas are about 2 to 4% [73].

For the moment the part of large hydro in Europe is about 90% [75]. So, an acceptable value for the average efficiency of hydroelectric plants in Europe would be 91.5% [2] from the value given in table B.7.
The capacity factor interpretation is quite different from other renewable energies. Its value can be quite high or low, depending on the flexibility wished. For a high flexibility, the installed capacity is large and the capacity factor low, for a flexible one it is the opposite.

For the moment, the installed capacity ranking is leaded by China and Brazil, representing the two continents with the most hydro projects. In Europe, the potential to install new hydroelectric plants is low. The focus is done on improving the efficiency and capacity, install pump/storage system and adding capacity to no powered damps[75] (small hydro). The potential of small hydro is highly criticized, for example, in [64]. The author multiply simply the rain fall over an area and the average altitude of a region in England, two times for the medium and high region. He found out that if all the rain potential energy is used (means damped rivers everywhere and 100% efficiency and no transportation/transmission lost), hydro in England could only deserve 7 kWh/day per person. In reality, a maximum of about 20% is only possible to achieve. So, in a objective of a green transition in Europe, the focus on small hydro wouldn't be a solution. Developing large project and improving the existing one is a step but the majority is already installed. From a global point of view, Africa has a really high potential for large hydroelectric projects, and small hydro is a good solution to electrify the rural areas. In the future a quiet amelioration is possible with a better design of the turbines (Francis for the large hydro and Kaplan for the small one) and overall thanks to the replacement of older ones.

Hydro	Current	Physical Limit	Prospection, 2050
Efficiency value [%]	91.5	100	92.5

Table B.8: Efficiency values used to know the total hydro energy quantity consumed. Unlike for the other sources, the values defined in the prospection aren't expected to change from a scenario to another because of the similar importance accorded to this technology.

B.0.11 Defining the current and limiting values for wind, sun and ocean energy conversion.

This part is dedicated to the analyse of the efficiencies used in sun, wind and ocean energy conversion technologies. Theses efficiencies are particular since the energy consumed is defined as almost an infinite free energy source. In all scenarios all of these efficiencies are set to 100%. Here, the model proposes to let the choice of taking it into account. It should also be mentioned that CSP technology is composed of a thermal cycle and a light-to-heat process. A distinction is made between the efficiency used as light-to-electricity and the heat-to-electricity. The last one is used by the scenarios. Again, the model gives the choice to the user to take it into account or not.

Wind

The maximum efficiency for a lonely wind turbine is 16/27 , as describe by the Betz limit (see demonstration at [76]). The average efficiency is at 35% [65]. The Betz limit can't be reach since they are vortex creation and other losses in the flow through the wind farms. The current purpose is not to reach higher efficiency conversion but to increase the charge factor, by increasing the high of the masts for example. Values chosen to run the program, if the quantity of wind taken from the nature should be known, are summarized in the table B.9.

wind	Current	Physical Limit
Efficiency value [%]	35	59.26

Table B.9: Efficiency values used to know the total wind energy quantity consumed from the nature.

[2] $0.1 * 82.5 + 92.5 * 0.9$

Sun

Values chosen to run the program, if the quantity of sun taken from the nature should be known, are summarized in the table B.11, at the end of this subsection. In the following details and motivation about this choice of values are presented per technology. The technologies studied are the CSP towers and PV panels to produce electricity and solar collectors for the heat production.

CSP. A part of the power transmitted by the concentration system (depending on C) is reflected and lost in convection and radiation. The power left is used in the thermodynamic cycle to be converted in power at maximum efficiency constraints by the Carnot law. Then the maximum theoretical global efficiency depends of the losses at the absorption phase and the operation temperature reached.
The efficiency depends on the operation temperature (the greater the better the Carnot efficiency) constraints by the losses mainly due to radiation (the greater the higher, Stefan-Boltzman law whis is proportional to T^4).
The technology of CSP is not mature and evolve a lot. The projects have a higher scale than before and the efficiency is higher. In a presentation about CSP performances forecast [77], we can observe the evolution of the CSP global efficiency, see table B.10.

	1988	2006	2010
Capacity [MW]	10	13.7	100
Efficiency [%]	7.9	13.0	16.1

Table B.10: Evolution of the performance of the CSP technology from a presentation at the electric power conference 2005 [77].

And is expected to reach 17.4% in 2020 according to the same article. This source[77] is from 2005, for the moment we are at 13-16% [78] of sun to power efficiency, which demonstrates a quite good estimation from the source [77].
To optimize the efficiency, the parameters are the operation temperature and the optical properties of the absorber. The goals is to find for the concentration factor C given, the optimal properties of the absorber and the operation temperature corresponding. A study from the Solar Energy Journal [24] analyses how to maximize CSP plant overall efficiency using theoretical material with selective wavelength property. According to this study, the optical properties of the absorber could be controlled using the wavelength dependent radiation distribution of the absorber. The sun radiations have a wavelength a way lower than the radiation losses from a typical black body used in CSP application. The wavelength determining the point where the radiation losses are greater than the sun radiation is called the cut-off wavelength. The perfect material then absorbs the sun radiation below the cut-off wavelength and doesn't for the higher wavelengths, skipping the radiation losses. The article found a theoretically maximum efficiency of about 73% at C=2000 using this kind of material for the absorber. This results were found for the following hypothesis: no conduction losses (isolation is perfect), perfect thermodynamic Carnot cycle, C=2000, ideal absorber (selective absorption properties) working at optimal temperature, the absorption at the wavelength cut-off is from 0 to 1 (which could no be not continue in reality the transition has a width).
According to the author, new discoveries of material with good selective abilities and material structuring methods could lead to the development of absorber with selective optical properties. But achieve to create material with a long lifespan under operating conditions will take time.

PV. Definition efficiency PV:

$$\eta_{sun-to-electricity} = \frac{\text{Maximum power output}}{\text{Incident solar radiant energy on the collector area}}$$

At $1000 W/m^2$, 25C° of cell temperature, and a spectrum of AM1.5.

According to a review about PV technologies [79], silicon amorph cells have an efficiency of 5-7%, uncrystalized 8-10% and up to 13% with a spectrum splitting triple junction. Use of multi-crystalline silicon solar cells is available and the efficiency is about 14-19%. According to this article, solar cells utilizing thin film poly crystalline silicon can reach a power conversion efficiency greater than 19%.

Concentrators:
The aim is to produce more power with less semiconducting materials. The drawback are the cost of focusing, tracking and cooling. From [79] it leads to an average of 1.62 times more power output and so efficiency. An experience described in the review, show an increase of 1.5 for solar panels when there is a higher tilt angle and concentrator in front of them. Concentrator could be used for solar farm but not in classical private rooftop installation. Then possibilities of improvement of the efficiency is larger for solar farm than rooftop projects.

The physical limit:
In [80], the author proposes several way to analyse the physical limit of PV converters firstly based on Carnot limit. He considers a system composed of the sun and the converter. The sun produce the inputs: a heat energy flux at a certain temperature (6000K) and entropy flux. The converter the outputs: energy flux as useful work (with an entropy flux =0) and a heat flux reject to the ambient. At an ambient temperature (300K) this has an associated entropy flux. The entropy generation at the conversion is another input. Knowing that the efficiency equals the useful work divided by the heat energy flux of the sun, the author found that, with the entropy flux of conversion at 0 the limit is reach for 95%. The hypothesis required that there is no entropy production during the absorption, transmission, and conversion. If the entropy production is not set to zero (except for the absorption) the maximum efficiency reachable is 93.3%, known as the Landsberg efficiency. Most photovoltaic system use cells converting diffuse light, allowing to not using sun tracking system. Because of a higher entropy flux than before, since the light comes from all possible angles, the efficiency decrease in comparison with the direct one. Then the author found the Landsberg efficiency as 73.7% in global. From the same article, a three level cell has a physical limit of 63.8% in direct light and 49.3% in global light. A single junction 40.8% in direct light and 31.0% in global.

Solar collectors. Flat plate collector could be single or double glazed. According to a study about solar collectors from the Progress in energy and Combustion Science journal [81], the efficiency depends of the range of operation, in terms of the delta of temperature and the radiation (depending on the location). For domestic hot water range of operation (about 0.04 C°m^2/W) their efficiency is about 60% for the double glazed and 55% for the single glazed. For pool heaters, at their dedicated range, the efficiency is about 75%. As remind the authors, the efficiency depends also of the angle of incidence which is obviously not zero during real application. For example, according to the same study, for a parabolic through collector the efficiency can decrease of 50% for a small difference of the angle of incidence (2 degrees). Then accurate tracking system is used for this technology, achieving the higher efficiency of all collector systems, which is about 75%, with a zero angle of incidence [81].

PVT technology. It exists also a mix of PV and solar collectors called PVT technology. In the review of solar photovoltaic technologies [79] mentioned at the previous PV paragraph, a hot water collector combined to a photovoltaic system experimental study is presented. The water undergoes a natural circulation and is pre-heated flowing in the system. The thermal efficiency found is about 39% and the electric one about 8.5%. According to the research described in this article, this technology could have a real potential in the domestic heating sector, providing electricity too. This technology was discussed to give some idea of possible evolutions of the sun-energy production but isn't implemented in the model.

Sun efficiency values [%]	Current	Physical Limit
CSP	17	73
$CSP_{only-thermal-cycle}$	40	78
PV	15	62.5
Solar Collectors	55	100

Table B.11: Efficiency values used to know the total energy quantity consumed from sun rays.

The value of the limiting PV efficiency is derived from (50+50*1.5)/2. The 50 value comes from the physical limit from three level cells and 1.5 from the amelioration thanks to concentrator in solar farms. It'is considered that half of installations are solar farms equipped with concentrators and the other half rooftop projects.

Ocean

Values chosen to run the program, if the quantity of energy from ocean taken from the nature should be known, are summarized in the table B.12, at the end of this subsection. In the following details and motivation about this choice of values are presented. For ocean energy, two technologies are taken into account: hydroturbines and flapping foils.

The proper efficiency of one hydroturbine is not representative of the future application for tidal energy. As for wind turbines, there will be farms of hundreds of turbines. It means than the flow is highly influenced by the farms and that the efficiency of each turbines depends on the flow, the farms, and the position of the turbine in the farm. None real big tidal projects exist for the moment so the efficiency expected is purely theoretical.

Tidal turbines efficiency is limited, as wind turbines, by the Betz limit at 16/27. This limit could be applied for wind and tidal turbines since the perfect assumption of the fluid is a good approximation but not to vapor turbines (thermodynamics effects). The study presented by Ross Vennell [82], demonstrated that tidal turbines grouped into large farms in high flow channel could produce power at a higher efficiency. But, as reminded by the author, it doesn't involve necessarily higher power production since the flow is slowed down by the farms along the channel. According to the author, the tidal farms has a good development in view as it can lead to better exploitation of the power in a channel flow.

Some studies try to estimate the scale of farm and number of turbines required to extract a certain amount of power from a channel flow [83]. According to the study, the efficiency of farms increases as the best turbines are placed in the corss-section with an output per turbines decreasing in shallow channels and increasing in tidal straits. The study achieve a theoretical efficiency of about 0.85% for the farm in a shallow channel, with a high number of turbines and a small power output for each turbine. This results can give an idea of what kind of limitation a real farm could be limited to; the numbers of turbines and assumptions presented here are to strong to achieve this efficiency in real projects.

It exists also another type of tidal energy converter: flapping foils system presented in a simulation study presented in the Renewable energy journal [84]. According to this article, such a system could generate power with the same level of power efficiency than hydroturbines even with lower stream velocity, which could maximize the numbers of usable tidal sites. According to the authors, one module of several foils could reach an efficiency about 80%.

Ocean	Current	Physical Limit
Efficiency value [%]	50	85

Table B.12: Efficiency values used to know the total ocean energy quantity.

B.0.12 Defining the current and limiting efficiency values for hydrogen production

Hydrogen vector could be used for transport, industries, and CHP plants. Energy is used to create and compress the hydrogen gas. There are many ways to create hydrogen from renewable primary energy sources. Here below are the main possible realizations that will be discussed in the following. Values chosen to run the program are summarized in the table B.15, at the end of this subsection.

- wind offshore - electrolysis
- green grid - electrolysis
- Independant PV units - electrolysis
- thermal solar - water splitting
- geothermal - water splitting
- biomass – anaerobic fermentation

Wind offshore. Electricity produced by wind offshore turbines is used to create directly hydrogen by electrolysis on site, i.e. on a platform in the sea. This method permits to avoid transmission losses, the high cost of submarine cables and the cost of the reinforcement of the grid to support the variable electricity production. The water needed for the electrolysis process comes from the sea. The efficiency of such a project, that doesn't exist yet, have been analyzed by K.Meier in a study analyzing the hydrogen production potential from Norwegian offshore wind [85].

The study analyses the creation of hydrogen from a 100MW offshore Norwegian wind farm located in the North-Sea. Another German offshore wind farm already exists near the targeted localization. The German's load factor is at an average of 38% and is used to study the hypothetic Norwegian wind farm.
The project is composed of an electrolyser, a system to desalinize the sea water and a compressor to inject the H2 gas at 100 bar in a pipeline towards the land. All of these elements would be on a platform. Two different technologies of electrolysers are studied: the solid oxide electrolyser (SOE) and the polymer electrolyte membrane (PEM) system. The main characteristics, adapted to this application (variation of the courant taken in account), are indicated in the following table B.13.

	PEM	SOE
feed in	fresh water	steam
pressure [bar]	21.9	1
$\eta_{electrolysis}$ [%]	62	66
temperature [°C]	< 100	500 to 1000

Table B.13: Main characteristics of solid oxide electrolyser (SOE) and polymer electrolyte membrane systems (PEM) according to a study analyzing the hydrogen production potential from Norwegian offshore wind [85].

The incoming water from sea should be vaporize for the SOE and demineralized for the PEM. The SOE has the advantage of a higher efficiency for the electrolysis process and doesn't use noble material but the outgoing H_2 gas has a lower pressure than for the PEM, meaning that the work of the compressor will be higher. The compressor efficiency used in the study of the article presented [85] before, is about 50% instead of the conventional 70% since it undergoes the fluctuations of the flow of hydrogen gas since there is a fluctuation of energy production from the wind turbines. Power converters need to supply the same voltage to the electrolyser and auxiliary systems despite the variation of the courant. The design used in the article is based on a capacity factor of the farm of 50%, assuming as the best factor for the electrolyser. Due to the variation of the courant, the efficiency of the electrolyser itself is then lower. The values used int the study are between 80% and 100% of the normal efficiency value. The author evaluates the average compression power and heat for the steam generation (for the

SOE) needed, adds the power for the auxiliary systems and finds an overall efficiency of the hydrogen production (see results table B.14). The study demonstrates that the results really depends on the design and the overall charge factor on the year of the wind farm.

	PEM	SOE
Hydrogen produced [t]	4105	3893
Overall specific energy demand [kWh/kg]	82.53	86.59
Total efficiency	40.37	38.48

Table B.14: Main results of the study of K.Meier [85].The results presented were computed for an average charge factor of 38% for the wind farm.

The study evaluated the production price to about 22 euros/kg of compressed H_2 gas. A profitable scenario, according to the author, could happen if the price of the fossil fuels increase follow by the electrolyser cost reduction.
With a better researched of the ideal power level of the electrolyser according to the output of the wind farm, a better production, efficiency and life time of the system could be achieved. Moreover, according to the author, the electrolyser technology itself is an immature technology and cost is waiting to drop in the future. Storage could help delivering the right power to the systems and stabilize the flow of hydrogen, increasing the efficiency of the system

Green grid. Due to the intermittence production of renewable, more and more present on the grid, an idea is to balance the primary frequency on the grid by producing more or less quantity of hydrogen with electrolyser at certain moment. According to frequency deviations, electrolysers would consume electricity to balance the grid and produce hydrogen.
A study from the International Journal of Hydrogen Energy [86] analyses such a project thanks to simulations with the Odyssey platform. “The electrolyser plant operator is purchasing electricity on the day-head market to produce hydrogen. He also offers to the TSO the possibility to increase/reduce its consumption by submitting downward and upward offers on the balancing mechanism and, [U+FB01]nally; he provides a frequency regulation service by adjusting its consumption according to frequency deviations”[86]. The PEM electrolyser has a stack power of 523kW an AC/DC converter with an efficiency of 90%. On a year, based on the French context, the study found an overall efficiency of about 54%, for 87 tons of hydrogen produced at 7 euro/kg.
Some electrolysers could be fitted to consume energy of wind farms. An operational simulation from the Renewable Energy journal [87] shows that is better to use an electrolyser adapted to a certain amount of power from the wind farm and a direct grid connection to send directly from the wind farm all energy above the electrolyser range; the joint exploitation of wind energy increases. According to this article, it means that it is better than only connect the wind farm to the grid or to connect it only to an electrolyser. The overall efficiency is about 56% for a study with a PEM electrolyser of 54 kW. The electrolyser is control based on tracking useful power wind.

Green grid closed. The idea of a buffer hydrogen producer is to consume the excess of energy produced in real time. It could need to consume a big excess in a fraction of time and so the electrolyser is over dimensioned compared to the average incoming excess. A study from the International journal of hydrogen energy [88] analyses the efficiency of a buffer included in a closed grid composed of PV, biomass (5kW), and wind farm (6kW) production. They define a controller to achieve to a possible production of H2, consuming only the excess of the energy on the grid. They achieved to an average efficiency of 21% for the hydrogen production.

PV independent units. A study of the International journal of hydrogen energy [89] analyses with the program HOMER the production of hydrogen for a company. The optimize design comprises 1000-kw PV modules, 200 batteries and 10-kW converter. It comprises an electrical station, transformer, rectifier AC/DC, electrolyser, water

treatment, gas/liquid separator and a hydrogen purifier. The necessity of hydrogen is during the day, fitting well with the PV supply in electricity.
The result is a global efficiency of 75% accounting that the used of electricity produced is 3.95 kWh per normal cubic meter of hydrogen.

Watter splitting. The method presented here is based on a solar hydrogen production via a two steps thermochemical redox cycles. Radiation from sun is use to drive the redox cycle. Dynamic simulation of such a system was conducted in in a study from the International journal of hydrogen energy [90]. The two phases process is the following:

$$\text{Thermal reduction: } MO_{ox} \rightarrow MO_{red} + 0.5O_2$$
$$\text{Water splitting step: } MO_{red} + H_2O \rightarrow MO_{ox} + H_2$$

They conclude to an efficiency of about 10% up to 14% with optimistic calculation. Upper limit is the one of a Carnot process. To heat the reactor, heat from geothermal source could be used according to the article and there would be no reflection losses as for radiation on the glasswindow of the reactor but losses from the heat transfer, so the overall efficiency should be as low as for the solar one. According to the authors, the critical limitation is that Ferrite based redox need to be ameliorate a lot to achieve a real potential.

Anaerobic fermentation. . Anaerobic fermentation consists in utilizing organic waste as a source of energy to produce hydrogen, in a dark fermentation process without oxygen. The main advantage is the production of hydrogen from waste.
The average municipal solid waste (MSW) are composed of 20% of food waste. It is a mix of proteins, starch and cellulose among others. According to [85] each of these elements should be degraded with its own parameters to achieve a perfect result. Since there are all mix together, a compromise should be achieved. According to this study, the main factors influencing the efficiency of the process are the PH control, the retention time in the reactor and the dilution rate (D). The PH control is important to initiate the process and then is adapted during the operation. A good retention time control permits to increase the concentration of biomass in the reactor. D is used to maintain the conditions perfect to produce the hydrogen.
The process studied is a two-stage process. One is used for the acidogenic hydrogenesis and the other for the methanogenesis. Due to the non-energy use of light, the acidogenic hydrogenesis reactions are incomplete and organic acids remain, but it allows creating hydrogen in big reactors at a large scale. The study reproduce the method at a small scale and at perfect conditions, 19.3% of the mass of the food waste is transformed in hydrogen. “The theoretical maximum yield of hydrogen fermentation is reported to be four moles of hydrogen per mole of glucose or eight moles of hydrogen per mole of sucrose, if all of the substrate would be converted to acetic acid” [91]. It corresponds to a theoretical maximum yield of 61% of g H2 by g of food waste.

For the moment, the best energetic efficiency with anaerobic fermentation is achieve by the fermentation from molasse, a product of sugar and is about 28%, much higher than in average [92]. According to the same article, the challenge is in general to achieve to the same result at a big scale production. Improvement to reduce cost and improving scale were done coupling an aerobic and anaerobic fermentation process by the team of researchers in China [93].

hydrogen efficiency values [%]	Current	propsection, 2050
wind offshore-electrolysis	39	55
Green-grid-electrolysis	55	65
Green-grid closed-electrolysis	21	35
PV independant units	75	90
Thermal solar - water splitting	10	25
Geothermal - water splitting	10	20
Biomass - anaerobic fermentation	15	35

Table B.15: Efficiency values used to evaluate the quantity of energy used to produced hydrogen. The electricity or heat consumed in the process comes exclusively from renewable sources. For example, for the offshore production, the efficiency doesn't take into account the wind to electricity conversion (by the windturbines) but only the elctricity produced (by the windtubines) to the hydrogen quantity. The main limating factor of the efficiency in this case is the fluctuation of the current produced.

C GP scenarios: representation of the evolution of the primary demand

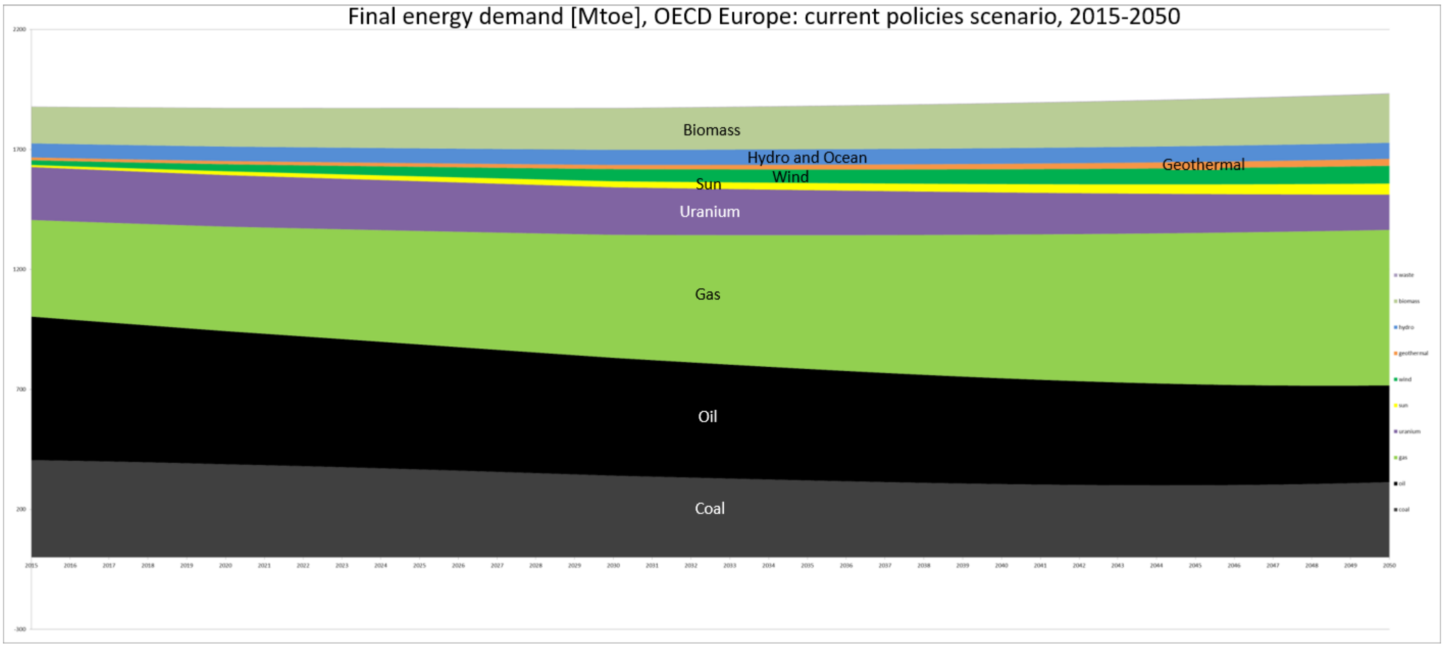

Figure C.1: OECD Europe, final energy demand, GP current sc.

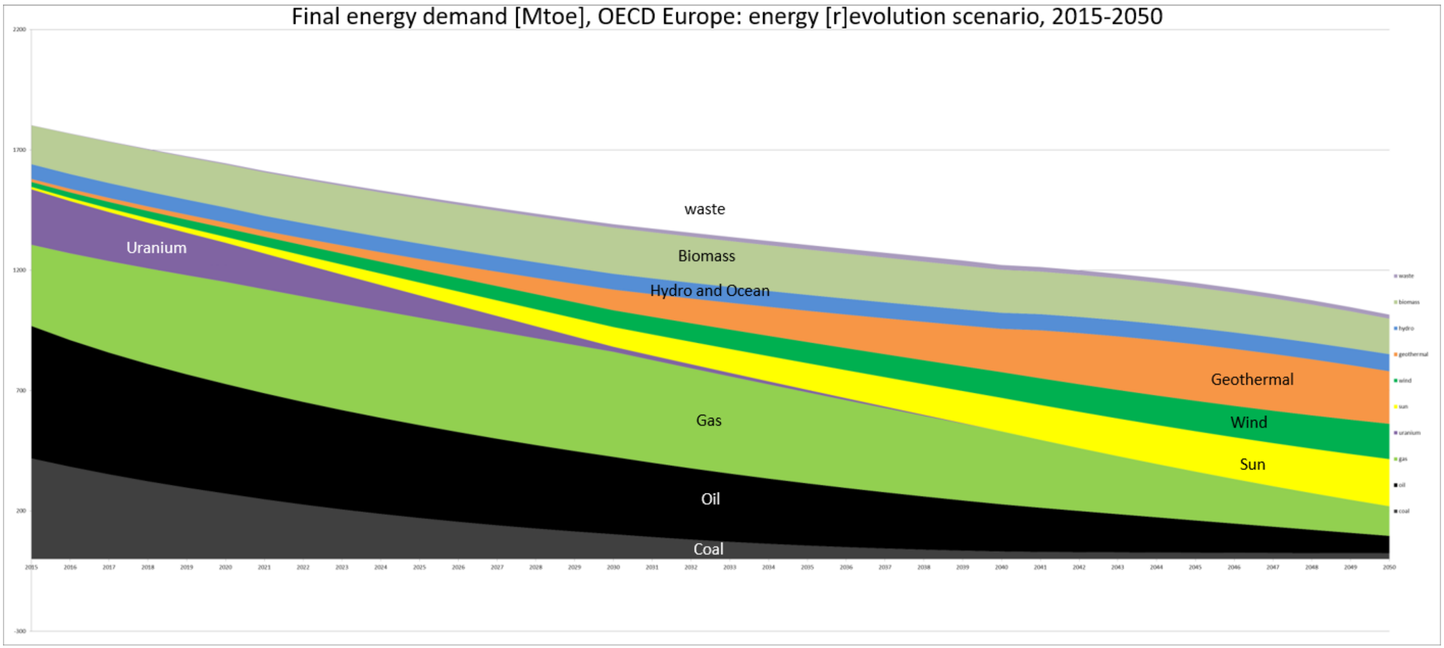

Figure C.2: OECD Europe, final energy demand, GP energy revolution sc.

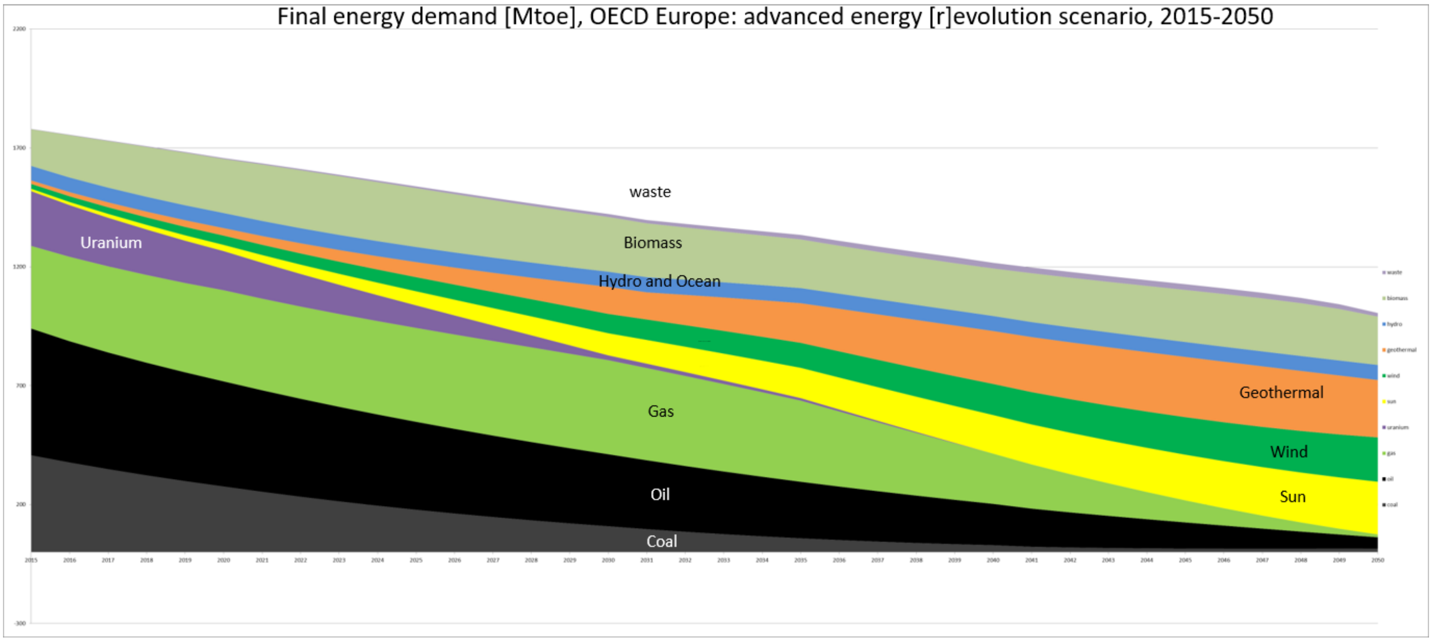

Figure C.3: OECD Europe, final energy demand, GP advanced energy revolution sc.

D Final values used in the energy balance model

Here are presented all values used for the efficiency, depending on the scenario.

	source of energy	technology	overall efficiency:	2015[%]	2050[%]	physical limit
Hydrogen						
		CHP plants electricity				60
			sc GP/iea 1	43	50	
			sc GP E[R]		50	
			sc GP E[R]+		55	
			sc Perso			
		CHP plants heat				100
			sc GP/iea 1	30	35	
			sc GP E[R]		40	
			sc GP E[R]+		45	
			sc Perso			
Biomass: waste						
		CHP plants electricity				60
			sc GP/iea 1	22	22	
			sc GP E[R]		28	
			sc GP E[R]+		28	
			sc Perso			
		CHP plants heat				100
			sc GP/iea 1	30	40	
			sc GP E[R]		40	
			sc GP E[R]+		40	
			sc Perso			
Biomass (other)						
		electricity plants				60
			sc GP/iea 1	42	45	
			sc GP E[R]		45	
			sc GP E[R]+		47	
			sc Perso			
		heat plants				100
			sc GP/iea 1	40	48	
			sc GP E[R]		48	
			sc GP E[R]+		48	
			sc Perso			
		CHP plants electricty				50
			sc GP/iea 1	34	45	
			sc GP E[R]		45	
			sc GP E[R]+		45	
			sc Perso			
		CHP plants heat				50
			sc GP/iea 1	36	45	
			sc GP E[R]		45	
			sc GP E[R]+		45	
			sc Perso			

Figure D.1: Efficiency values, energy balance model, part 1.

Geothermal						
		electricity plants				54
			sc GP/iea 1	12	16	
			sc GP E[R]		16	
			sc GP E[R]+		17	
			sc Perso			
		heat plants				100
			sc GP/iea 1	50	53	
			sc GP E[R]		53	
			sc GP E[R]+		53	
			sc Perso			
		CHP plants electricity				35
			sc GP/iea 1	6	6	
			sc GP E[R]		11	
			sc GP E[R]+		13	
			sc Perso			
		CHP plants heat				65
			sc GP/iea 1	45	51	
			sc GP E[R]		51	
			sc GP E[R]+		51	
			sc Perso			
Hydro						
		Hydroelectric damps				100
			sc GP/iea 1	91,5	92,5	
			sc GP E[R]		92,5	
			sc GP E[R]+		92,5	
			sc Perso			
Sun						
		Solar thermal CSP				78
			sc GP/iea 1	40	77	
			sc GP E[R]		77	
			sc GP E[R]+		77	
			sc Perso			
Uranium						
		nuclear plants				60
			sc GP/iea 1	36	39	
			sc GP E[R]		39	
			sc GP E[R]+		39	

Figure D.2: Efficiency values, energy balance model, part 2.

Natural gas						
		electricity plants				60
			sc GP/iea 1	56	59	
			sc GP E[R]		59	
			sc GP E[R]+		59	
			sc Perso			
		heat plants				100
			sc GP/iea 1	92	92	
			sc GP E[R]		92	
			sc GP E[R]+		92	
			sc Perso			
		CHP plants electricity				45
			sc GP/iea 1	37	42	
			sc GP E[R]		42	
			sc GP E[R]+		42	
			sc Perso			
		CHP plants heat				55
			sc GP/iea 1	47	50	
			sc GP E[R]		50	
			sc GP E[R]+		50	
			sc Perso			
Oil products						
		electricity plants				60
			sc GP/iea 1	39	42	
			sc GP E[R]		42	
			sc GP E[R]+		42	
			sc Perso			
		heat plants				100
			sc GP/iea 1	92	93	
			sc GP E[R]		93	
			sc GP E[R]+		93	
			sc Perso			
		CHP plants electricity				50
			sc GP/iea 1	37	40	
			sc GP E[R]		40	
			sc GP E[R]+		40	
			sc Perso			
		CHP plants heat				50
			sc GP/iea 1	42	45	
			sc GP E[R]		45	
			sc GP E[R]+		45	
			sc Perso			

Figure D.3: Efficiency values, energy balance model, part 3.

crude oil						
		oil refineries				100
			sc GP/iea 1	87,8	90	
			sc GP E[R]		90	
			sc GP E[R]+		90	
			sc Perso			
coal						
		electricity plants				60
			sc GP/iea 1	39	42	
			sc GP E[R]		42	
			sc GP E[R]+		42	
			sc Perso			
		heat plants				100
			sc GP/iea 1	90	92	
			sc GP E[R]		92	
			sc GP E[R]+		92	
			sc Perso			
		CHP plants electricity				25
			sc GP/iea 1	21	21	
			sc GP E[R]		21	
			sc GP E[R]+		21	
			sc Perso			
		CHP plants heat				75
			sc GP/iea 1	69	70	
			sc GP E[R]		70	
			sc GP E[R]+		70	
			sc Perso			

Figure D.4: Efficiency values, energy balance model, part 4.

Bibliography

[1] M. Wang, H. Lee, and J. Molburg. Allocation of Energy Use in Petroleum Refineries to Pretroleum Products. *Int J LCA 9*, pages 34–44, 2004.

[2] C. Deilmann and K.J. Bathe. Holistic method to design an optimized energy scenario and quantitatively evaluate promissing technologies for implementation. *International Journal of Green Energy 6*, pages 1–21, Jan 2009.

[3] GreenPeace. *Energy [r]evolution, a sustainable world, Energy Outlook 2015*, 2015.

[4] E. Dupont, H. Jeanmart, and R. Koppelaar. A Dynamic Function for the Energy Return on Investment of Wind Energy. *IMMC - Insistute of Mechanics - UCL*, 2017.

[5] Life Cycle Assessment of a HYSOL Concentrated Solar Power Plant: analyzing the effect of geographic location. *Energies 9,413*, May 2016.

[6] Nrel CSP Projects under construction. https://www.nrel.gov/csp/solarpaces/projects_by_status.cfm?status=Under%20Construction. Accessed: 2017-04-26.

[7] H.L. Zhang, J. Baeyens, J. Degrève, and G. Cacères. Concentrated solar power plants: Review and design methodology. *Elsevier. Renewable and Sustainable Energy Reviews 22*, pages 466–481, Mar 2013.

[8] SolarEnergy Projects in California. http://www.energy.ca.gov/sitingcases/solar/. Accessed: 2017-04-19.

[9] Ivanpah Solar Electric Generating System. https://www.nrel.gov/csp/solarpaces/project_detail.cfm/projectID=62. Accessed: 2017-04-19.

[10] X. Xu, K. Vignarooban, K. Hsu, and A.M. Kannan. Prospects and problems of concentrating solar power technologies for power generation in the desert regions. *Elsevier. Renewable and Sustainable Energy Reviews 53*, pages 1106–1131, Nov 2015.

[11] D.A. Baharoon, H.A. Rahman, W.Z. Omar, and S.O. Fadhl. Historical development of concentrating solar power technologies to generate clean electricity efficiently - A review. *Elsevier. Renewable and Sustainable Energy Reviews 41*, pages 996–1027, Jan 2015.

[12] O. Behar, A. Khellaf, and K. Mohammedi. A review of studies on central receiver solar thermal power plants. *Elsevier. Renewable and Sustainable Energy Reviews 23*, pages 12–39, Mar 2013.

[13] F.J. Collado and J. Guallar. Optical study of solar tower power plants. *Elsevier. Renewable and Sustainable Energy Reviews 20*, pages 142–154, Nov 2013.

[14] Advancing CSP Technology, Performances and Dispatchability. *SunShot AND NREL*, May 2016.

[15] Concentrating solar power: its potential contribution to a sustainable energy future 16. *EASAC policy report*, Nov 2011.

[16] Optics of solar central receiver systems: a review. https://www.osapublishing.org/oe/fulltext.cfm?uri=oe-24-14-A985. Accessed: 2017-05-20.

[17] F. Eddjibi, M.B. Amara, M. Balghouthi, and A. Guizani. Optical study of solar tower power plants. *Journal of Physics: Conference Series 596*, Apr 2015.

[18] Cosine Effect. http://www.energy.kth.se/compedu/webcompedu/WebHelp/S9_Renewable_Energy/B5_Solar_Energy/C2_Solar_Thermal_Energy/ID118_files/Cosine_effect.htm. Accessed: 2017-04-20.

[19] E. Leonardi and B. D'Aguanno. Crs4-2: A numerical code for the calculation of the solar power collected in a central receiver system. *Elsevier. Energy 36*, pages 4828–4837, May 2011.

[20] YT. Chen, A. Kribus, BH. Lim, and KK. Chong. Comparison of two sun tracking methods in the application of a heliostat field. *Journal of Solar Energy Engineering 126*, pages 638–682, 2004.

[21] KK. Chong and MH Tan. Range of motion study for two different sun-tracking methods in the application of heliostats field. *Solar Energy 85*, pages 1837–1887, 2011.

[22] A.L. Avila-Marin. Volumetric receivers in Solar Thermal Power Plants with central receiver system technology: A review. *Solar Energy 85*, pages 891–910, Mar 2011.

[23] B. Hoffschmidt. Receivers for Solar Tower Systems. Jun 2014.

[24] K. Burlafinger, A. Vetter, and C.J. Brabec. Maximizing concentrated solar power (CSP) plant overall efficiencies by using spectral selective absorbers at optimal operation temperatures. *Solar Energy 120*, pages 428–438, Aug 2015.

[25] Y. WU, N. REN, and C. Ma. Experimental study on optimized composition of mixed carbonate salt for sensible heat storage in solar thermal power plant. *Sol Energy 85*, pages 1957–2023, Aug 2011.

[26] C.S Turchi, M. Zhiwen, T. Neises, and M.J. Wagner. Thermodynamics study of advanced supercritical carbon dioxide power cycles for concentrating solar power systems. *Journal of SolarEnergy Engineering 135*, Nov 2013.

[27] R. Charcartegui, J.M. Munoz, D. Sanchez, B. Monje, and T. Sanchez. Alternatives cycles based on carbon dioxide for central receiver solar power plants. *Elsevier. Applied Thermal Engineering 31*, pages 872–879, Nov 2011.

[28] R.J. Zoschak and S.F Wu. Studies of the direct input of solar energy to a fossil-fueled central station steam power plant. *Elsevier. Solar Energy 17*, pages 297–305, Nov 1975.

[29] J.S.M. Jebamalai. Receiver Design Methodology for Solar Tower Power Plants. *Department of Energy Technology*, Aug 2016.

[30] K.C. HO and B.D. Iverson. Review of high-temperature central receiver designs for concentrating solar power. *Elsevier. Renewable and sustainable Energy Reviews*, pages 835–846, Aug 2013.

[31] B. Sakadjian, S. Hu, M. Maryamchik, T. Flynn, K. Santelmann, and Z. Ma. Fluidized-bed technology enabling the integration of high temperature solar receiver csp systems with steam and advanced power cycles. *Esevier. Internation Conference on Concentrating Solar Power. SolarPACES 2014. Energy Procedia 69*, pages 1404–1411, 2015.

[32] Agc mirrors. `http://www.agc-solar.com/agc-solar-products/solar-mirror/solar-mirror-thick.html#uid_114_desc`. Accessed: 2017-04-25.

[33] How do mirros reflect photons? `http://www.scientificamerican.com/article/how-do-mirros-reflect-ph/`. Accessed: 2017-04-25.

[34] C. Xu, Z. Wang, X. Li, and F. Sun. Energy and exergy analysis of solar power tower plants. *Elsevier. Applied Thermal Engineering 31*, pages 3904–3913, July 2011.

[35] V. Zare and M. Hasanzadeh. Energy and exergy analysis of a closed Brayton cycle based combined cycle for solar power tower plants. *Elsevier. Energy Conversion and Management*, pages 227–237, Sep 2016.

[36] G. Lambert, C. Hall, S. Balogh, A. Gupta, and M. Arnold. Energy, EROI and quality of life. *Eslevier. Energy Policy 64*, pages 153–167, August 2014.

[37] D. Murhpy, C. Hall, M. Dale, and C. Cleveland. Order from chaos: A preliminary protocol for determining the EROI of fuels. *Sustainability 3*, pages 1888–1907, July 2011.

[38] M. Dale, D. Krumdieck, and P. Bodger. A dynamic function for EnergyReturn on Investment. *Sustainability 3*, pages 1972–1985, October 2011.

[39] D. Waissbach, G. Ruprecht, A. Huke, K. Czerski, S. Gottlieb, and A. Hussein. Energy intensities, EROIs, and energy payback times of electricity generating power plants. April 2013.

[40] M.B Whitaker, G.A Heath, J.J. Burkhardt, and C.S. Turchi. Life Cycle Assessment of a Power Tower Concentrating Solar Plant and the Impacts of Key Design Alternatives. *Environmental Science Technology 47*, pages 5896–5903, May 2013.

[41] M. Rauge. Methodological Guidelines on Net Energy Analysis of Photovoltaic Electricity. *IEA Report 1 IEAPVPS T1207:2016*, Jan 2016.

[42] Revision of Primary Energy Factors in EU legislation. `http://www.eurelectric.org/media/184566/pef_note_2015_final-2015-030-0373-01-e.pdf`. Accessed: 2017-06-06.

[43] NASA Surface meteorology and Solar Energy. `https://eosweb.larc.nasa.gov/sse/global/text/direct_radiation`. Accessed: 2017-05-12.

[44] B. William and M. Geyer. Power from the Sun, available at powerfromthesun.net.

[45] L. Broman. Solar Engineering - a Condensed Course. *Högskolan Dalarna*, March 2006.

[46] Y. Thamn, T. Muneer, and B. Davison. Estimation of hourly averaged solar irradiation: evaluation of models. *Building Serv ResTechnol 31*, pages 9–25, 2010.

[47] R. Sioshansi and P. Denhlom. The value of CSP and thermal energy storage. *National Renewable Energy Laboratory*, Feb 2010.

[48] Thermal Energy Storage for CSP plants. `http://www.cttc.upc.edu/research/node/94`. Accessed: 2017-05-14.

[49] European Space Agency GlobCover Portal, ESA GlobCover 2009 Project. `http://due.esrin.esa.int/page_globcover.php`. Accessed: 2017-05-25.

[50] Review of the default primary energy factor (PEF) reflecting the estimated average EU generation efficiency referred to in annex iv of directive 2012/27/eu and possible extension of the approach to other energy carriers. `https://ec.europa.eu/energy/sites/ener/files/documents/final_report_pef_eed.pdf`. Accessed: 2017-06-06.

[51] R. Goh, M.Y. Othman, S. Mat, and K. Ruslan, H. Sopian. Review of heat pump systems for drying application. *Renewable and Sustainable Energy Reviews 15*, pages 4788–4796, Sep 2011.

[52] Technical Institute of Physics and Chemistry. *State of the art of Air-source Heat Pump for Cold Region*. Chinese Academy of Sciences, 2008.

[53] J. Martin and P. Wauters. *Installations thermodynmaiques motrices*. Presse Universitaires de Louvain, 2009.

[54] International Energy Agency. *Energy Technology Perspectives 2014*. IEA, 2014.

[55] Alyssa Kagel. The State of Geothermal Technology Part II: Surface Technology. *Geothermal Energy Association*, pages 1381–1390, Jan 2008.

[56] European Geothermal Energy Council. *Geothermal Electricity and Combined Heat and Power*, 2009.

[57] Jesper Ahrenfeldt, Tobias.P. Thomsen, Ulrick Henriksen, and Lasse.R Clausen. Biomass gasification cogeneration - A review of state of the art technology and near future perspectives. *Elsevier*, *Aplied Thermal Engineering*, pages 1407–1417, Dec 29 2011.

[58] Toms Prodanuks, Ivars Veidenbers, Ginta Cimdina, Salami Mohannad, and Dagnija Blumberga. Emergy analysis of biomass CHP. Case study. *International Scientific Conference "Environmental and Climate Technologies"*, *CONECT 2015*, *Riga*, *Latvia*, pages 366–371, Oct 2015.

[59] Antonia Proka, Matthijs Hisschemöller, and Elissaios Papyrakis. The scale of transition: an integrated study of the performance of CHP biomass plants in the Netherlands. *Journal of Integrative Environmental Sciences*, pages 225–241, Oct 10 2014.

[60] Micro CHP report powers discussion on UK energy future. *Elsevier. Fuel Cells Bulletin*, pages 3–4, Apr 2013.

[61] N. Thilak Raj, S. Iniyan, and R. Goic. A review of renewable energy based cogeneration technologies. *Elsevier. Renewable and Sustainable Energy Reviews*, pages 3640–3648, Aug 2011.

[62] Fuel cell CHP passes the point of no return. `http://www.decentralized-energy.com/articles/print/volume-15/issue-2/features/fuel-cell-chp-passes-the-point-of-no-return.html`. Accessed: 2017-04-15.

[63] I. Verhaert, G. Mulder, and M. DePaepe. Evaluation of an alkaline fuel cell system as micro-CHP. *Energy Conversion and Management 126*, pages 434–445, Aug 2016.

[64] David JC MacKay. *Without the hot air*. UIT Cambridge Ltd, 2009.

[65] Eurelectric working group in collaboration with VGB. Efficiency in Electricity Generation. *ETE03*, pages 1–4, July 2003.

[66] H Lund, B Möller, B.V. Mathiesen, and A. Dyrelund. The role of district heating in future renewable energy systems. *Elsevier. Renewable and Sustainable Energy Reviews*, pages 1381–1390, Jan 19 2010.

[67] Sadiq.J. Zarrouk and H. Moon. Efficiency of geothermal power plants: A worldwide review. *Elsevier. Goethermics 51*, pages 142–153, Jan 2014.

[68] F. Bertrand, Gr. Tchanche, T Lambrinos, A. Frangoudakis, and G. Papadakis. Low-grade heat conversion into power using organic Rankine cycles – A review of various applications. *Elsevier. Renewable and Sustainable Energy Reviews 15*, pages 3963–3979, Aug 21 2011.

[69] R. DiPippo. Geothermal power plants: Evolution and performance assesments 53. *Elsevier. Geothermics*, pages 291–307, Jul 2015.

[70] F. Cao, H. Li, Q. Ma, and L. Zhao. Design and simulation of a geothermal-solar combined chimney power plant. *Elsevier. Energy Conversion and Management 84*, pages 186–195, May 2014.

[71] La production d'énergie géothermique en France. `http://www.geothermie-perspectives.fr/article/production-denergie-geothermique-en-france`. Accessed: 2017-02-26.

[72] Wood and Pellet Heating. `http://energy.gov/energysaver/wood-and-pellet-heating`. Accessed: 2017-04-06.

[73] Giorgio Simbolotti. Biomass for Power Generation and CHP. *IEA Energy Technology Essentials ETE03*, pages 1–4, Jan 2007.

[74] S. Soltani, S.M.S. Mahmoudi, M. Yari, and M.A. Rosen. Themodynamic analyses of an externally fired gas turbine combined cycle integrated with a biomass gasification plant. *Elsevier. Energy Conversion and Management Vol.70*, pages 107–115, Jan 2013.

[75] IRENA. Hydropower. *IRENA Working Paper, Volume 1: Power Sector*, Jun 2012.

[76] M. Blackwood. Maximum efficiency of a wind turbine. *Mathematical modeling Vol 6, artcl 2*, 2016.

[77] R.P. Charles, K.W. Davis, and J.L. Smith. Assesment of Concentrating Solar Power Technology cost and performance forecasts. *Presented at Electric Power 2005*, Apr 2005.

[78] G.A. Health and J.J. Burkhardt. Meta-Analysis of estimates of life cycle greenhouse gas emissions from concentrating solar power. *Conference Paper of NREL, NREL/CP-6A20-52191*, Sept 2011.

[79] B. Parida, S. Iniyan, and R. Goic. A review of solar photovoltaic technologies. *Elsevier. Renewable and Sustainable energy reviews 15*, pages 1625–1636, Jan 2011.

[80] M.A. Green. Third generation photovoltaics, advanced solar energy conversion. *Springer Series in Photonics 12*, 2008.

[81] S.A Kalogirou. Solar thermal collectors and applications. *Elsevier. Progress in Energy and Combustion Science 30*, pages 231–295, Feb 2004.

[82] R. Vennell. Exceeding the Betz Limit with Tidal Turbines. *Elsevier. Renewable energy 53*, Aug 2013.

[83] R. Vennell. Realizing the potential of tidal currents and the efficiency of turbines farms in a channel. *Elsevier. Renewable Energy 47*, pages 95–102, May 2012.

[84] H.R. Karbasian, J.A. Esfahani, and E. Barati. Simulation of power extraction from tidal currents by flapping foil hydrokinetic turbines in tandem formation. *Elsevier. Renewable Energy 81*, pages 816–824, Apr 2015.

[85] K. Meier. Hydrogen production with sea water electrolysis using Norwegian offshore wind energy potentials 5:104. *Int J Energy Eng*, May 2014.

[86] B. Guinot, F. Montignac, B. Champel, and D. Vannucci. Profitability of an electrolysis based hydrogen production plant providing grid balancing services. *Elsevier. International Journal of Hydrogen Energy 40*, pages 8778–8787, June 2015.

[87] R. Valdés, J.H. Lucio, and L.R. Rodriguez. Operational simulation of wind power plants for electrolytic hydrogen production connected to a distributed electricity generation grid. *Elsevier. Renewable Energy 53*, pages 249–257, Dec 2012.

[88] C. Sanchez and D. Gonzalez. Experimental characterization of a grid-connected hydrogen energy buffer: hydrogen production. *Elsevier. International Journal of Hydrogen Energy 38*, pages 9741–9754, June 2013.

[89] R. Bourdies, A. Khellaf, A. Aliane, L. Ihaddaden, and F. Khida. PV system design for powering an industrial unit for hydrogen production. *Elsevier. International Journal of Hydrogen Energy 39*, pages 15188–15195, June 2014.

[90] M. Lange, M. Roeb, C. Sattler, and R. Pitz-Paal. Efficiency assessment of a two-step thermochemical water-splitting process based on a dynamic process model. *Elsevier. International Journal of Hydrogen Energy 40*, pages 12108–12119, Aug 2015.

[91] S. Sung, L. Raskin, J.J. Simmons, S. Padmasiri, and T. Duangmanee. Hydrogen Production by anaerobic microbial communities exposed to repeated heat treatments. *Water Environment Research Vol 79 n 9*, pages 975–983, Sept 2007.

[92] I. Dincer. Green methods for Hydrogen Production. *Elsevier. International Journal of Hydrogen Energy*, pages 1954–1971, Sept 2011.

[93] D. Li, L. Qin, and H. Chen. Aerobic and anaerobic sequential culture fermentation to produce bio-hydrogen from steam-exploded cornstalk. *Elsevier. International Journal of Hydrogen Energy 39*, pages 8992–8999, Apr 2014.

Rue Archimède, 1 bte L6.11.01, 1348 Louvain-la-Neuve www.uclouvain.be/epl